Spring 1-1-2011

Limits to Continuity of Unsaturated, Compacted Soils

Joonyong Lee
University of Colorado at Boulder, joonyong.lee@colorado.edu

LIMITS TO CONTINUITY OF UNSATURATED, COMPACTED SOILS

by

JOONYONG LEE

B.S., Konkuk University, 2003

M.S., University of Colorado, 2007

A thesis submitted to the

Faculty of the Graduate School of the

University of Colorado in partial fulfillment

of the requirement for the degree of

Doctor of Philosophy

Department of Civil, Environmental, and Architectural Engineering

2011

This thesis entitled:
Limits to Continuity of Unsaturated, Compacted Soils
written by Joonyong Lee
has been approved for the Department of Civil, Environmental, and Architectural Engineering

_____

Professor Dobroslav Znidarcic, Committee Chair

_____

Professor Hon-Yim Ko

_____

Professor John McCartney

Date_____

The final copy of this thesis has been examined by the signatories, and we
Find that both the content and the form meet acceptable presentation standards
Of scholarly work in the above mentioned discipline.

Joonyong, Lee (Ph.D., Civil, Environmental and Architectural Engineering)

Limits to Continuity of Unsaturated, Compacted Soils

Thesis directed by Professor Dobroslav Znidarcic

Geotechnical engineers are interested in flow phenomena of unsaturated soils, as they play an important role in interpreting the stability and deformation of slopes, retaining walls, and pavements under unsaturated conditions. Fundamental material characteristics of flow phenomena such as soil-water retention curve (SWRC), which is required to define the driving potential for the flow process, and hydraulic conductivity function (HCF), which is required to define the resistance to the flow process, are still primary concerns for characterizing the flow phenomena in unsaturated soils. Characterizing the SWRC and the HCF in flow phenomena of unsaturated soils is a challenge for many researchers even though the several measurement techniques have been proposed.

A flow pump system (FPS) was developed in early 1990 at the University of Colorado in order to characterize unsaturated soils. FPS has been improved over the past 20 years for characterizing the flow phenomena of unsaturated soils, and the new FPS technique is developed for measuring the suction response and SWRC induced by the flow pump during drying and wetting cycles. And, HCF is evaluated by using an inverse problem solution approach.

Three materials such as a uniform sand and well graded soils are used in this study for investigating flow phenomena in unsaturated soils. The following conclusions are drawn from the research result. The prediction models commonly used for HCF cannot properly represent the actual hydraulic conductivity of unsaturated soils. The results also show that the liquid-phase flow of pore water stops at relatively high degree of saturation and low suction. The threshold

saturation and corresponding hydraulic conductivity values are difficult to determine for each material, and this confirms the hypothesis that hydraulic conductivity for unsaturated soils must be determined through careful experimentation and that no prediction model is valid for all soils. This research developed an adequate methodology to conduct such experiments straightforward, and paved a rational way to predict suction changes in soils due to environmental conditions.

CONTENTS

TABLES

FIGURES

CHAPTER 1

INTRODUCTION

Many geotechnical engineers still use classical soil mechanics theory proposed by Karl Terzaghi in various geotechnical engineering problems. However, classical soil mechanics theory is based on an assumption that soil is either completely saturated cohesive material or completely dry material, even though unsaturated soil conditions are often present in the field. That is to say, soils are multiphase system consisting of pore water, solid soil particles, and pore air. Therefore, analysis with classical soil mechanics theory is either ineffective or inappropriate for fully describing the stress distributions or failure conditions in many soils in the field (Lu and Likos, 2004).

Unsaturated soil mechanics can be separated into three general phenomena, flow phenomena, stress phenomena, and deformation phenomena. Governing theories and models for both liquid and gas flow in unsaturated soils can explain flow phenomena, and many seepage related problems in geotechnical engineering can be effectively treated through the application of the governing theories and models. Stress phenomena are important in many traditional geotechnical engineering problems such as lateral earth pressure, bearing capacity, and slope stability analyses. In order to explain stress phenomena under unsaturated conditions, theories for describing the states of stress and failure require consideration of thermodynamic properties of

the pore water in terms of soil suction, material variables such as grain size and grain size distribution, state variables such as the degree of saturation, and consequent interparticle forces such as suction-induced effective stress or suction stress (Lu and Likos, 2004). Also, the unsaturated soil deformation phenomena, such as swelling or shrinking soil characteristics, caused by changes in the moisture condition of the soil should be considered. Among these three representative phenomena in unsaturated soil mechanics, many researchers are interested in flow phenomena under unsaturated conditions, especially fundamental material characteristics of unsaturated flow phenomena such as soil-water retention curve (SWRC) required to define the driving potential for the flow process and hydraulic conductivity function (HCF) required to define the resistance to the flow process. Also, these fundamental material characteristics of flow process are related to the stability and deformation of slopes, retaining walls, and pavements. Therefore, appropriate approach for the SWRC and HCF should be needed for geotechnical engineering field.

Issues

In comparison with direct measurement of unsaturated hydraulic conductivity, the prediction models for the HCF from the SWRC are attractive for their fast and simple use and low cost (Vogel and Cislerova, 1998). In spite of these advantages, prediction models for the HCF have some significant limitations. Among issues in prediction models for the HFC, existing models often can predict the HCF exactly in comparison with experimental dat. One of the reasons for this deficiency is the restriction of using the parameter values in the SWRC fitting model for the HCF, since models for the HCF use same parameter values as in the SWRC. This is due to the inaccuracies in the determination of the SWRC caused by an insufficient representativeness of the sample for the porous medium in question, or errors of measurement, or

inexact curve fitting through the experimental data (Vogel and Cislerova, 1988). Previous models for HCF are sensitive to these inaccuracies in determination of the SWRC. Also, previous prediction models for the HCF were particularly found to lead to significant discrepancy from the actual HCF at low water contents (McCartney and Parks 2009). Figure 1.1 shows differences of the van Genuchten's fitting curve parameter α values between for the SWRC and the HCF, when the van Genuchten's curve parameter α for HCF is obtained not from the fit to the SWRC, but from the fit to the hydraulic conductivity data directly. The data in Figure 1.1 indicates that prediction model for the HCF with α value obtained the fit to the SWRC generally misestimate the actual hydraulic conductivity value.

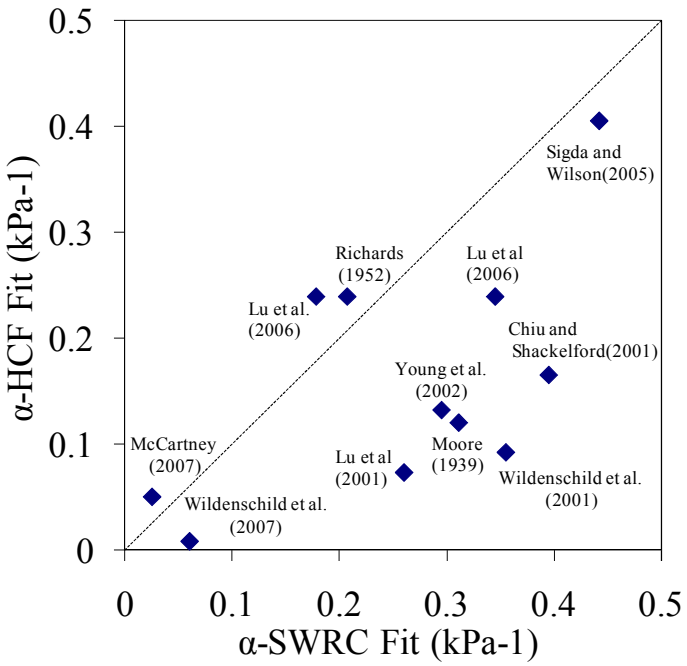

Figure 1.1. Comparison between α parameters for different soils obtained from fitting van Genuchten (1980) model to the HCF and SWRC data (McCartney and Parks, 2009)

A second issue with respect to the HCF is a limit for the liquid-phase water flow in unsaturated conditions. Previous prediction models for the HCF do not provide limit between the

liquid-phase water flow and vapor-phase water flow on the hydraulic conductivity of the soil. The unlimited decrease in the hydraulic conductivity with increasing soil suctions produces a termination of liquid-phase water flow due to a discontinuity in the liquid-phase (Ebrahimi-B et al., 2004). When the liquid-phase in the soil becomes discontinuous at a specific suction value, vapor-phase water flow dominates in the migration of moisture in the soil instead of the liquid-phase water flow. However, the boundary between liquid and vapor phase transport is difficult to assess (McCartney and Zornberg, 2010). A recent study (Ebrahimi-B et al, 2004) has suggested that the lower limit for the hydraulic conductivity is based on the residual water content and vapor-phase water flow theory, and the overall HCF for entire suction range is added the HCF for vapor-phase water flow to the HCF for liquid-phase water flow. Figure 1.2 shows their suggested overall HCF. However, we need to observe the tendency of the HCF by experimental approach, since they also used the HCF prediction model to determine the termination of liquid-phase water flow instead of the actual HCF data.

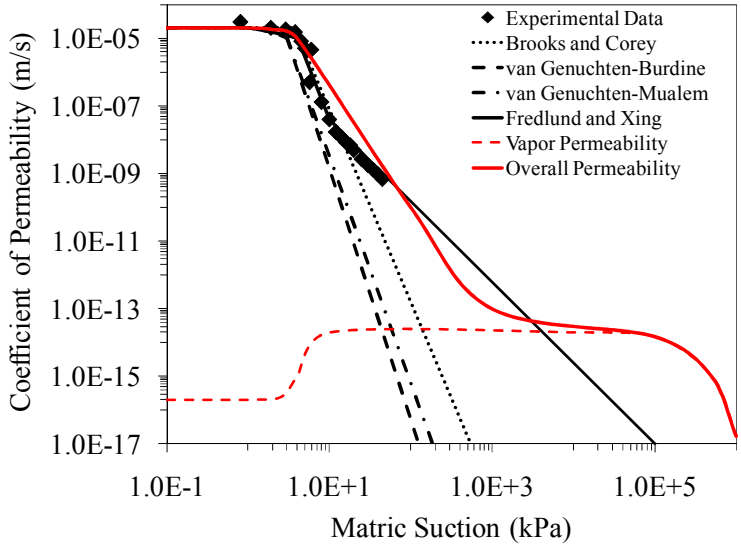

Figure 1.2. Variation of liquid water, vapor, and overall HCF with soil suction for a loamy sand soil (Ebrahimi-B et al, 2004)

Objectives

The goal of this research is to measure the suction response and the SWRC during hydraulic hysteresis using a new measurement technique, referred to as the "*Maintained Suction Measurement"* approach together with the conventional axis translation technique, triaxial equipment and a flow pump system (FPS) originally developed at the University of Colorado at Boulder (Znidarcic et al, 1991). Also, the proper HCFs corresponding to drying and wetting cycles are evaluated using an inverse problem solution approach corresponding to the suction response result with time and the SWRC result. Also, the previous measurement technique with the FPS, "*Suction Drop Measurement*" developed by Hwang (2002) is reviewed, and suction responses, SWRCs, and HCFs between two measurement techniques are discussed. Finally, the infiltration test technique with FPS is developed without preceding drying cycle.

CHAPTER 2

BACKGROUND OF FLOW PHENOMENA IN UNSATURATED SOILS

The flow phenomena in unsaturated soils is different from that under saturated conditions, because the unsaturated soil is a multiphase system consisting of three phases: pore air, pore water, and solid soil particles, whereas saturated soil consists of only pore water and solid soil particles. In order to understand the flow behavior in unsaturated soils, reviews about fundamental concepts such as phase relationships for unsaturated soils, governing equations, SWRC, hydraulic conductivity function HCF, and the numerical solution approach are needed.

2.1 Phase Relationship for Unsaturated Soils

Soils under the unsaturated condition consist of three phase compositions: pore air, pore water, and solid soil particles. The gravimetric water content is defined as the ratio of mass of water to mass of solids, whereas volumetric water content is defined as the ratio of the volume of water to total volume. The following relationships can be defined with respect to Figure 2.1.

$$w = \frac{M_w}{M_s} \;;\; n = \frac{V_v}{V_t} = \frac{e}{1+e} \;;\; e = \frac{V_v}{V_s} = \frac{n}{1-n} \;;\; S_r = \frac{V_w}{V_v} \;;\; \theta = \frac{V_w}{V_t} = \frac{V_v}{V_t} \times \frac{V_w}{V_v} = n \times S_r \tag{2.1}$$

where w is the gravimetric water content, n is porosity, e is void ratio, S_r is degree of saturation, and θ is volumetric water content.

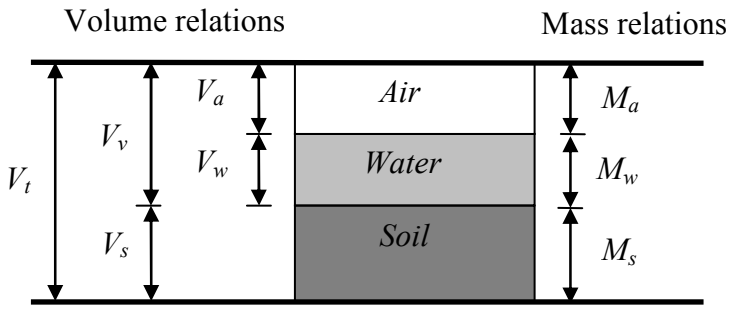

Figure 2.1. Phase diagram for unsaturated soils (Fredlund and Rahardjo, 1993)

The volumetric water content (θ) can be used to describe the quantity of the change in water storage of a soil specimen in the situation where there are no changes in both the total volume of the soil and the volume of water in the pores during water flow. Thus, the volumetric water content (θ), and porosity (n) are appropriate for rigid soil specimens such as compacted or overconsolidated soils. In compressible specimens, the gravimetric water content (w) and void ratio (e) are more appropriate, because the mass and volume of solids do not change during water flow. Changes in the gravimetric water content (w) reflect changes in the mass of the water in the soil, while changes in the void ratio (e) reflect changes in the volume of voids (McCartney, 2007).

2.2 Capillarity and Soil Suction

As shown in Figure 2.2, the water rises above free water level because of the surface tension in the contractile skin and the tendency of water to wet the surface of the glass tube when the capillary tube is submerged under water. This phenomenon can be explained by the relationship between the vertical resultant of the surface tension and the weight of water column, and we can obtain the maximum height of water in the capillary tube through the following Equations (2.2) and (2.3).

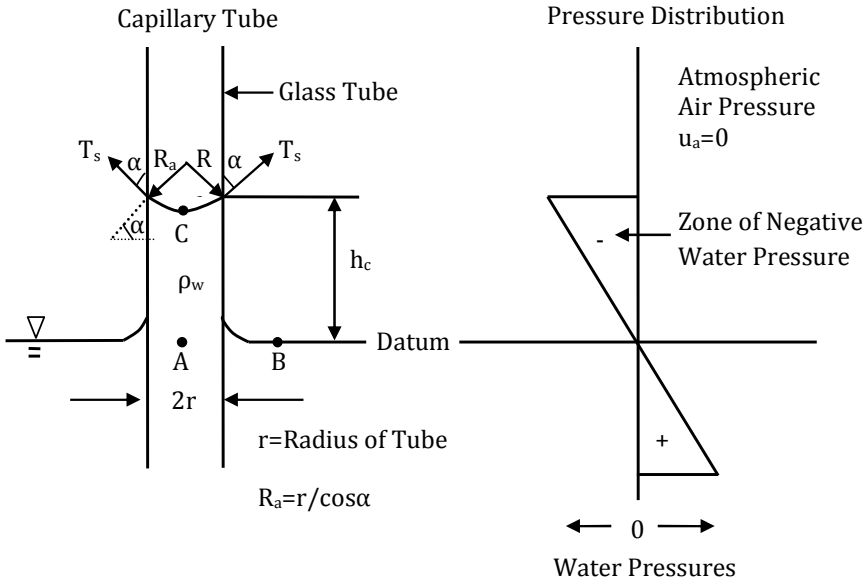

Figure 2.2. Physical model and phenomenon related to capillarity (after Fredlund and Rahardjo, 1993)

$$2\pi r T_s \cos\alpha = \pi r^2 h_c \rho_w g \tag{2.2}$$

$$h_c = \frac{2T_s}{\rho_w g r} \tag{2.3}$$

where r is radius of the capillary tube, T_s is the surface tension of water, α is contact angle, h_c is capillary height, and g is gravitational acceleration.

Points A, B, and C are in hydrostatic equilibrium. Therefore, the total head at points A, B, and C are the same. At point A and B, pressure heads and elevation heads are all zero, thus the total head at point A and B are 0. Therefore, the total head at point C is also 0. Also, the elevation head at point C is h_c, so the pressure head at point C must be $-h_c$ because the total head at point C is 0. Therefore, we can express the water pressure, $u_{w,C}$ at point C as follows.

$$u_{w,C} = -\rho_w g h_c \tag{2.4}$$

Since the gauge air pressure is 0 at point C and the water pressure, u_w is $-\rho_w g h_c$, the matric suction is defined as follows.

$$(u_a - u_w) = \rho_w g h_c \tag{2.5}$$

Substituting Equation (2.3) into Equation (2.5), we can get the matric suction by the relationship between the surface tension and the radius of the capillary tube, and we can see that the capillary phenomenon is related to the matric suction,

$$(u_a - u_w) = \frac{2T_s}{r} \tag{2.6}$$

Soil suction is commonly referred to as the free energy state of soil water (Edlefsen and Anderson, 1943). The free energy of the soil water can be measured in terms of the partial vapor pressure of the soil water (Richards, 1965). The thermodynamic relationship between soil suction and the partial pressure of the pore-water vapor can be written as follows (Thomson, 1871).

$$\psi_T = -\frac{RT}{v_{w0} w_v} \ln\left(\frac{u_v}{u_{v0}}\right) = -\frac{RT}{v_{w0} w_v} \ln(RH) \tag{2.7}$$

where Ψ_T= soil suction or total suction (kPa)

R = universal (molar) gas constant [i.e., 8.31432J/(mol K)]

T = absolute temperature [i.e., T=(273.16+$t°$) (K)]

$t°$ = temperature ($°C$)

v_{w0} =specific volume of water or the inverse of the density of water [i.e., $1/\rho_w$ (m^3/kg)]

ρ_w = density of water [i.e., 998kg/ m^3 at $t°$=20 $°C$]

w_v = molecular mass of water vapor [i.e., 18.016 kg/kmol]

u_v = partial pressure of water vapor (kPa)

u_{v0}= saturation pressure of water vapor over a flat surface of pure water at the same temperature (kPa).

RH=relative humidity

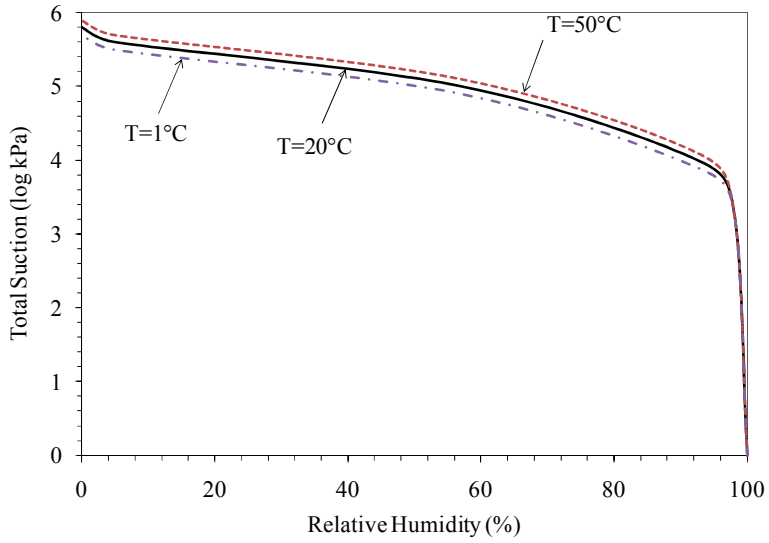

Figure 2.3. Theoretical relationship between RH and total suction (Likos and Lu, 2001)

In Equation (2.8), the soil suction, ψ_T is the total suction comprised of the matric suction and osmotic suction, and the relationship between the total suction, matric suction and osmotic suction is as follows:

$$\psi_T = \psi_m + \psi_o \tag{2.8}$$

where ψ_m is matric suction and ψ_o is osmotic suction

Matric suction describes the component of suction arising from interactions between the pore water and the soil solids, or soil matrix, and osmotic suction is suction arising from the presence of dissolved solutes (Lu and Likos, 2004). Generally, in the absence of changes in dissolved salt concentration, the change of the matric suction is more significant than the change of osmotic suction in the change of the total suction because osmotic suction remains constant over the entire range of water content if the concentration of dissolved solutes does not change.

2.3 Governing Equation for Transient Liquid-Phase Water Flow

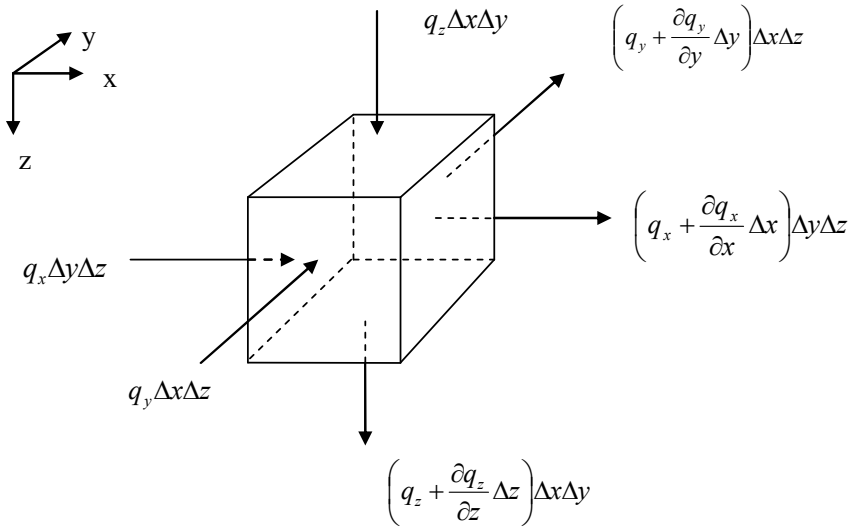

Figure 2.4. Elemental volume of soil and continuity requirements for fluids flow (Lu and Likos, 2004).

Figure 2.4 shows a representative element of soil. The total inflow of water is

$$q_{in} = \rho\left(q_x \Delta y \Delta z + q_y \Delta x \Delta z + q_z \Delta x \Delta y\right) \tag{2.9}$$

and the total outflow of water is:

$$q_{out} = \rho\left[\left(q_x + \frac{\partial q_x}{\partial x}\Delta x\right)\Delta y \Delta z + \left(q_y + \frac{\partial q_y}{\partial y}\Delta y\right)\Delta x \Delta z + \left(q_z + \frac{\partial q_z}{\partial z}\Delta z\right)\Delta x \Delta y\right] \tag{2.10}$$

where ρ is the density of water (kg/m^3), q_x, q_y, and q_z are the liquid-phase water fluxes in the x, y, and z directions, respectively (m/s).

From Equations (2.9) and (2.10), the net flux of inflow and outflow is:

$$q_{in} - q_{out} = -\rho\left[\frac{\partial q_x}{\partial x}\Delta x \Delta y \Delta z + \frac{\partial q_y}{\partial y}\Delta y \Delta x \Delta z + \frac{\partial q_z}{\partial z}\Delta z \Delta x \Delta y\right] \tag{2.11}$$

The rate of water loss or gain by element during a transient process is given as follows:

$$\frac{\partial(\rho\theta)}{\partial t}\Delta x\Delta y\Delta z \tag{2.12}$$

Equation (2.12). Also, the rate of water loss or gain is conservative, and is equal to the net flux and of inflow and outflow for a given elemental volume of soil according to mass conservation, also called continuity principle (Lu and Likos, 2004). Therefore, Equation (2.11) is equal to Equation (2.12), or :

$$\frac{\partial(\rho\theta)}{\partial t}\Delta x\Delta y\Delta z \tag{2.12}$$

$$-\rho\left(\frac{\partial q_x}{\partial x}\Delta x\Delta y\Delta z+\frac{\partial q_y}{\partial y}\Delta y\Delta x\Delta z+\frac{\partial q_z}{\partial z}\Delta z\Delta x\Delta y\right)=\frac{\partial(\rho\theta)}{\partial t}\Delta x\Delta y\Delta z \tag{2.13}$$

or

$$-\rho\left(\frac{\partial q_x}{\partial x}+\frac{\partial q_y}{\partial y}+\frac{\partial q_z}{\partial z}\right)=\frac{\partial(\rho\theta)}{\partial t} \tag{2.14}$$

Equations (2.13) and (2.14) are called the governing equation for unsteady or transient liquid-phase water flow in both saturated and unsaturated soil.

Darcy's law is given as follows:

$$q_x=-k_x(h_m)\frac{\partial h}{\partial x}\qquad q_y=-k_y(h_m)\frac{\partial h}{\partial y}\qquad q_z=-k_z(h_m)\frac{\partial h}{\partial z} \tag{2.15}$$

Substituting of Equation (2.15) into Equation (2.14), give the following result:

$$\frac{\partial}{\partial x}\left[k_x(h_m)\frac{\partial h_m}{\partial x}\right]+\frac{\partial}{\partial y}\left[k_y(h_m)\frac{\partial h_m}{\partial y}\right]+\frac{\partial}{\partial z}\left[k_z(h_m)\left(\frac{\partial h_m}{\partial z}+1\right)\right]=\frac{\partial\theta}{\partial t} \tag{2.16}$$

where h_m is matric suction head and $k(h_m)$ is HCF.

The right-hand term in Equation (2.16) can be rewritten as follows:

$$\frac{\partial\theta}{\partial t}=\frac{\partial\theta}{\partial h_m}\frac{\partial h_m}{\partial t} \tag{2.17}$$

or

$$C(h_m) = \frac{\partial \theta}{\partial h_m} \tag{2.18}$$

where $C(h_m)$ is the specific moisture capacity function representing the slope between volumetric water content and suction head given as the SWRC.

The governing equation for transient unsaturated liquid-phase water flow known as Richards' equation can be derived by substituting Equation (2.17) and (2.18) into Equation (2.16), or

$$\frac{\partial}{\partial x}\left[k_x(h_m)\frac{\partial h_m}{\partial x}\right] + \frac{\partial}{\partial y}\left[k_y(h_m)\frac{\partial h_m}{\partial y}\right] + \frac{\partial}{\partial z}\left[k_z(h_m)\left(\frac{\partial h_m}{\partial z} + 1\right)\right] = C(h_m)\frac{\partial h_m}{\partial t} \tag{2.19}$$

Thus, two characteristic functions are required for the solution of Richards' equation, i.e., the HCF and the specific moisture capacity function from the SWRC.

2.4 Soil Water Retention Curve (SWRC)

As previously mentioned, the SWRC is one of relationships needed to describe the unsaturated soils. The SWRC defines the relationship between soil suction and the amount of water in soil, expressed by gravimetric water content (m_w/m_s), volumetric water content (v_w/v_t), normalized water content (Θ), or degree of saturation (S_r). Table 2.1 shows the summary of advantages and disadvantages of various designations for the amount of water in a soil.

In general, the SWRC reflects that the soil suction is high at a relatively low water content, whereas the difference between the pore-water potential and the potential of free water decreases as the volumetric water content increases and the corresponding soil suction is relatively low at relatively high water content (Lu and Likos, 2004). Figure 2.5 presents the typical SWRC of sand, silt, and clay. The reason that the SWRCs of sand, silt, and clay have

different shapes is that three materials will have different pore and grain size distributions. Other factors such as organic material content, and the mineralogy also affect the shapes of the SWRC. Figure 2.6 shows the effect of the hysteresis and scanning curves on the SWRC. The drying curve is significantly different from the wetting curve. Therefore, a decision must be made as to which process is to be modeled (i.e., the drying or wetting process) and then the appropriate unsaturated soil property function estimated from the SWRC (Tami et al., 2004a).

Table 2.1. Summary of advantages and disadvantages of various designations for the amount of water in a soil (Fredlund, 2006)

Designation	Advantages	Disadvantages
Gravimetric water content, w	-Consistent with usage in classical soil mechanics -Most common means of measurement -Does not require a volume measurement -Reference is "mass of soil" which remains constants	Does not allow differentiation between change in volume and change in degree of saturation Does not yield the correct air entry value when the soil changes volume upon drying
Volumetric water content, Θ	-Is the basic form that emerges in the derivation of transient seepage in unsaturated soils -Commonly used in databases of results obtained in soil science	Requires a volume measurement Rigorous definition requires a volume measurement at each soil suction Is the designation least familiar and least used in geotechnical eng.
Degree of saturation, S_r	-Most clearly defines the air entry value -Appears to be the variable most closely controlling unsaturated soil behavior	Requires a volume measurement Does not reveal when the soil undergoes volume change

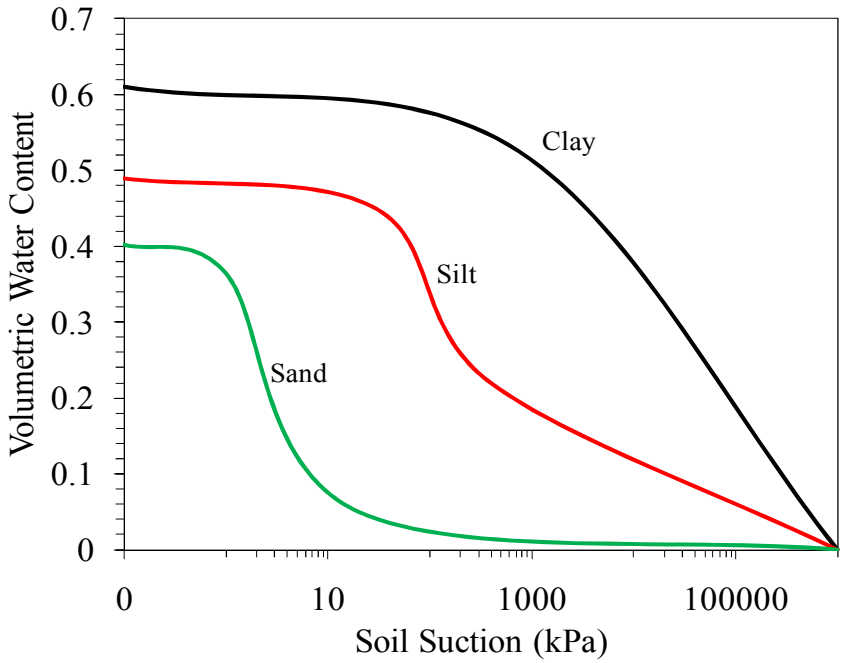

Figure 2.5. A typical example of SWCC for fine sand, silt, and clay (Lu and Likos, 2004)

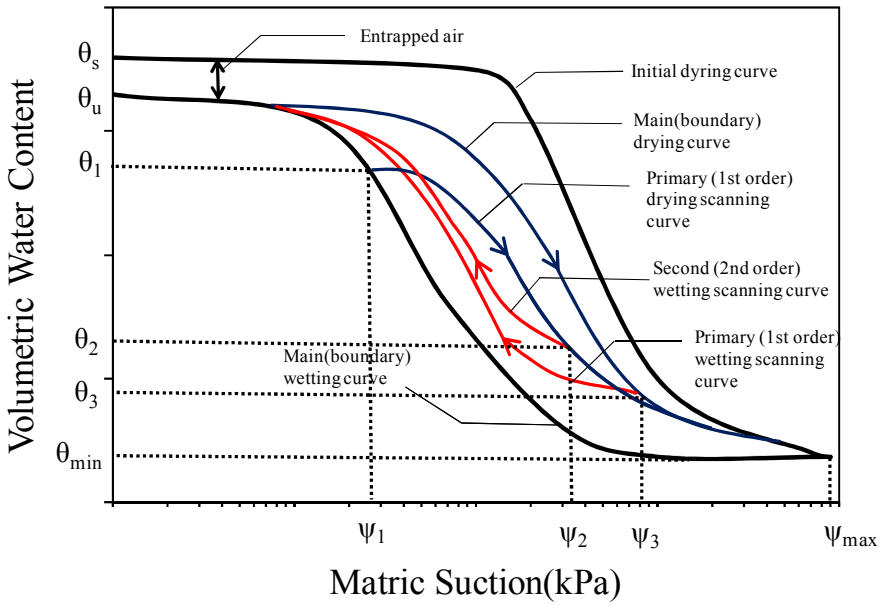

Figure 2.6. Bounding and scanning curves that comprise the drying and wetting behavior of an unsaturated soil (Pham et al., 2003a,b)

Currently, many researchers use SWRC equations for representation of the SWRC experimental data or empirical data in order to solve the governing equation numerically. Numerous SWRC equations have been suggested including Gardner (1958), Brooks and Corey (1964), Farrel and Larson (1972), van Genuchten (1980), Williams et al. (1983), and Fredlund and Xing (1994). Among numerous SWRC equations, only three SWRC equations are commonly used for geotechnical engineering application, i.e., the Brooks and Corey (1964), van Genuchten (1980), and the Fredlund and Xing (1994).

Each SWRC equation has different curve fitting parameters. First, Brooks and Corey proposed a SWRC equation in 1964. According to their model, the SWRC equation is expressed by two-part power law relationship incorporating a pore size distribution index, $1/b$ ($=\lambda$):

$$\theta = \begin{cases} \theta_s & \psi < \psi_e \\ \theta_r + (\theta_s - \theta_r)\left(\dfrac{\psi_e}{\psi}\right)^{1/b} & \psi \geq \psi_e \end{cases} \tag{2.20}$$

where θ_r is the residual volumetric water content, θ_s is the saturated volumetric water content, ψ_e is the air entry pressure, and $1/b$ is a pore size distribution index (which is inverse of the original Brooks and Corey parameter, λ).

This equation has a discontinuity at the air entry pressure value in the SWRC. This discontinuity sometimes is one of the reasons why Brooks and Corey equation shows some numerical problems in numerical saturated-unsaturated flow problems.

Second, van Genuchten developed a SWRC equation using three fitting parameters, i.e.,α, m, and n in 1980:

$$\theta = (\theta_s - \theta_r)\left[\frac{1}{1+(\alpha\psi)^n}\right]^m + \theta_r \tag{2.21}$$

The parameter α approximates the inverse of inflection point, the parameter n is related to the pore size distribution of the soil, and the parameter m is related to the overall symmetry of the characteristic curve (Lu and Likos, 2004). The van Genuchten equation can be expressed in terms of suction ψ (or suction head, h) and air-entry pressure ψ_e (or air entry head, h_e). Unlike the Brooks and Corey model, this model can predict the hydraulic conductivity over the entire range of soil suctions excluding discontinuity.

Finally, Fredlund and Xing proposed the SWRC equation in 1994.

$$\theta = C(\psi)\theta_s\left[\frac{1}{\ln[e+(\psi/a)^n}\right]^m \quad \text{or} \quad \theta = C(\psi)\left[\frac{1}{\ln[e+(\psi/a)^n}\right]^m \tag{2.22}$$

where $C(\psi)$ is a correction factor which defines $C(\psi) = \left[1 - \frac{\ln(1+\psi/\psi_r)}{\ln[1+10^6/\psi_r)}\right]^m$ and α, m, and n are fitting parameter.

In each of the aforementioned SWRC equations, definitions of the residual water content are different. Brooks and Corey(1964) defined the residual water content is defined as the water content at which suction reaches infinity, whereas van Genuchten(1980) defined the residual water content at which the slope of the SWRC and coefficient permeability go to zero when the suction becomes large (van Geuchten, 1980). However, it is difficult to determine the residual water content when experimental data are limited, and there has been some disagreement about the definition of residual water content. Many researchers use currently the residual water content only as a fitting parameter with no real physical significance (Vanapalli et al, 1998). Fredlund and Xing (1994) proposed the method to estimate the residual state and the air entry value with their proposed SWRC equation at the suction values between 0 and 10^6 kPa. Figure 2.7 shows an example of the comparison of three SWRC equations with experimental data for a

sandy soil (Lu and Likos, 2004), and Table 2.2 shows the values of fitting curve parameters in each equation corresponding to SWRC data for a sandy soil.

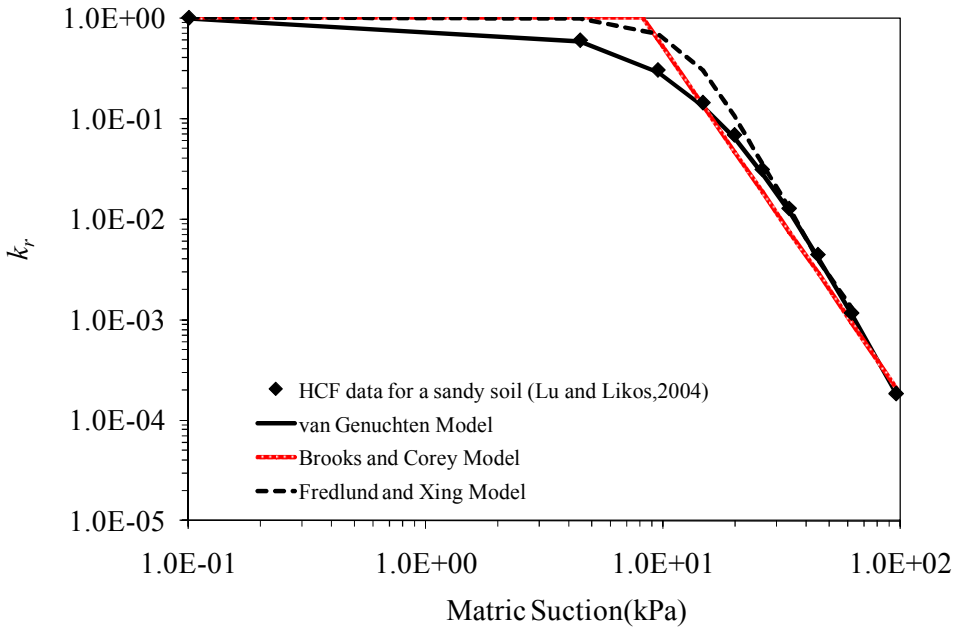

Figure 2.7. The comparison of three SWRC equations (SWRC data for a sandy soil from Lu and Likos, 2004)

Table 2.2. Parameter values in each model (SWRC data for a sandy soil from Lu and Likos, 2004)

Brooks and Corey model	*van Genuchten model*	*Fredlund and Xing model*
θ_s=0.5	θ_s=0.5	a=13
θ_r=0.1	θ_r=0.1	n=2.8
1/b=0.58	n=1.9738	m=0.5
ψ_b=8.2kPa	m=0.49338	θ_s=0.5
	α=0.052	

2.5 Hydraulic Conductivity Function (HCF) in Unsaturated Soils

Figure 2.8 presents a typical HCF curve. The HCF curves of sand, silt, and clay have different shapes due to different pore and grain size distributions, proportions of sand and clay fractions, clay mineralogy, compaction conditions, volume changes, stress state. In general, coarse grained soils have a higher hydraulic conductivity than fine grained soils when saturated.

However, the decrease in the hydraulic conductivity of unsaturated coarse grained soils is much faster than the decrease in fine grained soils after the air entry value. Fine grained soils can retain more water under higher suctions, thus there are more pathways available for water flow. The coarse grained soils quickly approach residual saturation, meaning there are few pathways available for water flow (McCartney, 2007). The HCF for unsaturated soils can be plotted as a function of suction or volumetric water content. Therefore, the HCF is related to the SWRC and hysteresis can be also observed in HCF, like the SWRC, as shown in figure 2.9.

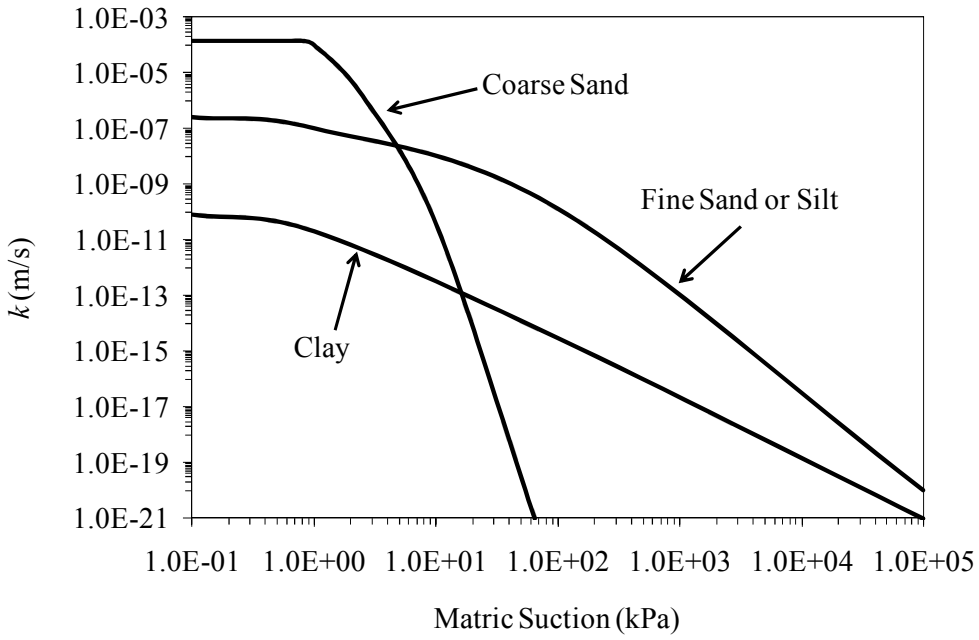

Figure 2.8. HCFs for different materials (McCartney, 2007)

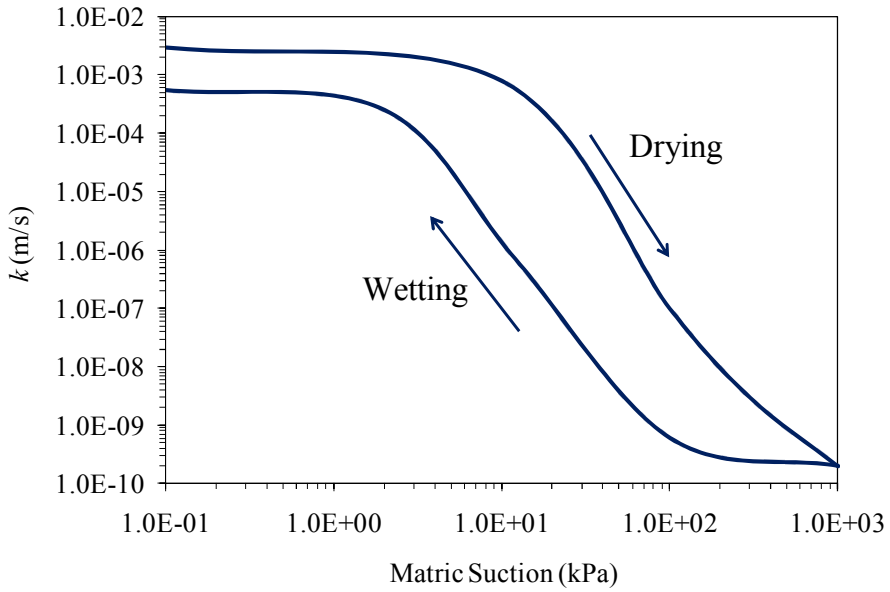

Figure 2.9. Hysteresis of the HCF (Lu and Likos, 2004)

Brooks and Corey (1964) and van Genuchten (1980) derived close form expressions for the HCF by substituting their proposed SWRC equations into statistical model proposed by Burdine (1953). Also, van Genuchten derived close form expression for the HCF based on Mualem theory (1976b). Fredlund and Xing (1994) have developed relative HCF model with their proposed their SWRC equation and the statistical pore size distribution model of Childs and Collis-George (1950). In the Brooks and Corey model, the HCF can be expressed in terms of suction, ψ or suction head, h and air entry pressure, ψ_e or air entry head, h_e. This prediction model for HCF also has a discontinuity at the air entry pressure value like the SWRC.

$$k = k_s \times \begin{cases} 1 & \psi < \psi_e \\ \left(\frac{\psi_e}{\psi}\right)^{2+b'/b} & \psi \geq \psi_e \end{cases} \tag{2.23}$$

where θ_r is the residual volumetric water content, θ_s is the saturated volumetric water content, ψ_e is the air entry pressure, $1/b$ is a pore size distribution index (which is inverse of the original Brooks and Corey parameter, λ), and b'=3 in Burdine theory or 2.5 in Mualem theory.

van Genuchten (1980) developed a HCF model using the same fitting parameters *α, m,* and *n* as the SWRC in 1980. The van Genucthen HCF model can be expressed by basis of both Burdine theory (1953) and Mualem theory (1976b). The HCF model based on Mualem theory in our research is only considered because the HCF model based on Burdine theory shows the lesser agreement with experimental data than the Mualem theory (van Genuchten 1980).

$$k = k_s \times \frac{\left[1-(\alpha\psi)^{n-1}\left[1+(\alpha\psi)^n\right]^{-m}\right]^2}{\left[1+(\alpha\psi)^n\right]^{0.5m}} \tag{2.24}$$

Finally, Fredlund and Xing proposed the HCF model in 1994.

$$k_r(\psi) = \frac{\int_{\ln(\psi_{aev})}^{b} \frac{\theta(e^y)-\theta(\psi)}{e^y}\theta'(e^y)dy}{\int_{\ln(\psi_{aev})}^{b} \frac{\theta(e^y)-\theta_s}{e^y}\theta'(e^y)dy} \tag{2.25}$$

where y is a dummy variable of integration representing $\ln(\psi)$, b is $\ln(10^6)$, ψ_{aev} is the air-entry pressure, and θ' is the derivative of the Fredlund and Xing's soil-water characteristic function which respect to ψ.

Figure 2.10 shows the example of comparison with three prediction models, and fitting parameter values for each model are the same as the table 2.2 in chapter 2.4. There is little discrepancy between the experimental data and three models in case of the SWRC, whereas the van Genuchten model shows the best fit with experimental data in case of the relative hydraulic conductivity. However, it could not be guaranteed that the van Genuchten model would always predict well other experimental data.

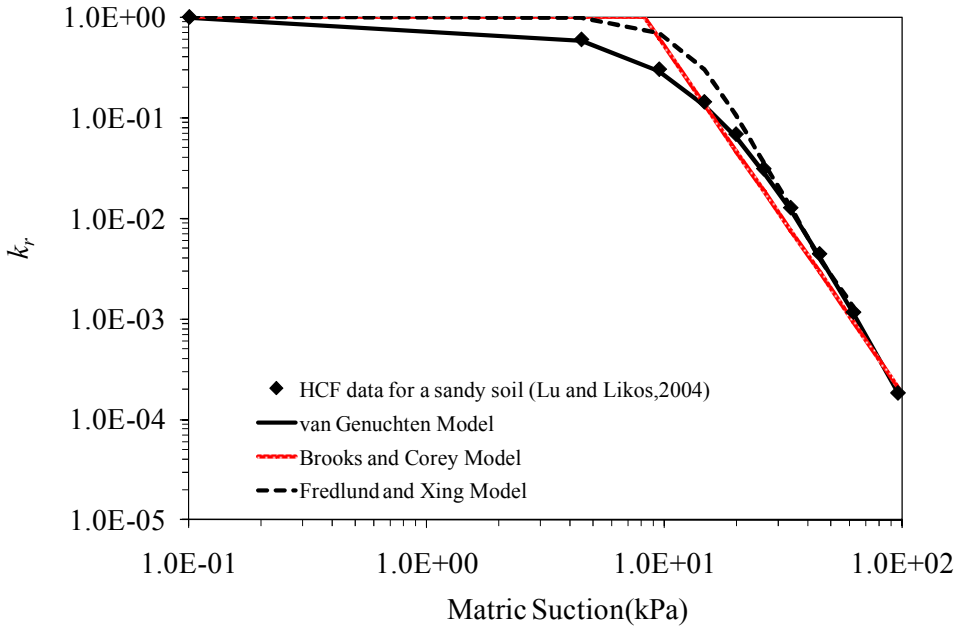

Figure 2.10. The comparison of three prediction models for the HCF (HCF data for a sandy soil from Lu and Likos, 2004)

2.6 Cavitation

Caviation is easily explained by a thermodynamic phase diagram, as shown in figure 2.11. Cavitation occurs when the liquid state translates to the vapor state across the vaporization curve along a path of decreasing pressure. If the liquid state translates to the vapor state along a path of increasing temperature, it is called boiling. In measurement system in unsaturated soils, cavitation occurs when negative pore water pressure approaches the gauge cavitation pressure, since the liquid phase pressure exchanges the liquid vapor pressure. If cavitation occurs in measurement systems, the continuity in the liquid phase between measurement system and the soil pore water is broken, and further suction cannot be measured under cavitation. Therefore, the limit of the measurement system depends on cavitation pressure when the negative pore water pressure and atmospheric pressure are used in measurement system. Boulder area in Colorado is located above mean sea level of 1500 m, lower limit (cavitation pressure) is about 80 kPa, since lower limit is about 95 kPa at mean sea level of 0 m and the lower limit decreases as

elevation above mean sea level increases. Figure 2.12 shows the gauge cavitation pressure and atmospheric pressure in terms of the elevation above mean sea level. In order to avoid cavitation in measurement system, the axis translation technique (Hilf, 1956) is commonly used. Axis translation technique uses the pore water pressure and pore air pressure instead of the negative pore water pressure and atmospheric pressure. By applying high back pressure, the range of the measuring suction increases, and the measurement system can avoid the cavitation up to back pressure value.

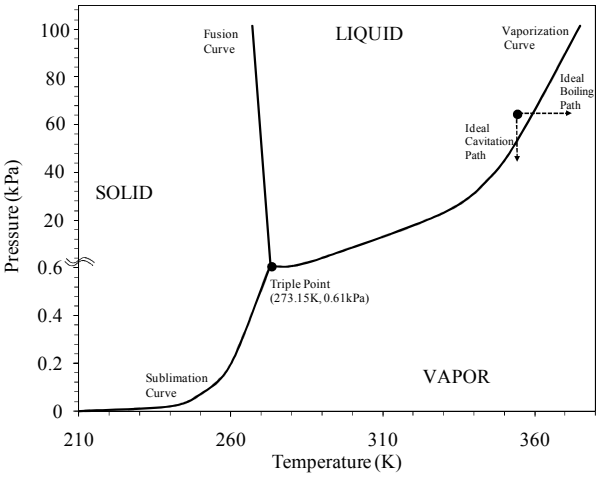

Figure 2.11. Thermodynamic diagram for pure water (Lu and Likos, 2004)

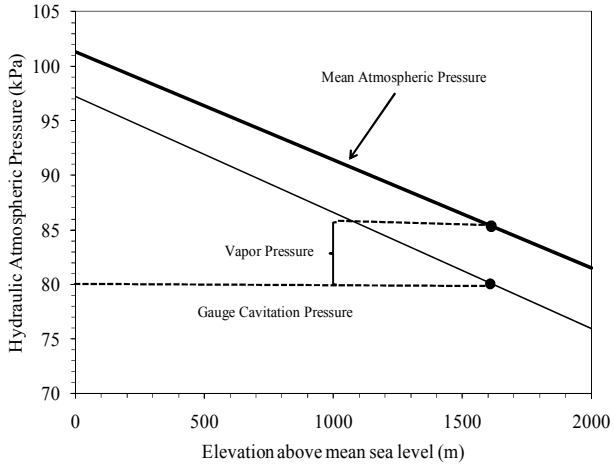

Figure 2.12. Gauge cavitation pressure and mean atmospheric pressure (Lu and Likos, 2004)

2.7 Numerical Solution of the Richards' Equation

A finite difference discretization technique is used to solve the governing equation. Generally, volumetric water content based form cannot describe flow in the saturated zone, and flow in layered soils is also not easily simulated, and head based form has a problem to run into mass conservation errors (Huang et al, 1996). For these reasons, the mixed form of the governing equation is used for numerical simulation. Equation (2.26) shows the mixed form formulation of governing equation. By using an implicit Euler backward approximation of the derivative, first, second, and third terms of left hand side in Equation (2.26) become Equations (2.27), (2.28), and (2.29), respectively. Therefore, Equation (2.26) in discretized form becomes equation (2.30).

$$\frac{\partial \theta}{\partial t} - \frac{\partial k(h)}{\partial z} - \frac{\partial}{\partial z}\left[k(h)\frac{\partial h}{\partial z}\right] = 0 \tag{2.26}$$

$$\frac{\partial \theta}{\partial t}(z,t) = \frac{\theta_j^{n+1} - \theta_j^n}{\Delta t} = \frac{\theta(z,t+\Delta t) - \theta(z,t)}{\Delta t} \tag{2.27}$$

$$\frac{\partial k(h)}{\partial z}(z,t) = \frac{k_{k+1/2}^{n+1} - k_{k-1/2}^{n+1}}{\Delta z} \tag{2.28}$$

where $k_{k+1/2}^{n} = \dfrac{2}{1/k(h_j^n) + 1/k(h_{j+1}^n)}$

$$\frac{\partial}{\partial z}\left[k(h)\frac{\partial h}{\partial z}\right] = \frac{1}{\Delta z}\left[k_{j+1/2}^{n+1}\frac{h_{j+1}^{n+1} - h_j^{n+1}}{\Delta z} - k_{j-1/2}^{n+1}\frac{h_j^{n+1} - h_{j-1}^{n+1}}{\Delta z}\right] \tag{2.29}$$

$$\left[\frac{\theta_j^{n+1} - \theta_j^n}{\Delta t}\right] - \left[\frac{k_{k+1/2}^{n+1} - k_{k-1/2}^{n+1}}{\Delta z}\right] - \frac{1}{\Delta z}\left[k_{j+1/2}^{n+1}\frac{h_{j+1}^{n+1} - h_j^{n+1}}{\Delta z} - k_{j-1/2}^{n+1}\frac{h_j^{n+1} - h_{j-1}^{n+1}}{\Delta z}\right] = 0 \tag{2.30}$$

The Picard iteration procedure (Celia et al., 1990) is used to use an iteration to advance Equation (2.30) from one time level to the next, as shown in Equation (2.31). In each time step, iterative scheme starts with initial estimates $h_j^{n+1,0}$ and increments $\delta h_j^{n+1,m+1}$ is determined and updated during the iteration loop. And iterative scheme ends when increment is sufficiently small. Equation (2.30) becomes Equation (2.32) by using the Picard iteration procedure.

$$h_{j+1}^{n+1,m+1} = h_j^{n+1,m} + \delta h_j^{n+1,m+1} \tag{2.31}$$

$$\left[\frac{\theta_j^{n+1,m+1} - \theta_j^n}{\Delta t}\right] - \left[\frac{k_{k+1/2}^{n+1,m} - k_{k-1/2}^{n+1,m}}{\Delta z}\right] - \frac{1}{\Delta z}\left[k_{j+1/2}^{n+1,m}\frac{h_{j+1}^{n+1,m+1} - h_j^{n+1,m+1}}{\Delta z} - k_{j-1/2}^{n+1,m}\frac{h_j^{n+1,m+1} - h_{j-1}^{n+1,m+1}}{\Delta z}\right] = 0 \tag{2.32}$$

Substituting Equation (2.33) (Taylor series expansion of the derivatives) to Equation (2.32), the first and third terms in left hand side of Equation (2.32) becomes Equation (2.34) and (2.35). Second term in left hand side of Equation (2.32) gives the right hand side of Equation (2.32). Terms including δh_j move to left heand side, and rest of them move to right hand side. Therefore, the standard finite difference approximation in space becomes Equations (2.36) and (2.37). R_j^{n+1} is an error measure for the finite difference spatial approximation coupled with the Picard iteration.

$$\theta_j^{n+1,m+1} = \theta_j^{n+1,m} + \left.\frac{d\theta}{dh}\right|_j^{n+1,m} \delta h_j^{n+1,m+1} \tag{2.33}$$

$$\frac{C_j^{n+1,m}}{\Delta t}\delta h_j^{n+1,m+1} + \left[\frac{\theta_j^{n+1,m} - \theta_j^n}{\Delta t}\right] \tag{2.34}$$

$$-\frac{k_{j+1/2}^{n+1,m}}{\Delta z^2}\left[h_{j+1}^{n+1,m}+\delta h_{j+1}^{n+1,m+1}\right]+\frac{1}{\Delta z^2}\left[k_{j+1/2}^{n+1,m}+k_{j-1/2}^{n+1,m}\right]\left[\psi_j^{n+1,m}+\delta h_j^{n+1,m+1}\right]-\frac{k_{j-1/2}^{n+1,m}}{\Delta z^2}\left[h_{j-1}^{n+1,m}+\delta h_{j-1}^{n+1,m+1}\right] \tag{2.35}$$

$$LHS=-\frac{k_{j+1/2}^{n+1,m}}{\Delta z^2}\left[\delta h_{j+1}^{n+1,m+1}\right]+\left[\frac{k_{j+1/2}^{n+1,m}+k_{j-1/2}^{n+1,m}}{\Delta z^2}+\frac{C_j^{n+1,m}}{\Delta t}\right]\left[\delta h_j^{n+1,m+1}\right]-\frac{k_{j-1/2}^{n+1,m}}{\Delta z^2}\left[\delta h_{j-1}^{n+1,m+1}\right] \tag{2.36}$$

$$RHS=-\left[\frac{\theta_j^{n+1,m}-\theta_j^n}{\Delta t}\right]+\left[\frac{k_{j+1/2}^{n+1,m}-k_{j-1/2}^{n+1,m}}{\Delta z}\right]+\frac{k_{j+1/2}^{n+1,m}}{\Delta z^2}\left[h_{j+1}^{n+1,m}\right]-\frac{1}{\Delta z^2}\left[k_{j+1/2}^{n+1,m}+k_{j-1/2}^{n+1,m}\right]\left[h_j^{n+1,m}\right]$$
$$+\frac{k_{j-1/2}^{n+1,m}}{\Delta z^2}\left[h_{j-1}^{n+1,m}\right]=R_j^{n+1} \tag{2.37}$$

The governing equation is solved using a Picard iteration technique with Thomas algorithm. In each time step, iteration scheme starts with initial estimates $h_j^{n+1,0}$. Every k on left hand side and θ and h on right hand side can be calculated using known $h_j^{n+1,m}$ at all nodes . Left hand side coefficient, k is stored in a, b, and c, vectors tri-diagonal matrix, $R_j^{n+1,m}$ is calculated and check convergence. [A] $\delta h_j^{n+1,m+1}=R^{n+1,m}$ is solved to get all $\delta h_j^{n+1,m+1}$. From Equation (2.31), $h_j^{n+1,m+1}$ is obtained, and move to next iteration after updating current estimates. If convergence, time step moves to next. In order to validate our code, the simple infiltration is simulated with the hydrostatic initial conditions and same boundary conditions during ten days. Figure 2.13 presents the material properties, SWRC and HCF used in the numerical simulation, and Figure 2.14 shows the comparison of our result with the commercial programs, UNSAT-H and SEEP/W.

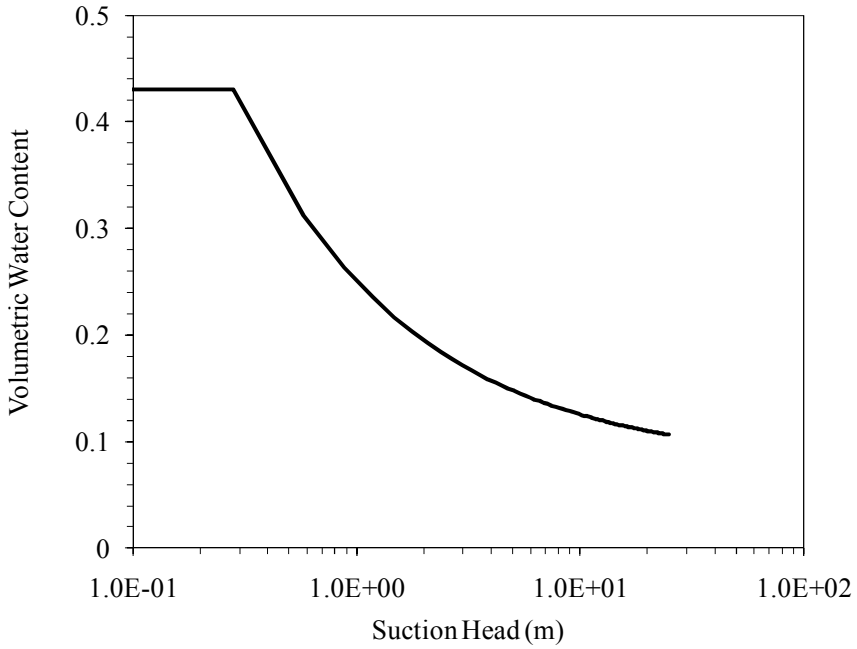

(a)

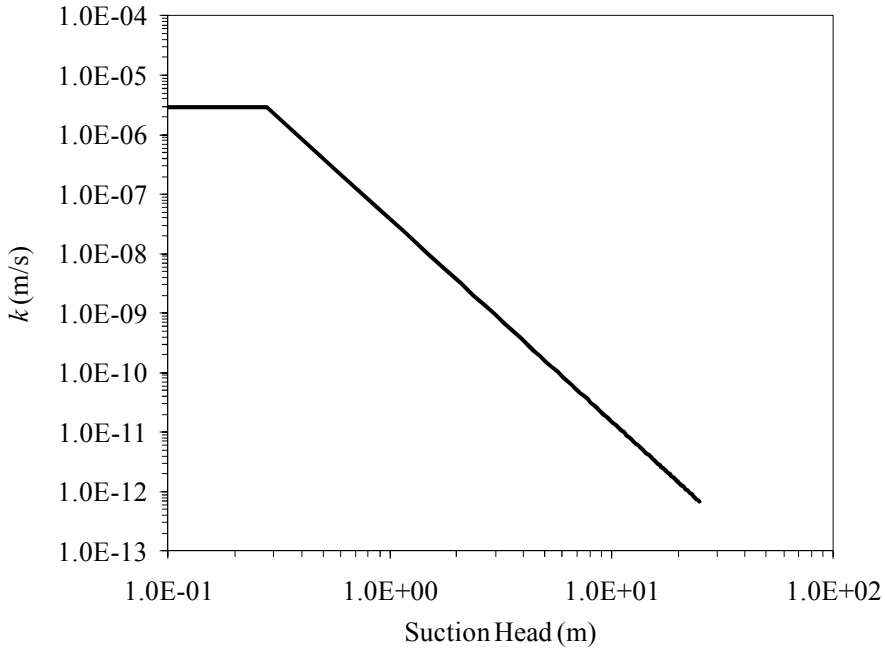

(b)

Figure 2.13. SWRC and HCF for example of numerical simulation: (a) SWRC; (b) HCF

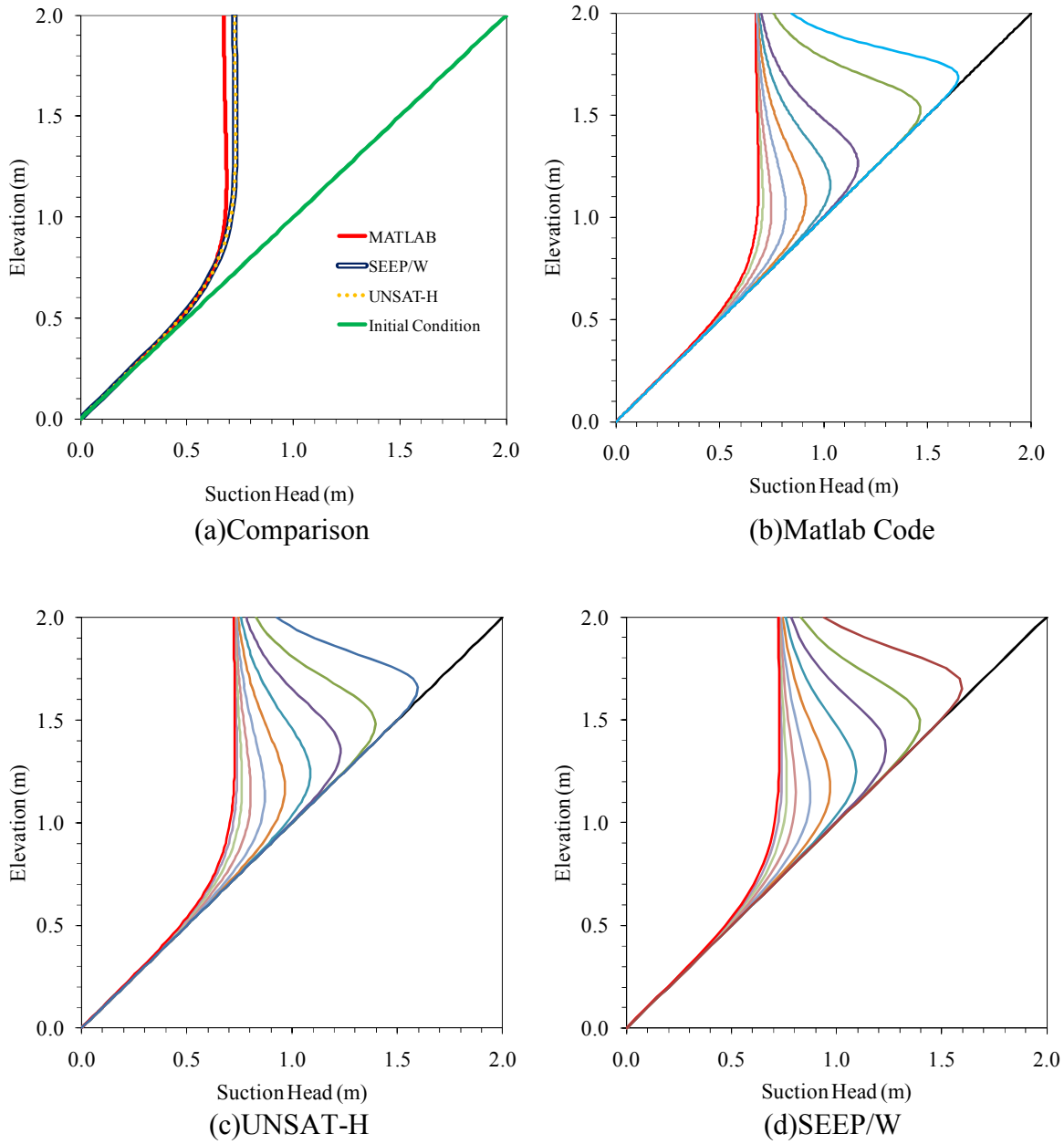

Figure 2.14. Comparison of numerical simulation results

CHAPTER 3

OVERVIEW OF MEASUREMENT TECHNIQUES

For the past 100 years, many measurement techniques for the SWRC and the HCF have been developed (Briggs and McLane, 1907; Gardner; 1937; Spanner, 1951; Hilf,1956; Fawcett and Collis-Geroge, 1967; Hamilton et al., 1981; Daniel, 1983; Meerdink et al, 1996; Khanzode, 2002; Parks, 2010). The measurement techniques for the SWRC can be classified into two groups as matric suction measurement or total suction measurement. The matric suction measurement is generally used for low suction range, whereas the total suction measurement is used for high suction range. There are two methods to measure the HCF; one is the steady state measurement of flux or hydraulic gradient for known flow field geometry corresponding to a specific value of suction or water content. For steady state measurement technique, the flux, gradient, and water content of soil water system do not vary with time. The second measurement method is a transient measurement technique solving the governing equation for one dimensional flow systems under controlled boundary conditions from measurements of flux or moisture content profiles at known location and times. For transient measurement technique, the flux, gradient, or water content of the soil water system are not constant with time. In this chapter, fundamental measurement techniques for the SWRC and the HCF are reviewed.

3.1 Measurement Techniques for SWRC

One of the most commonly used suction measurement technique is a pressure plate using the axis translation technique controlling the difference between positive pore air pressure and positive pore water pressure instead of atmospheric air pressure and negative pore water pressure and measuring the corresponding water content of soil in equilibrium with the applied matric suction. The desired suction range depends on the air entry value of the High Air Entry (HAE) ceramic plate. Figure 3.1 shows the schematic drawing of the pressure plate axis translation apparatus. The soil specimen is placed on the ceramic plate in the pressure vessel. The ceramic plate should have much higher air entry value than soil and the maximum air pressure applied to the pressure vessel. After that, air pressure is applied to pressure vessel while keeping the water pressure on the saturated ceramic plate constant, and this will cause air to enter the pores and water to drain from soil specimen to base of ceramic plate. The water content of the soil specimen can be obtained from the volume of outflow of water measured using a constant head burette until outflow of water ceases. The end of outflow of water means that the system is in equilibrium under the imposed matric suction. This is one point on the SWRC. This procedure is repeated several times with applying different air pressure levels into the pressure vessel until the desired suction value is reached. Figure 3.2 shows another common measurement technique, hanging column test for the SRWC. This technique is generally appropriate for the low suction about 10 kPa. Suction is imposed to the soil specimen throughout maintaining the water level in a manometer tube below the high air entry porous plate. During testing, outflow can be measured with time using the constant head Mariotte burette until outflow ceases. From the volume of the outflow, the volumetric water content can be obtained inversely at the induced suction. After

reaching the equilibrium, other volumetric water content or degree of saturation of the soil specimen can be obtained with different suction values using the same procedure.

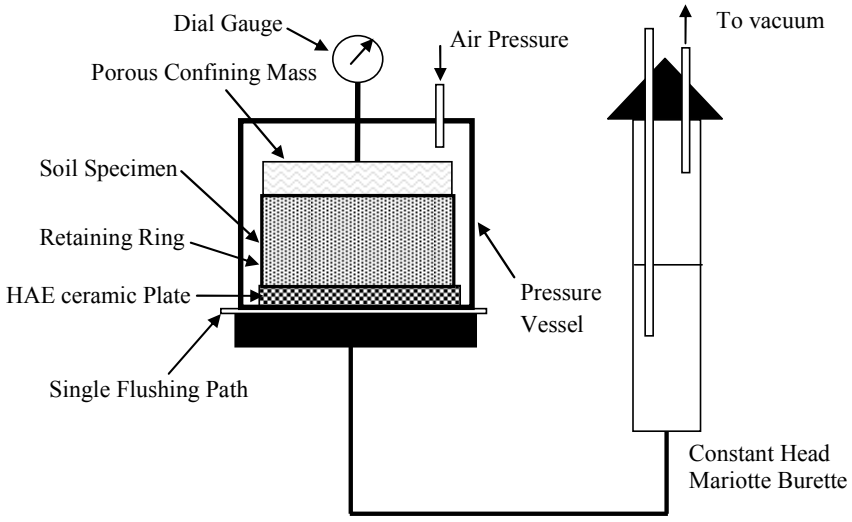

Figure 3.1. Pressure plate apparatus

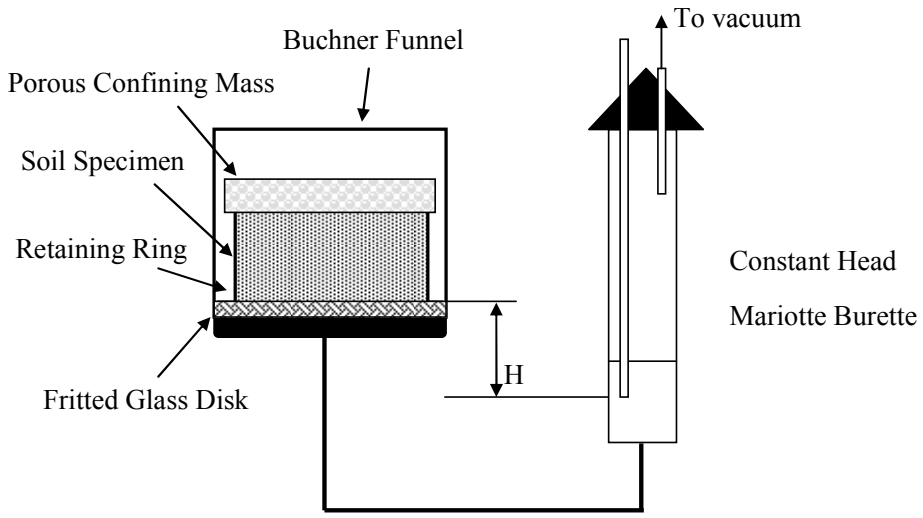

Figure 3.2. Hanging column apparatus

Centrifuge technique was developed in early 1900's by Briggs and McLane (1907) and has been improved by several researchers. It takes a lot of time to obtain the SWRC by using

conventional suction measurement method such as a pressure plate or a tempe cell, but the centrifuge technique shortens the time to obtain the SWRC. Equation (3.1) is a nonlinear relationship between soil suction and centrifugal radius suggested by Gardner (1937), and Figure 3.3 shows the principle of the centrifuge technique for the measurement of soil suction. The saturated soil specimen is placed on a HAE ceramic plate as the outflow boundary. Different soil suction values can be measured by draining a saturated soil specimen through varying either r_1 using the height of ceramic cylinder or test speed (i.e., ω), as shown in Figure 3.4

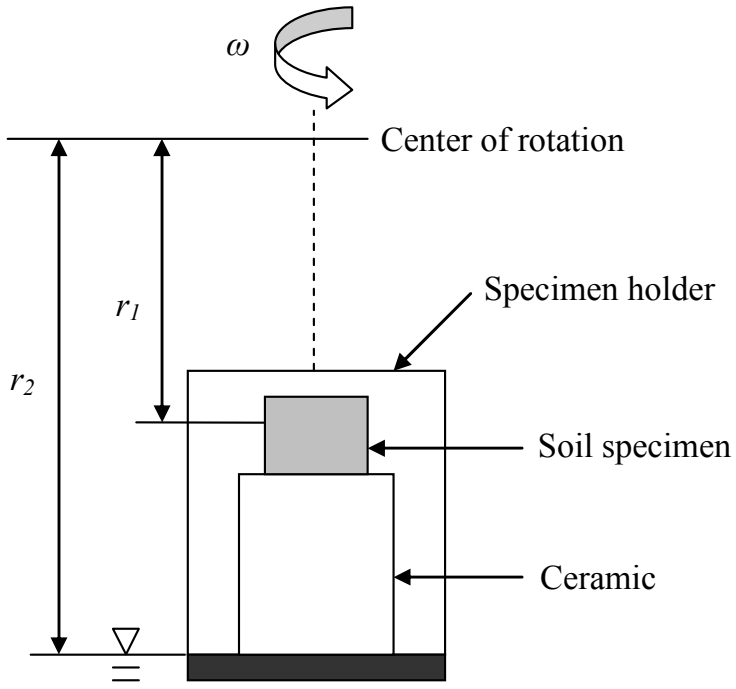

Figure 3.3. Soil suction measurement principle of the centrifuge (Khanzode et al, 2002)

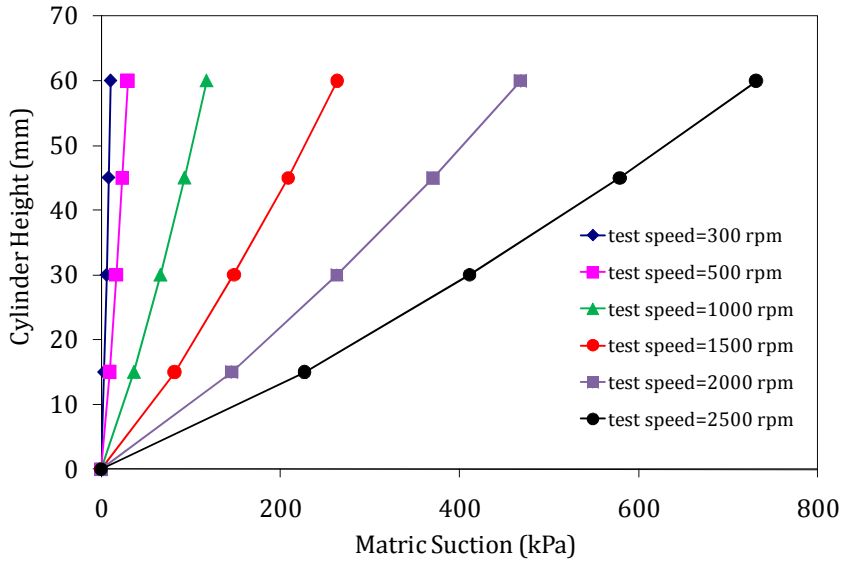

Figure 3.4. Soil suction values associated with different test speeds, ω and different ceramic cylinders (Khanzode et al, 2002)

$$\psi = \frac{\rho\omega^2}{2g}\left(r_1^2 - r_2^2\right) \tag{3.1}$$

where ψ=the suction in the soil specimen, ρ=the density of pore fluid, ω= the angular velocity, r_1=the radial distance to the midpoint of the soil specimen, r_2= the radial distance to the free water surface, and g=the acceleration due to gravity.

Total suction measurement techniques are usually used in high suction ranges. As mentioned in Equation (2.7) and Figure 2.3, the total suction is affected by the relative humidity. There are two representative total suction measurement techniques to measure the relative humidity. One is direct measurement (e.g., thermocouple psychrometer), and another is in-direct measurement (e.g., filter paper method). Thermocouple psychrometer measures the relative humidity on the basis of the temperature difference between a nonevaporation surface, or reference junction, and an evaporation surface, or measurement junction (Spanner, 1951). In filter paper method, the bottom filter paper at the bottom of soil sample contacts directly with soil sample (matric suction measurement), while the perforated disk is placed between the top of

soil sample and the filter paper in order to non-contact between soil sample and top filter paper (i.e., total suction measurement). Water flow occurs at the bottom portion, and the water vapor flow occurs at the top portion. After reaching equilibrium condition, the water content of the filter paper is measured, and the suction is obtained from the calibration curve.

3.2 Measurement Techniques for HCF

The instantaneous profile method (Hamilton et al., 1981; Daniel, 1983; Meerdink et al., 1996) is one of the transient measurement techniques. The instantaneous profile method uses the vertical or horizontal soil column which has several measurement ports for suction head and water content at 10% interval of soil column in general. In each measurement port, the suction head can be measured by using tensiometers or thermocouple psychrometers, and the volumetric water content corresponding to the suction head can be inferred from the SWRC. Figure 3.5 shows the typical horizontal soil column. At boundary, $x=0$, the flow pump is installed, and the end of soil column at boundary, $x=L$, is open to the atmosphere. In the case of horizontal soil column, the gravity fluid flow is negligible.

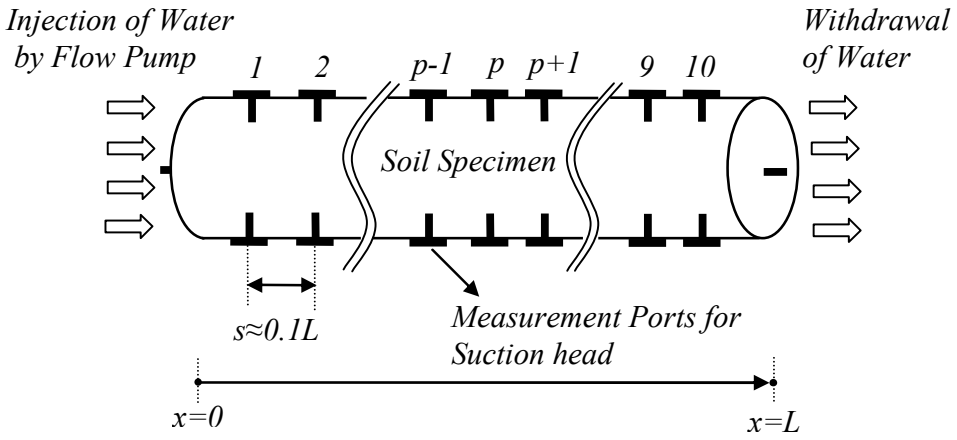

Figure 3.5. Schematic drawing of the IPM

First, water is injected by flow pump at boundary, $x=0$ causing time-dependent changes of suction head along the soil column. From the measurements of suction head, the hydraulic gradient, i, can be obtained by Equation (3.2) from one point to another.

$$i(x_p, t_q) = \frac{h_p - h_{p-1}}{l_{from\ x=p-1\ to\ x=p}} \tag{3.2}$$

Also, the volume of water passing from point, x_p to L at time interval, Δt from $t=q$ to $t=r$, can be obtained from the volumetric water content inferred from the SWRC, and cross sectional area of the soil column.

$$\Delta V_w = A\int_{x_p}^{L}\theta(x,t_r)dx - A\int_{x_p}^{L}\theta(x,t_q)dx \tag{3.3}$$

where A is the cross-sectional area of the soil column.

Therefore, the hydraulic conductivity corresponding to suction head value can be obtained by using Darcy's law and Equation (3.4).

$$v = \frac{length}{time} = \frac{\Delta V_w}{A}\frac{1}{\Delta t} = k \times i$$
$$k = \frac{\Delta V_w}{A \times \Delta t \times i} \tag{3.4}$$

However, the instantaneous profile method has several disadvantages such as great amount time required to complete test and inherent inaccuracy for measurement of the HCF.

Parks (2010) developed the permeameter using a 15 g-ton centrifuge at the University of Colorado at Boulder which has a 1.4 meter arm. Figure 3.8 shows the schematic drawing of CU centrifuge permeameter, which is designed to investigate the hydraulic properties of unsaturated soils with a sample size of 230 mm in diameter and 305 mm in height. The permeameter can control the infiltration and drainage from the soil sample during centrifugation. At the top of the

soil sample, the infiltration rate is applied using a spray nozzle until the steady state condition, and then the infiltration is stopped. Then, drainage is allowed at the bottom of the soil sample until equilibrium.

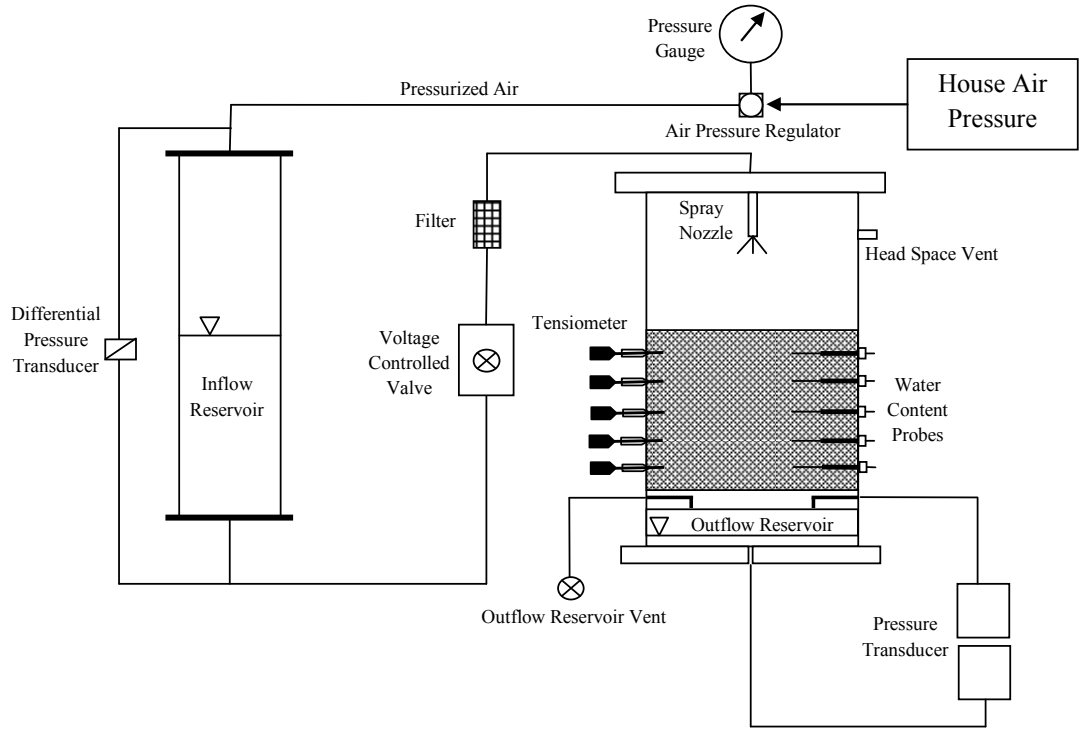

Figure 3.6. Schematic drawing of CU centrifuge permeameter (Parks, 2010)

The SWRC can be obtained from measurement of suction and water content simultaneously using tensiometers and dielectric sensors by controlling flow rate through a single specimen in a single test. For transient conditions, the HCF can be obtained using inverse problem solution approach of Equation (3.5). For steady state conditions, the HCF can be obtained using the Equation (3.6).

$$\frac{\partial\theta}{\partial\psi}\frac{\partial\psi}{\partial t}=\frac{1}{\rho g}\left[K\frac{\partial^2\psi}{\partial z^2}-\frac{\partial K}{\partial\psi}\left\{\left(\frac{\partial\psi}{\partial z}\right)^2-\rho\omega^2(r_0-z)\frac{\partial\psi}{\partial z}\right\}-K\rho\omega^2\right] \tag{3.5}$$

$$K(\psi) = \frac{vg}{\left[\frac{1}{\rho}\frac{d\psi}{dz} - \omega^2\left(r_0 - z\right)\right]} \tag{3.6}$$

where v=the discharge velocity applied to the specimen, equal to the flow rate divided by the specimen area, ψ=the suction in the soil specimen, ρ=the density of pore fluid, ω= the angular velocity, r_0=the radius from the center of rotation to the base of the specimen, z=(r- r_0) where r is the radius from the center of the specimen, and g=the acceleration due to gravity.

CHAPTER 4

EQUIPMENTS AND MATERIAL PROPERTIES

The flow pump system (FPS) was developed at the University of Colorado at Boulder, and this system has been improved over the last 20 years (Znidarcic et al, 1991). The FPS is designed based on the principle of the conventional axis-translation technique, and the conventional triaxial equipment. Figure 4.1 shows the schematic drawing of the FPS. This technique utilizes a flow pump for precise control of flow rates and precision differential transducer for measuring induced head differences (Znidarcic et al, 1991). The cylindrical soil sample is encased within a latex membrane inside a triaxial cell. One back pressure chamber is connected to the bottom of the soil sample, and another is connected to the top. The back pressure chamber connected to top can apply water pressure or air pressure to the top portion of the soil specimen. The confining pressure is applied by adjusting the chamber pressure. The flow pump is connected to the bottom of the soil specimen, and the water reservoir. During testing, the refill valve on the flow pump control panel is closed, and the flow pump operates for inflow to or outflow from the soil specimen. The differential transducer measures the pressure difference between top and bottom of the soil specimen induced by the flow pump. A LVDT measures the axial displacement of the soil sample during testing.

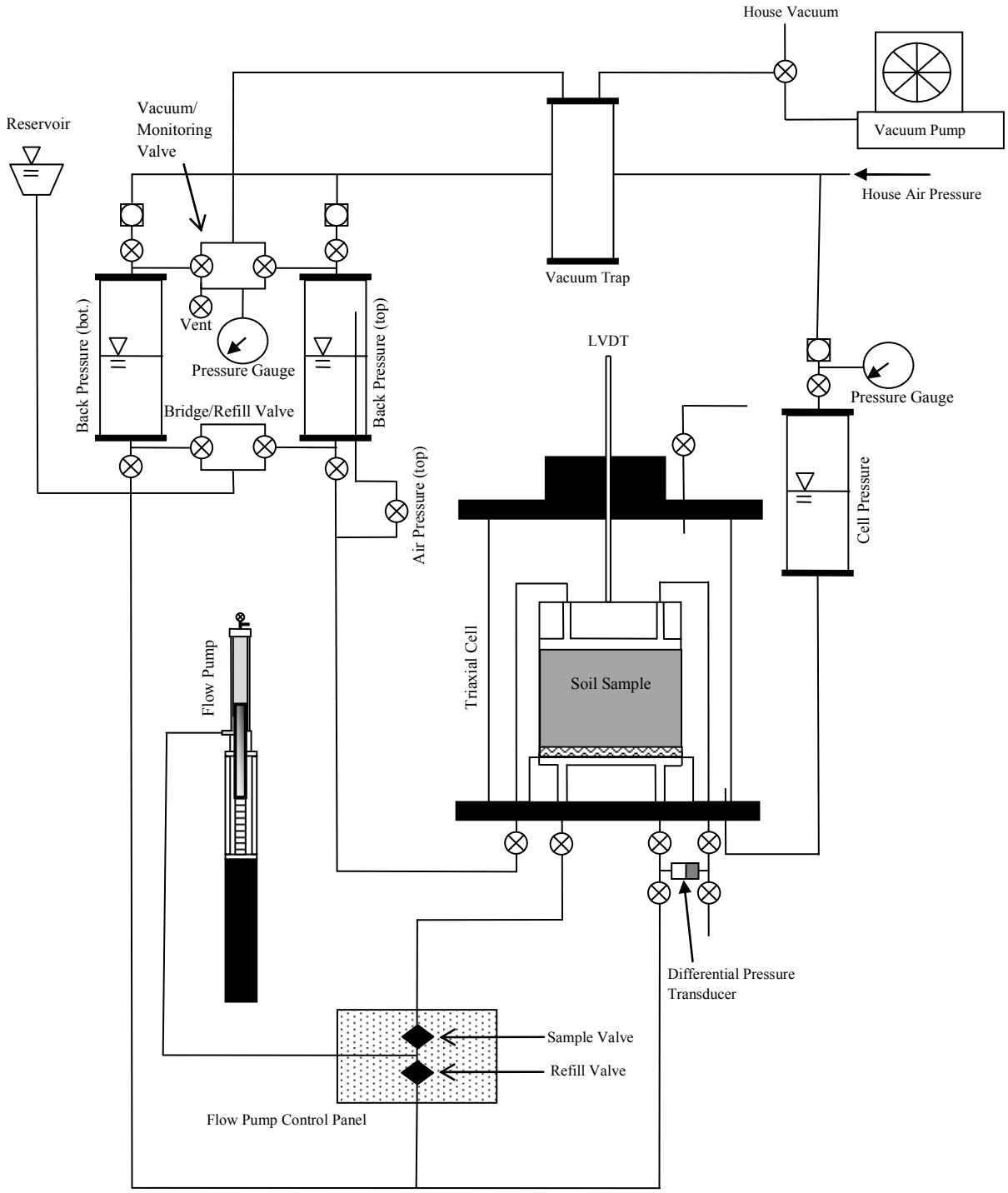

Figure 4.1. Schematic drawing of the FPS

The FPS is also used for the infiltration test in unsaturated soils. For infiltration test, the FPS changes in part from Figure 4.1 to Figure 4.2. Figure 4.2 shows the schematic drawing of the FPS for infiltration test in unsaturated soils. During the infiltration test, differential transducer measured the pressure difference between the atmospheric air pressure and negative water pressure at the bottom of the soil sample induced by flow pump instead of pore air pressure and pore water pressure. In Boulder area, the limit of the measurement for the negative water pressure is about 80 kPa. Right back pressure chamber connected to the top of the soil specimen is removed in Figure 4.1, and new tube is connected from the top of the soil sample to the scale to measure the outflow volume induced by flow pump through the soil specimen. From this tube, the volume of outflow from top of the soil specimen can be measured, and this can be compared with volume of water calculated from flow pump position. The other tube connected to the transducer at the other port at the top platen in Figure 4.1 is also removed, and the valve at that port is closed during the infiltration test in order to flow directly from the soil specimen to the scale. Left back pressure chamber plays only a role as a reservoir for resetting the flow pump.

Before the infiltration test with unsaturated soil samples, several initial suction tests are conducted. Two kinds of the tests are used for measurement of the initial suction. Figure 4.3 shows the basic apparatus for initial suction test, and tensiometer test is also conducted to check the validity of the initial suction test. Several soil samples, which have different initial suction values and water contents, are tested to obtain the SWRC.

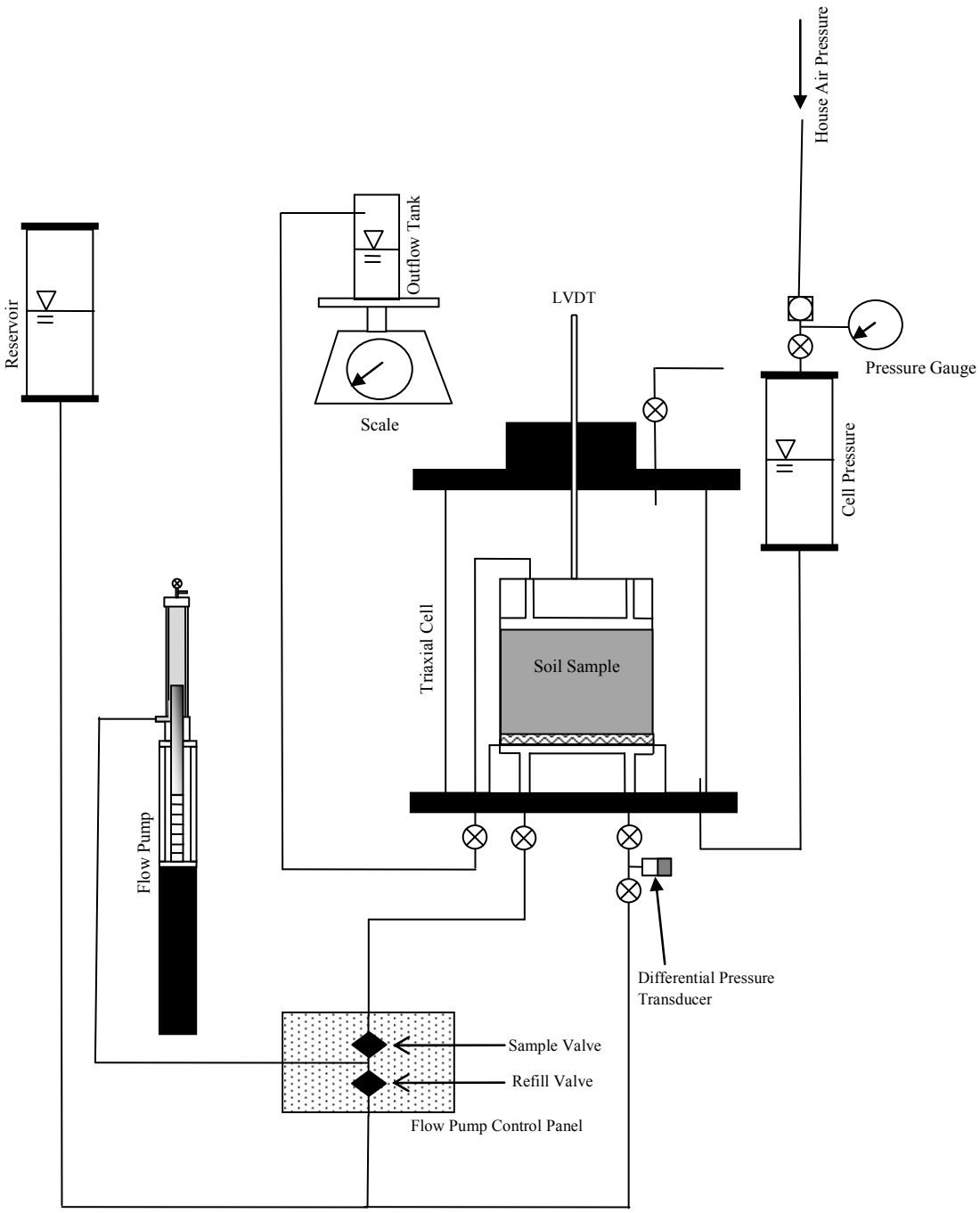

Figure 4.2. Schematic drawing of the FPS for the infiltration test

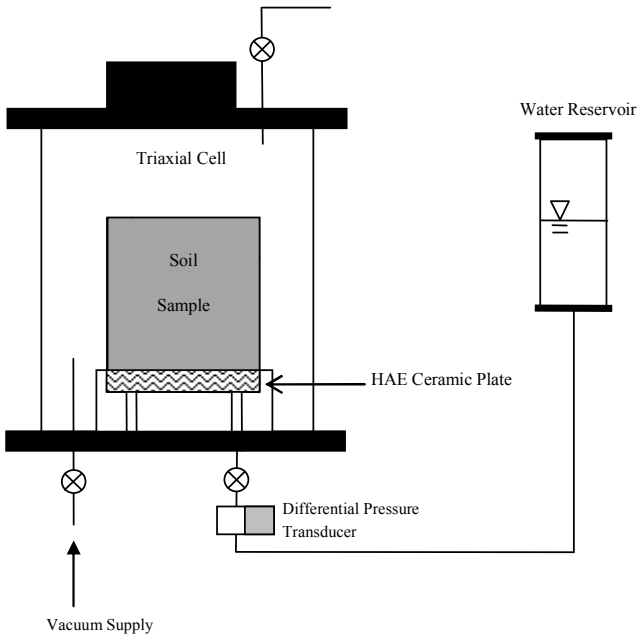

Figure 4.3. Basic Apparatus for the Initial Suction Test

4.1 Flow Pump System (FPS)

4.1.1. Flow Pump

The flow pump gives a continuous steady water flow for either wetting or drying cycles through operating the pump up or down direction and controlling the flow pump speed precisely. Operating flow pump in the infusion mode follows the wetting cycle, whereas operating it in the withdrawal mode follows the drying cycle. If the flow pump reaches the target position (i.e., top or bottom position of the flow pump), the flow pump automatically is reset for several seconds with high pump speed and continuously operates. The flow pump is connected to two lines on the flow pump control panel; one is connected to the water reservoir (left back pressure chamber in Figure 4.1) and another is connected to the bottom of the soil specimen for control of withdrawal and infusion of water into the soil specimen. Opening and closing of the two valves on the flow pump control panel can be controlled by the computer which is also used for the data

acquisition. The flow pump can operate precisely from 1E-05 to 5E+00 mm/s, since Darcy's velocity is defined as multiplying pump speed by the ratio of the piston area to sample area. The flow pump permits to push water into the soil sample or pull out water at the bottom of the soil sample up to the volume of water, 240 cm^3, since the piston area is 7.92 cm^2 and the height is 30 cm.

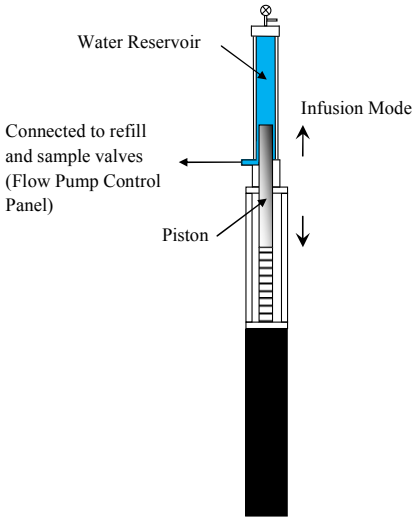

Figure 4.4. Schematic drawing of the flow pump

4.1.2. Differential Transducer

A differential transducer, manufactured by Validyne Engineering Corporation, is connected to the bottom of the soil specimen and to the back pressure chamber in order to measure the pressure difference between the reference pressure at the top of the soil specimen and the induced water pressure generated by the flow pump operation at the bottom of the soil specimen.

In the hydraulic conductivity test under saturated conditions, the transducer measures difference of pore water pressures between the bottom and top portions, whereas the transducer measures the difference between pore air pressure at the top of the soil specimen controlled by

the back pressure and the pore water pressure at the bottom of the soil specimen induced by the flow pump under unsaturated conditions.

The measured pressure value is sent to a data acquisition system which collects and displays the data during the test. The calibration coefficients of the transducer #38, #42, and #50 membranes are 11.11kPa/volt, 17.87kPa/volt, and 120.44kPa/volt, respectively.

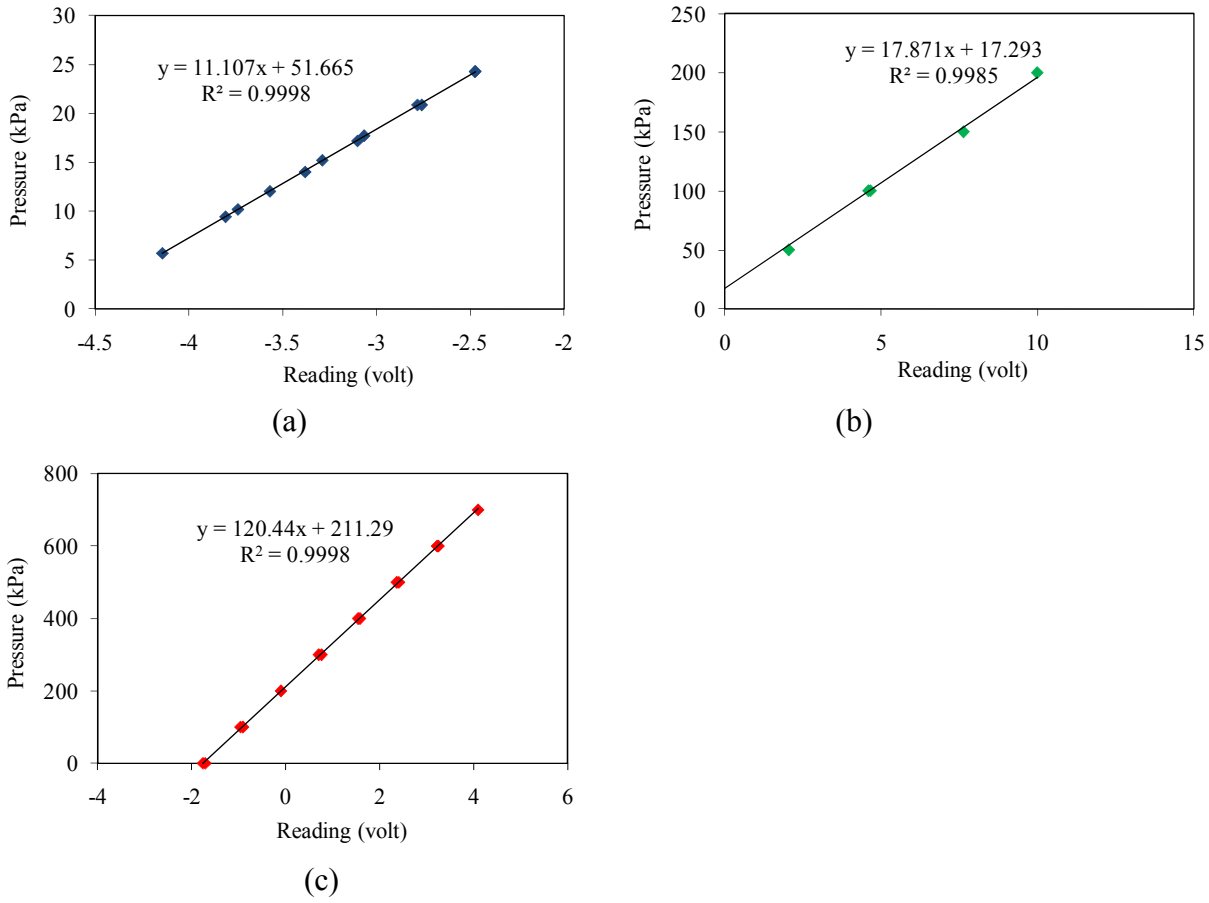

Figure 4.5. Calibrations of the transducers : (a) #38 membrane; (b) #42 membrane; (c) #50 membrane

4.1.3. High Air Entry Ceramic Plate and Filter Paper

The surface tension at the air-water interface in the pores of the HAE ceramic plate or the filter paper acts as a "membrane" to separate the air and water pressure without having soil present. The HAE ceramic plate or fine filter paper is installed between the soil specimen and the bottom platen, and the saturated pores of the HAE ceramic plate or the filter paper provide a

hydraulic connection between the soil pore water and the water reservoir below the filter paper. The effective pore size of the filter paper, or HAE ceramic plate controls the maximum difference between the air pressure and water pressure that can be sustainable in the test. As the radius of the pore becomes smaller, the air-entry pressure becomes larger. Two fine filter papers are polyethersulfone membranes manufactured by GE® water and process technologies, and the pore sizes of the filter are 0.8 and 0.22 micron, respectively.

Table 4.1 shows the head loss of HAE ceramic plates and fine filter papers induced by flow pump. In case of HAE ceramic plates, higher head loss is induced by flow pump than fine filter papers. Therefore, the head loss corresponding to the flow pump speed should be considered during the measurement of hydraulic conductivity and suction when HAE ceramic plate is used for test. However, the head loss of fine filter papers induced by flow pump is ignored because head loss corresponding to flow pump speed during test is very small. Figure 4.6 and 4.7 show the fine filter paper and HAE ceramic plate. The air entry values of 0.5 bar, 1 bar, and 3 bar HAE ceramic plates are generally 55 kPa, 170 kPa, and 400 kPa, respectively. The air entry values of 0.8 micron filter and 0.22 micron filter are about 40 kPa and 300 kPa, respectively.

Table 4.1. Comparison between fine filter paper and 1bar HAE

Pump Speed (m/s)	Flow Rate (m/s)	0.5 Bar Plate	1 Bar Plate	3 Bar Plate	0.8 Micron Filter	0.22 Micron Filter
1.00E-06	2.21E-07		2.0371	9.6792		
5.00E-06	1.11E-06	0.2196	11.7963	54.5877	0.0087	0.0218
1.00E-05	2.21E-06	0.4250	23.3035	111.4591		0.0458
5.00E-05	1.11E-05	2.4010			0.0928	0.2288
1.00E-04	2.21E-05					0.4850
5.00E-04					1.3365	

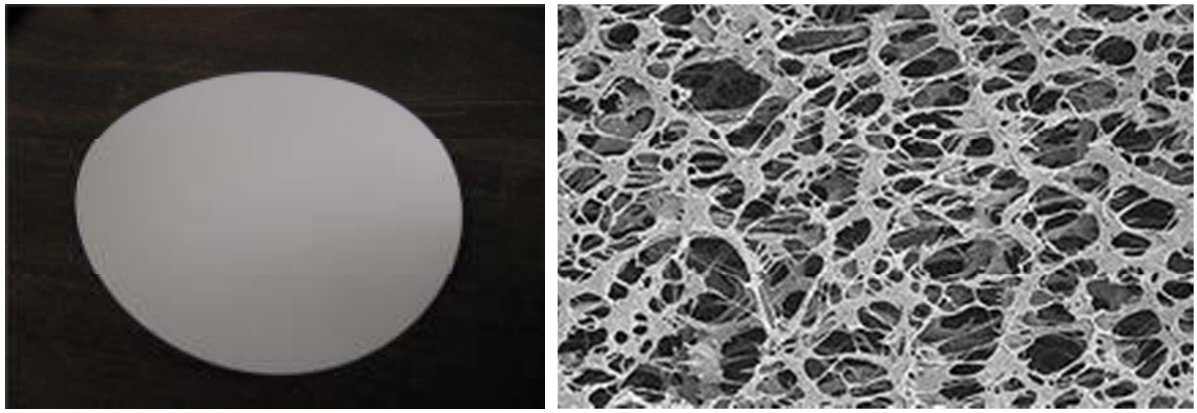

(a) (b)

Figure 4.6. 0.22 micron filter: (a) Fine filter paper; (b) 4000X magnification picture

Figure 4.7. HAE ceramic plates

4.1.4. Vacuum Pump

Vacuum pump, which has a capability of 22 in Hg, is installed and connected to top portion of the soil specimen throughout two back pressure chambers. Initial high vacuum is applied in order to make water in all parts of FPS to be deaired before testing and make easy to be full saturation of the soil sample. Initial high vacuum procedure (Rad and Clough, 1984) leads to promote the saturation of different soils (e.g., initial water content, particle size, relative density, or level of cementation), spend less time to be saturated, and be saturated at atmospheric pressure using a sufficiently low absolute pressure. The beneficial effects of the vacuum procedure increase as the soil particle size decreases or the desired final degree of saturation increases, or both (Rad and Clough, 1984).

4.1.5. Top and Bottom Platens

The top and bottom platens hold the soil specimen in the middle of the triaxial cell. There are two holes and grooves for water and air flow in each platen. The diameter of the bottom platen is designed 1 cm larger than the diameter of the top platen and the soil specimen (6.75 cm). This is because air is prevented to go to the FPS during test when the fine filter paper is used. For this reason, the same diameter of the fine filter paper as the bottom platen (i.e., larger diameter than the soil specimen) should be prepared, and the latex rubber membrane is installed around bottom platen, top platen, and soil specimen with O-rings in order to prevent air to the FPS. Figure 4.8 shows the schematic drawing of the specimen assembly.

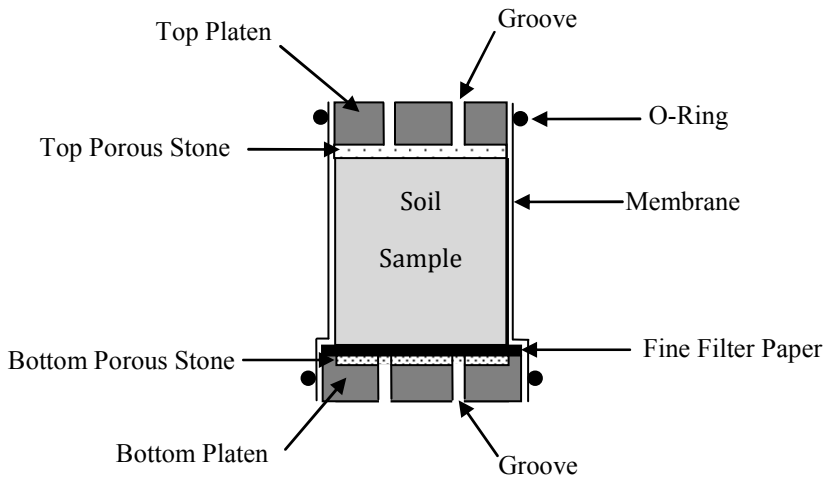

Figure 4.8. Schematic drawing of the specimen assembly

4.2 Material Properties

In our research, three materials, Bonny silt, Pocheon sand, and F-75 Ottawa sand are chosen as the test materials. Bonny silt, or as it is sometimes termed Bonny loess was taken from a sedimentary formation at the Bonny dam site in eastern Colorado. Specific gravity of Bonny silt is 2.6. This soil has classified as “CL-ML” according to the Unified Soil Classification

System (USCS). F-Series foundry grades from Ottawa, IL are mined and manufactured to U.S Silica®. Among several kinds of F-Series foundry grades, F-75 Ottawa sand, which consists of rounded to sub-angular grains and provides high strength and excellent permeability, was used. Specific gravity of F-75 Ottawa sand is 2.63. Pocheon sand is representative of weathered granite, which is widely distributed in Korea, and commonly found in the field. The voids between soil particles are formed by the weathering process. Pocheon sand shows large deformation due to loading, and the deformation depends largely on the porosity. Pocheon sand was taken from Pocheon, Gyunggi-do, Korea. The specific gravity of Pocheon sand is 2.67. This soil has approximately 17.2% passing the #200 sieve and classified as "SM" according to the Unified Soil Classification System (USCS). Figure 4.9 shows grain-size distributions of the three soils. Bonny silt has 75 % fine material, and Pocheon sand has 85% coarse material. F-75 Ottawa sand represents a coarse material. Figures 4.10 to 4.12 show the saturated hydraulic conductivity versus void ratio in each soil by using the constant flow rate method in the FPS. This scatter of data points is caused by slight variation on soil structure in different samples.

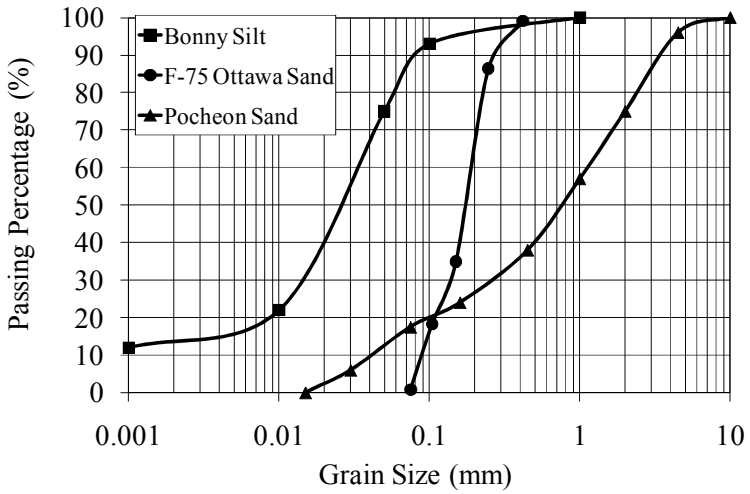

Figure 4.9. Grain-size distributions of each soil

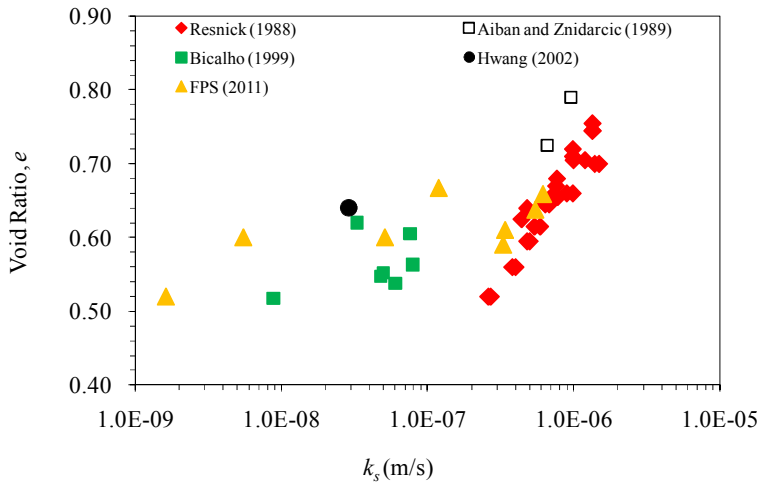

Figure 4.10. Saturated hydraulic conductivity of Bonny silt

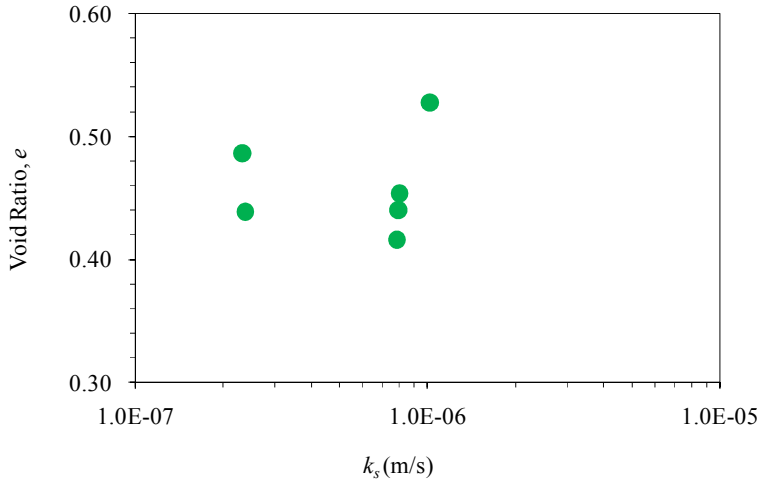

Figure 4.11. Saturated hydraulic conductivity of Pocheon sand

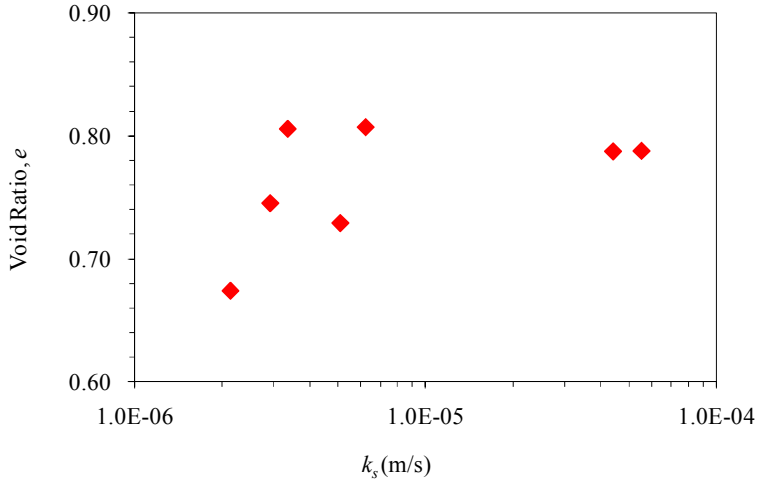

Figure 4.12. Saturated hydraulic conductivity of F-75 sand

CHAPTER 5

TEST PHILOSOPHY AND EXPERIMENTAL PROCEDURES

The flow pump system (FPS) gives the suction-time and suction-saturation curves, the primary relationship needed for interpreting the response of unsaturated soils and the link between theory and the material properties in unsaturated soil mechanics. The technique produces a complete, continuous curve and is less labor intensive than some other techniques. This technique is especially suitable for characterization of suction-time or suction-saturation relationship through the soil elements for both drying and wetting cycles with an arbitrary number of hysteresis cycles in between, where stress state and volume change are important. Two types of test procedures, *Maintained Suction Measurement*, and *Suction Drop Measurement* (Hwang, 2002) are presented for the measurement of the suction response and the SWRC. Also, the optimization process for the proper HCF is presented with the suction response and the SWRC results. Finally, initial suction test and infiltration test with unsaturated soil specimen using the FPS are introduced.

5.1 Test Philosophy

5.1.1. Maintained Suction Measurement

Figures 5.1 and 5.2 show the entire test process of maintained suction measurement. In order to conduct maintained suction measurement for the SWRC, the FPS in Figure 4.1 is used. When the flow rate via withdrawal is applied at the bottom of the fully saturated soil sample as shown in Figure 5.3 (b), continuous suction response is obtained up to first target suction value (withdrawal stage), as shown in Figure 5.1. In this stage, continuous suction response in Figure 5.1 represents the bottom boundary. If the applied flow rate is much smaller than the hydraulic conductivity value corresponding to the measured matric suction, the induced gradients are negligible and the entire suction responses represent the SWRC, since the profiles of the water content or suction change uniformly within the soil sample. However, applying lower flow rates would result in a long testing time, and the rate would need to decrease as the suction increases. Also, the flow pump has a lower limit for pump speed at 1E-05 mm/s. Therefore, the applied flow rate is generally higher than hydraulic conductivity as suction increases. If the applied flow rate is higher than the hydraulic conductivity value corresponding to the suction value, the suction and water content at the bottom boundary change more rapidly than the top portion of the soil specimen. This means that the suction and water content distributions during withdrawal stage are non-uniform, as shown in Figure 5.4 (a). Water content and saturation calculated in this stage represent the average values for the soil sample, since the water content and saturation are calculated by volume of the outflow using the flow pump position. The saturation or water content obtained in this stage is called the average saturation or the average water content.

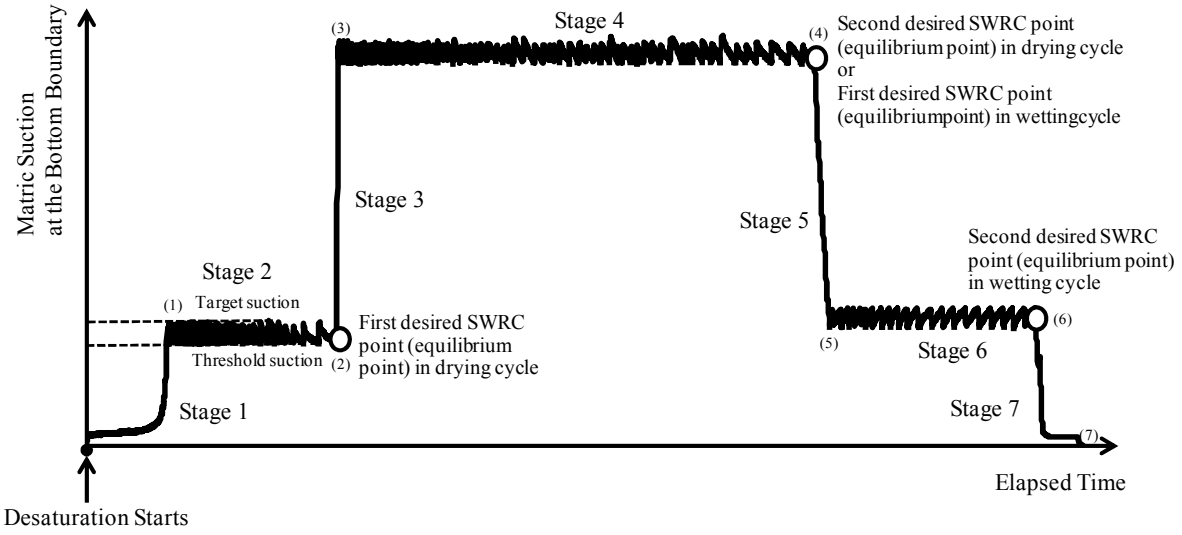

Withdrawal Stage (Drying Cycle) and Infusion Stage (Wetting Cycle)
Suction increases (stage 1 and 3) or decreases (stage 5 and 7) due to withdrawal or infusion of water using flow pump up to target suction value

Suction Equilibration Stage
Flow pump repeats stopping at target suction and starting at the threshold suction value intermittently during several hours in order to reach water content in equilibrium through the soil sample (stages 2, 4, and 6)

Figure 5.1. Suction response in maintained suction measurement

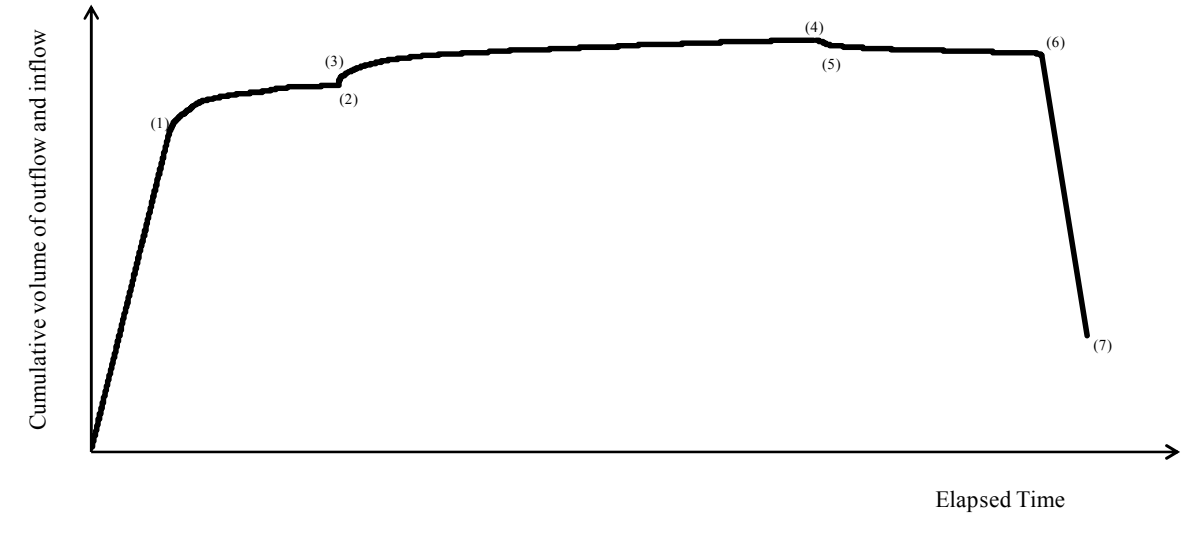

Figure 5.2. Cumulative volume of outflow and inflow in maintained suction measurement

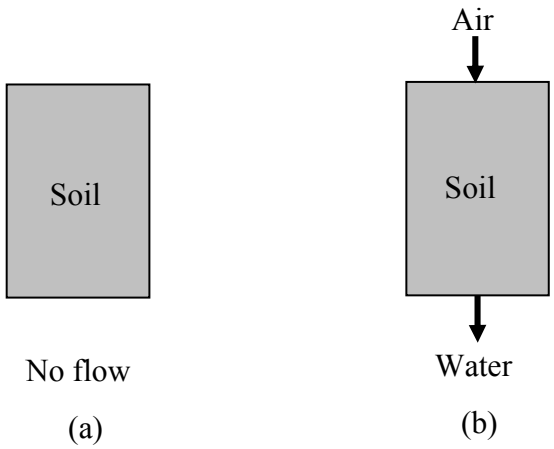

Figure 5.3. Directions of air and water flow during drying procedure in FPS: (a) before test; (b) withdrawal stage

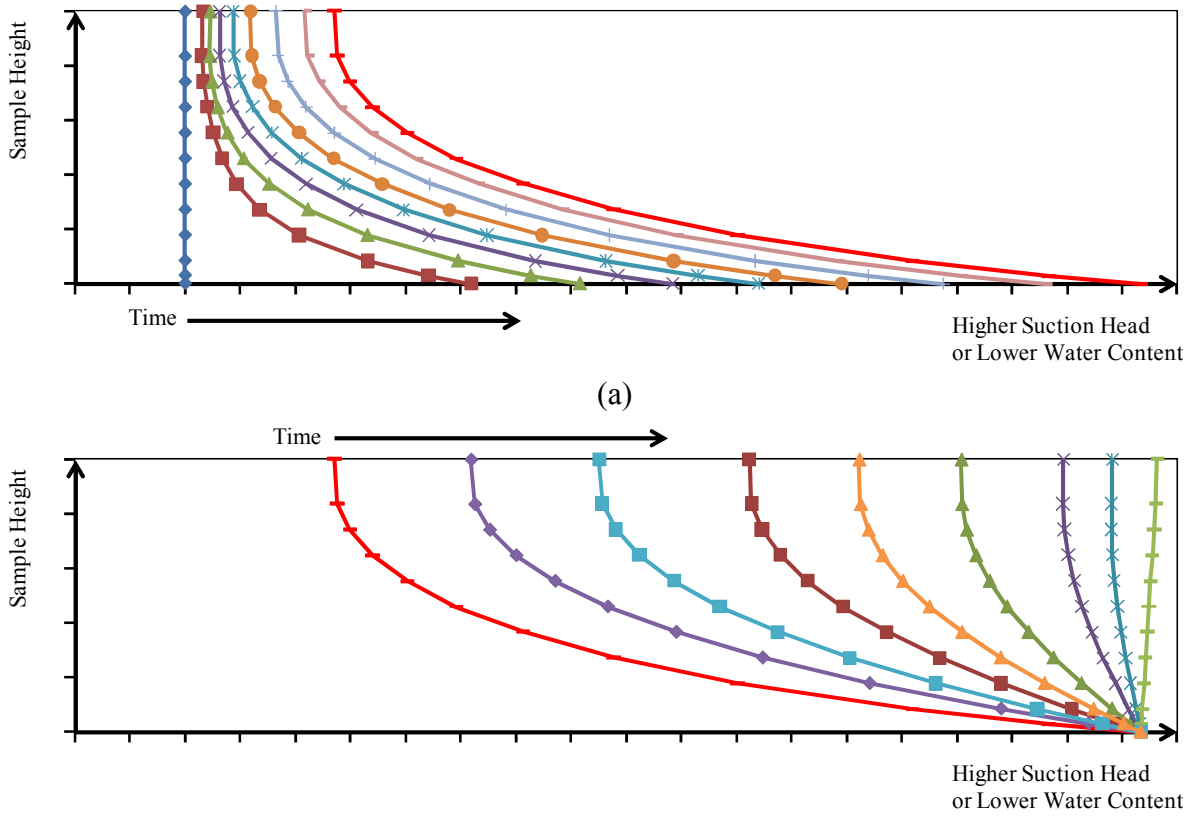

Figure 5.4. Suction and water content profiles of soil specimen during drying cycle: (a) Withdrawal Stage; (b) Suction Equilibration Stage

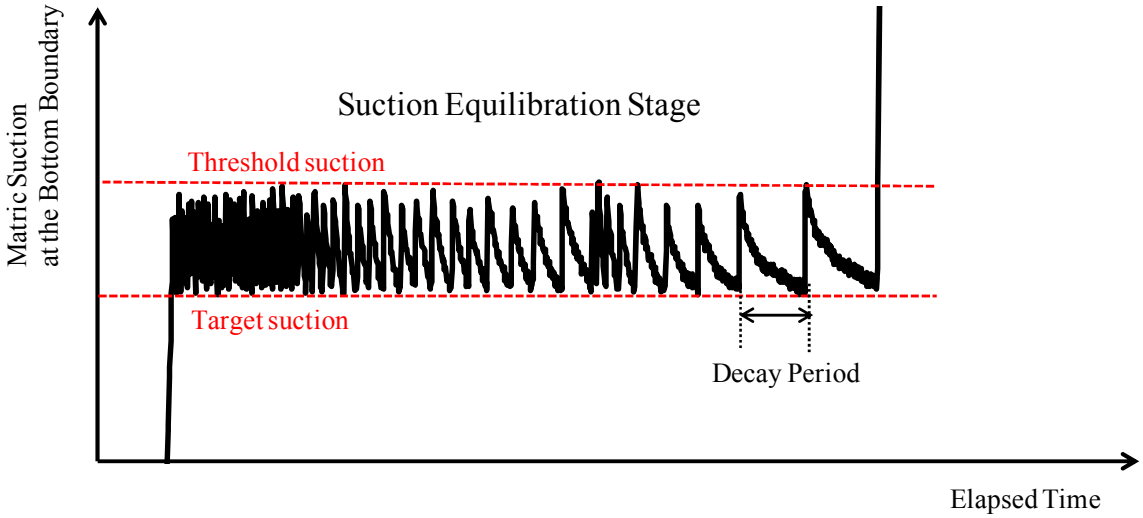

Figure 5.5. Equilibrium stage during test

When the suction reaches the target value, the flow pump repeats stopping and starting intermittently during several hours in order to reach water content at equilibrium (uniform suction and water content profiles of the soil specimen), as shown in Figures 5.1 and 5.5 (Suction Equilibration Stage). The suction interval between stopping and starting the flow pump is set up throughout the threshold value. When suction reaches target value, the flow pump stops, and suction goes down to threshold suction value. At the threshold suction value, flow pump starts again. This is called "*Suction-Feedback Control Loop*" (McCartney and Znidarcic, 2010). Also, the time interval (*Decay Period*) between target and threshold values can be estabilished. If decay period exceeds our target value, generally 5000 seconds(i.e, the longer decay period, the close the suction is to a uniform equilibrium water content and finite suction) the soil specimen reaches water content at equilibrium, and the outflow of water at the bottom ceases as shown in Figure 5.2. A target decay period of 5000 seconds was selected empirically by observing the condition when no measurable flow rate is reached in testing and from numerical analysis looking at the suction distribution of the soil specimen during suction equilibration stage. Figure

5.4 (b) shows the suction and water content profiles of soil specimen during suction equilibration stage. The saturation calculated at this point is first desired point of the SWRC during drying cycle. After obtaining the first desired point for the SWRC, flow pump restarts, suction response will go to the second target value, and the same procedure is repeated, as shown in Figure 5.1.

After completing the drying cycle, the wetting cycle is conducted with opposite direction of flow pump operation, as shown in Figure 5.6 (a). This means the piston of the flow pump pushes water into the soil sample. The final desired SWRC point in drying cycle is the same as first desired SWRC point in wetting cycle. The same process as the drying cycle is conducted in order to obtain several desired SWRC points in wetting cycle. Figure 5.7 shows the suction and water content profiles in the soil specimen during infusion stage and equilibrium stage of wetting cycle. From suction response result(i.e., Figure 5.1), transient suction-saturation (or water content) curve can be obtained by using the amount of water pulled out(drying cycle) or pushed in(wetting cycle) by flow pump operation. Figure 5.8 shows the typical transient suction-saturation curve converted from Figure 5.1.

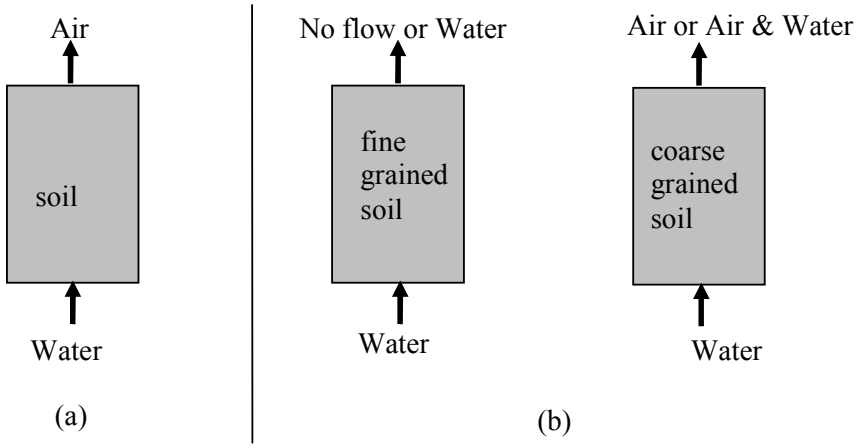

Figure 5.6. Directions of air and water flow during the wetting procedure in the FPS; (a) infusion stage; (b) infusion stage after air entrapment value

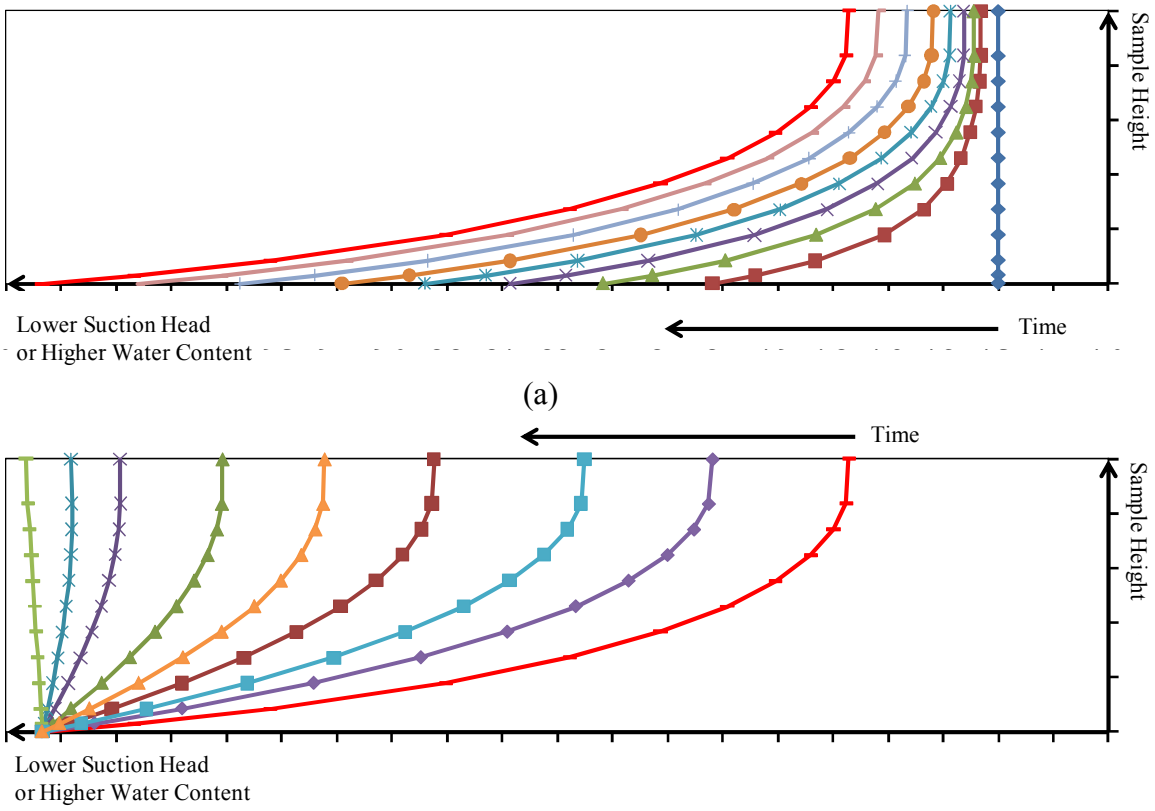

Figure 5.7. Suction or water content profiles of the soil specimen during wetting cycle: (a) Infusion Stage; (b) Suction Equilibration Stage

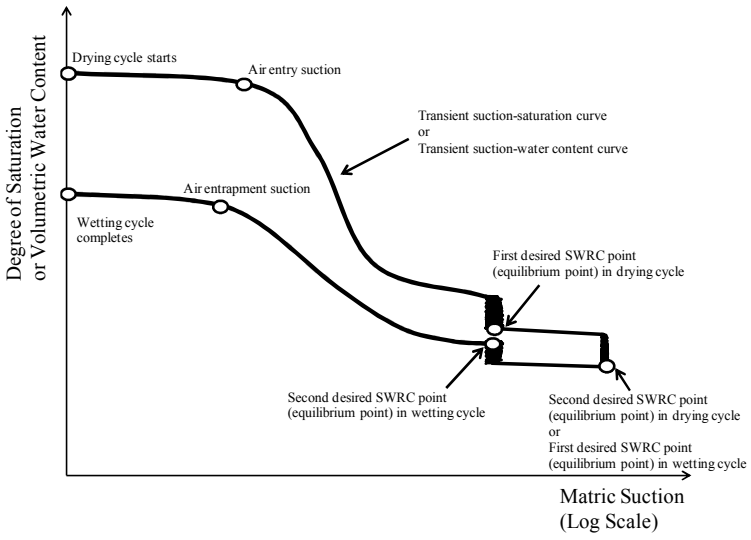

Figure 5.8. Conversion from suction response curve to transient suction-saturation curve

5.1.2. Suction Drop Measurement

Hwang (2002) developed the "*method of suction drop measurement*" using the flow pump system at the University of Colorado at Boulder. Figure 5.9 shows the principle of the suction drop measurement.

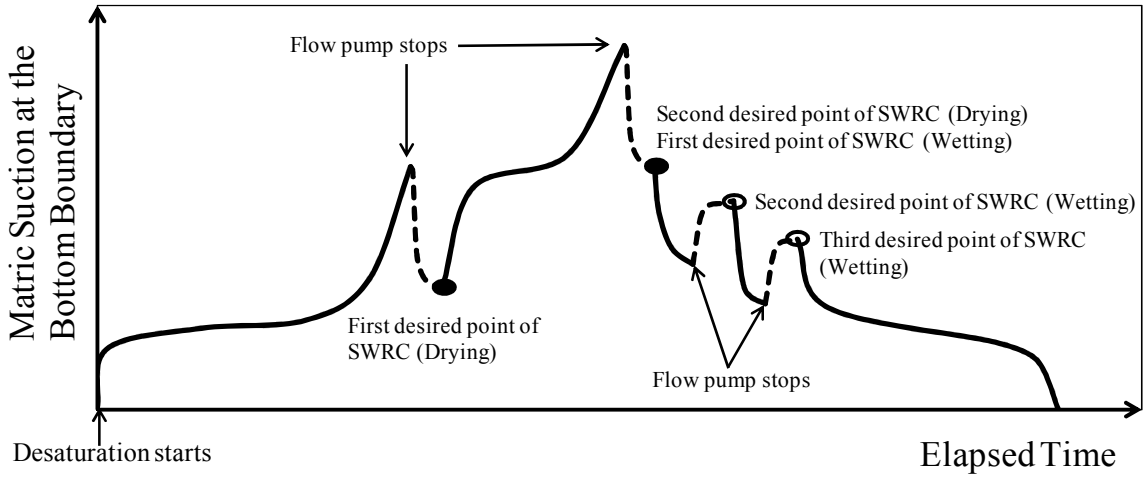

Figure 5.9. Principle of suction drop measurement (Hwang, 2002)

The suction at the bottom of the soil sample is induced using a flow pump connected to the bottom of the soil sample like suction feedback control loop measurement. This stage is called withdrawal stage. When flow rate is applied to the bottom of the soil sample and the induced suction at the bottom reaches the target value, the flow pump stops. The induced suction at the bottom of the soil sample drops gradually, and the soil sample reaches the steady state after several hours, as shown in Figure 5.9. This stage is called suction drop stage. Figure 5.10 shows the suction and water content profiles of soil specimen when flow rate is applied to soil sample, and the suction and water content profiles to reach the steady state when flow pump stops. The wetting process is dominant at the bottom of the soil specimen, whereas drying cycle is dominant the top during the equilibration period, as shown in Figure 5.10 (b). Even though the characteristics and values of the SWRC and HCF between drying and wetting cycles are

significantly different from each other, the effect of a wetting process at the bottom of the soil sample during suction drop stage is neglected in measuring the SWRC. This effect on the SWRC will be discussed further in Chapter 7. When the soil sample reaches the steady state, this is first desired SWRC point during drying cycle, as shown in Figure 5.9. After obtaining first SWRC point, the same procedure is repeated several times for several desired SWRC points.

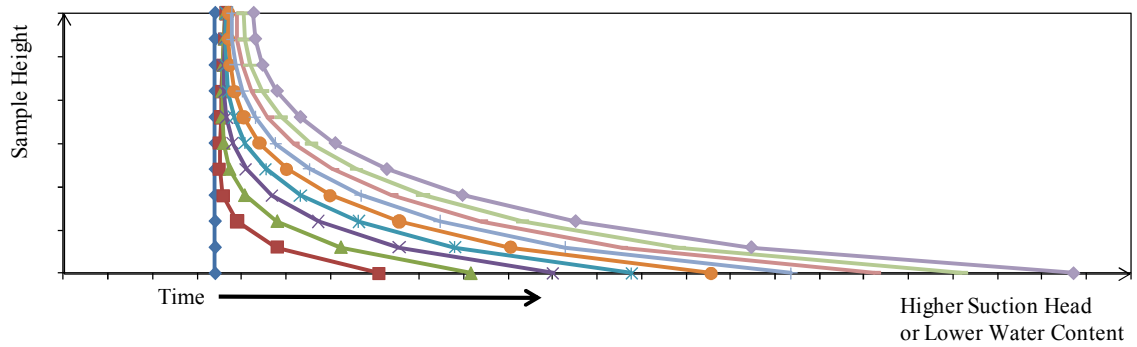

(a)

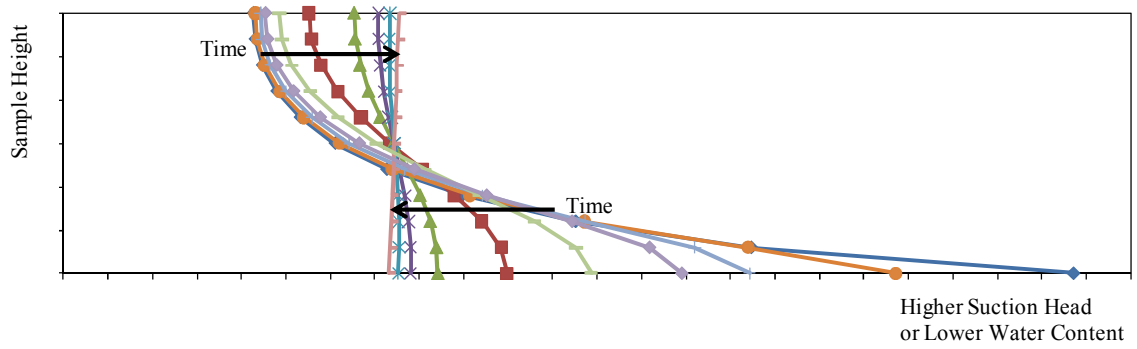

(b)

Figure 5.10. Soil profiles during drying cycle: (a) When flow rate is applied; (b) When flow pump stops

After obtaining the last SWRC point in drying cycle, the flow pump operates via the infusion mode. When the flow pump operates in infusion mode, pressure at the bottom of the soil specimen increases (or suction decreases), and this is called infusion stage. When the pressure reaches the target value, flow pump stops, and induced pressure at the bottom of the soil sample decreases (or suction increases) in order to reach the steady state in opposite direction of drying

cycle, and soil specimen reaches the steady state after several hours in figure 5.9. This is called pressure drop stage. Figure 5.11 shows the suction and water content profiles during pressure increasing stage and pressure drop stage. Figure 5.12 shows the typical transient suction-saturation curve obtained from suction response result.

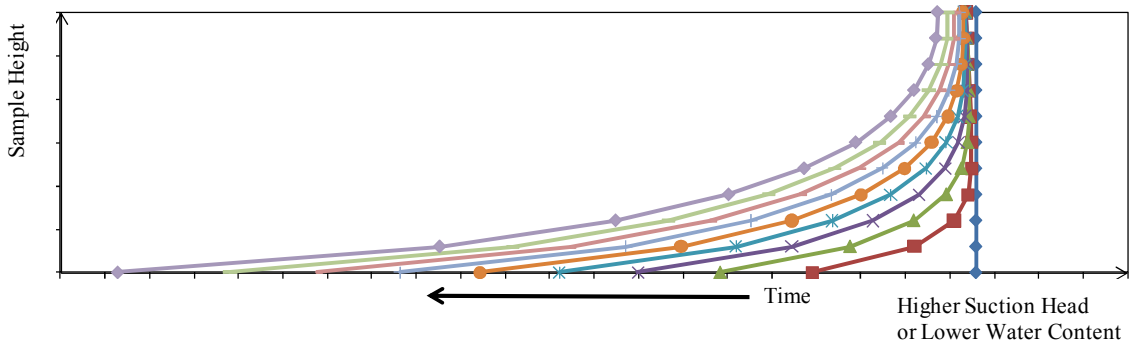

(a)

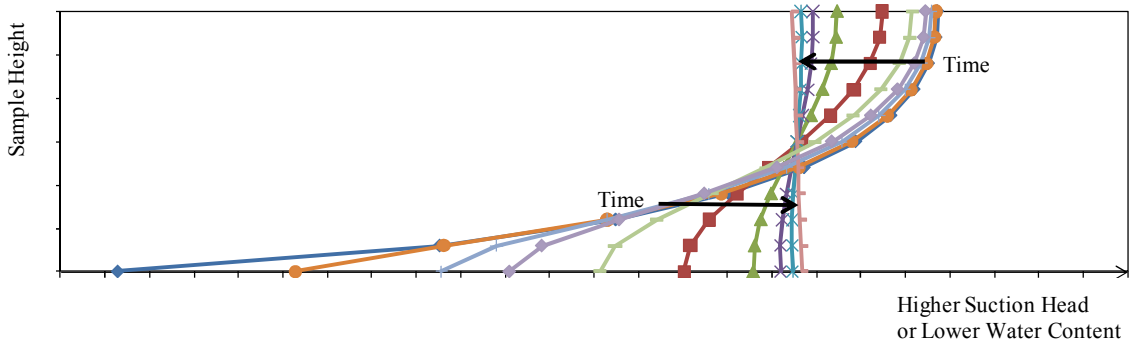

(b)

Figure 5.11. Soil profiles during wetting cycle: (a) When flow rate is applied; (b) When flow pump stops

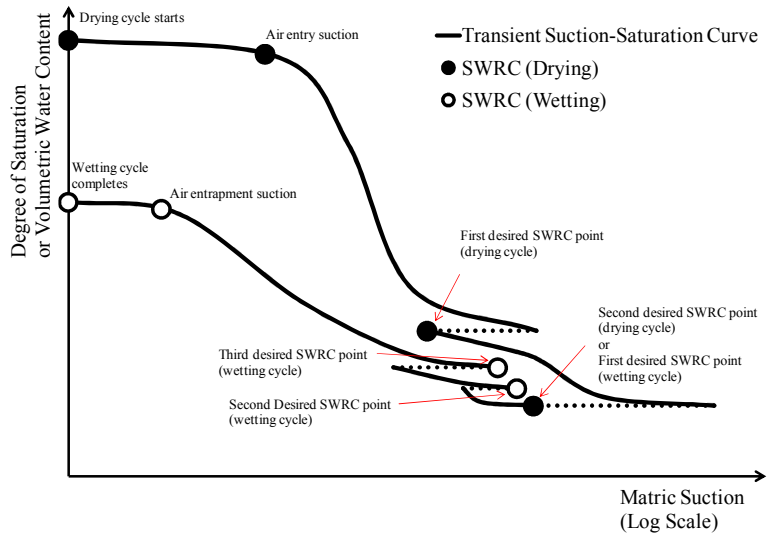

Figure 5.12. Conversion from suction response curve to transient suction-saturation curve

5.1.3. Infiltration Test

The FPS can be also used for the infiltration test in unsaturated soils without a preceding drying test. The FPS configuration changes from Figure 4.1 to 4.2 for the infiltration test. Figure 5.13 illustrates the principle of the infiltration test. In Zone I before the infiltration test, the initial suction of the soil sample is measured with fully saturated HAE ceramic plate. The soil sample, which has an initial suction, is placed on the saturated HAE ceramic plate with a good contact between the sample and the bottom platen, and the triaxial cell is closed as soon as possible to prevent the water content loss in the soil sample. After the sample is placed on the saturated ceramic plate, the sample tends to draw water instantly from the ceramic plate, and equilibrium is reached between the sample and ceramic plate after several minutes. In general, a smaller sample and a higher hydraulic conductivity of the ceramic plate will result in a shorter response time for the measuring system (Bicalho, 1999).

After equilibrium between ceramic plate and soil specimen is reached, the infiltration rate is applied at the bottom of the soil specimen in Zone II. During the infiltration test, a differential

transducer measures the pressure difference between the atmospheric air pressure and the water pressure at the bottom of the soil specimen induced by the flow pump. After completing the infiltration test, the flow pump stops, and pressure goes to zero. The flow pump position corresponding to zero pressure during infiltration test can be known, since the zero pressure value is obtained after stopping the flow pump. With flow pump position at zero pressure during infiltration test, degree of saturation of the soil specimen can be obtained from the volume of inflow pushed by the flow pump. The hydraulic conductivity value corresponding to degree of saturation of the soil specimen can be measured by using the constant flow rate method in Zone III.

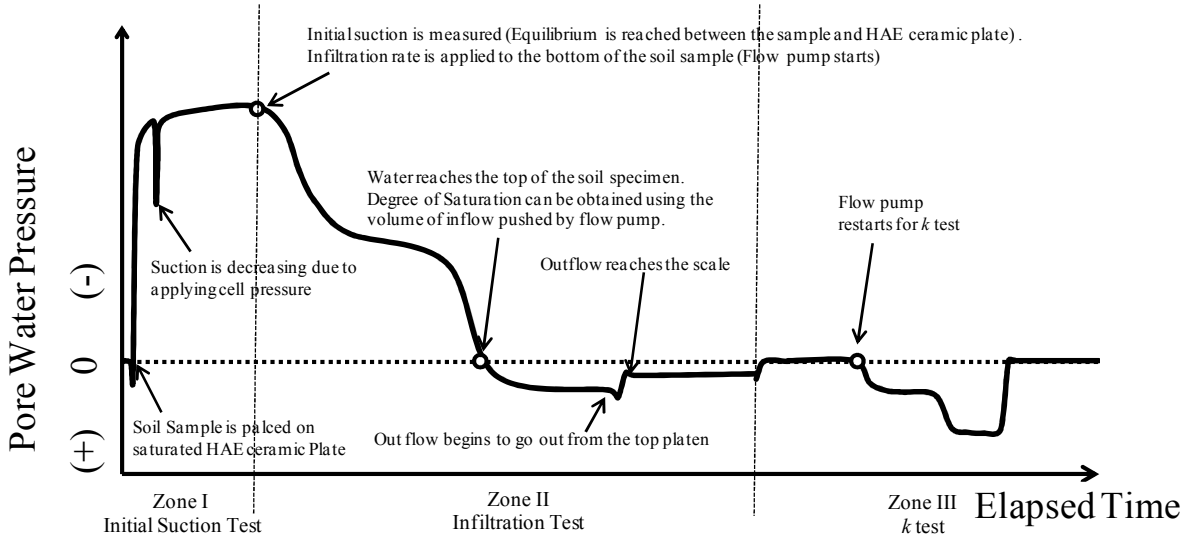

Figure 5.13. Infiltration test with an unsaturated soil sample

5.1.4. Optimization Process for HCF

For evaluation of the proper HCF corresponding to each suction response result (i.e., withdrawal stage and infusion stage in maintained suction measurement, the finite difference code UNSAT-H version 3.01, developed by Pacific Northwest National Laboratory (Fayer, 1990), and PEST version 5, developed by Watermark Numerical Computing are used. UNSAT-

H is designed to simulate unsaturated water flow in one dimension (typically vertical), and PEST is designed to minimize the weighted sum of squared difference between model-generated observation values and those actually measured in the laboratory.

In every FPS test, the soil specimen is surrounded by a latex membrane, and a constant reference air back pressure is applied at the top of the soil specimen. Therefore, the side boundaries are impermeable, and top boundary is also impermeable to water flow (no additional water flux is going to be added or removed at the top of soil specimen during drying cycle). During the suction increasing stage and suction decreasing stage, the specified unit flux is applied by a flow pump which is connected to the bottom of the soil specimen. In UNSAT-H, the side boundaries are not considered, as only one dimensional flow is simulated.

As mentioned in Chapter 2, two material properties are needed in order to solve Richards' equation. First material property is the SWRC, and second is the HCF. The first material properties (i.e., SWRC) and the solution of Richards' equation (i.e., suction response results as a function of time during withdrawal or infusion stage) are directly obtained from maintained suction measurement. Since the curve fitting parameters of the HCF are unrelated to the SWRC (i.e., λ in Brooks and Corey model and α and n in van Genuchten model) can be used in UNSAT-H program, PEST can adjust the parameters of the HCF model until the fit between UNSAT-H outputs and experimental data is optimized.

5.2 Test Procedures (Maintained Suction and Suction Drop Measurements)

5.2.1. Preparation of Soil Sample

There are two methods of preparation for soil specimen. One is that soil specimen is compacted at the desired water content in the mold outside the triaxial cell, especially in cohesive soils such as clay or silt. Compacted soil specimen is placed on bottom platen in good

contact with the fine filter paper or HAE ceramic plate and top platen is placed on the top of the soil sample. The latex rubber membrane is sealed around bottom platen, top platen, and soil specimen with O-rings.

In the case of the cohesionless soil, the split mold is mounted on the bottom platen with the fine filter paper or HAE ceramic plate inside the triaxial cell and the membrane is stretched in place by applying high vacuum. Then, the soil is poured into the forming jacket with a funnel to desired height, the top platen is placed on the top of the soil specimen, and the membrane is rolled over the top platen and fastened with O-rings. Two tubes, one connecting to a back-pressure chamber and another connecting to a transducer, are fixed in two holes of top platen. Vacuum, close to the absolute vacuum in Boulder, CO (approaximately -80 kPa), is applied to the top of the soil specimen in order to prepare the soil specimen for saturation and keep the shape of soil specimen. The coarse porous stone is installed between the soil sample and top platen in order to prevent the migration of the soil particle to the back pressure chamber, but air and water can move freely in the coarse porous stone. In both cases, a small load is applied vertically in order to keep the soil sample in good contact with the fine filter paper.

5.2.2. Saturation of Soil Sample and FPS

One of the most important aspects of the test is that the soil sample and all parts of system should be fully saturated before beginning the test in order to know the initial degree of saturation precisely. Air remaining inside two back-pressure chambers, the transducer, flow pump, and joints between the tubes and the bottom of the triaxial cell should be removed before installing the soil specimen. The soil sample then is placed inside triaxial cell, high vacuum is immediately applied to the sample, and the triaxial cell is closed. After the water fills the triaxial cell, vacuum should be applied for at least several hours. After this, air remaining in voids is

removed by deaired water flow from bottom to top of the soil specimen using the two bottom lines connected to the flow pump and the back pressure chamber with an applied vacuum. After checking the outflow of water from top portion of the soil sample, high confining pressure and high back pressure are applied to the soil specimen for two reasons. First, high back pressure helps the soil specimen to be fully saturated easily through driving the pore air into solution in the pore water. Second, high back pressure allows for the measurement of higher desired suction.

5.2.3. Saturated Hydraulic Conductivity Test by Using Constant Flow Rate

Before beginning a flow test under unsaturated conditions, the hydraulic conductivity test is performed under fully saturated condition by using the constant flow rate. Pressure differences using several proper constant flow pump speeds and the flow pump directions are measured. From the head difference induced by flow pump, the hydraulic gradients can be obtained, as follows:

$$i = \frac{\Delta h(mm)}{l(mm)} \tag{5.1}$$

where Δh is head loss and l is the height of the soil sample.

Darcy's velocity can be calculated, as follows:

$$v(mm/s) = pump\ speed(mm/s) \times \frac{pump\ area(=792mm^2)}{sample\ area(mm^2)} \tag{5.2}$$

The hydraulic conductivity is can be calculated, as follows:

$$k(mm/s) = \frac{v}{i} \tag{5.3}$$

5.2.4. Transient Flow Test for Suction Response and SWRC

Back-pressure is already applied to pore-water at the bottom and top of the soil specimen in order to be fully saturated. Before beginning the flow test under unsaturated conditions, the water at the top portion of the equipment is replaced to air. First, the valve connecting the water at the bottom of the right back pressure chamber is closed. Water at the top platen, the top porous stone, and the tube connecting top platen and right back pressure chamber should be drained out by injecting air through the small tube inside of the right back pressure chamber and by opening valve connecting the upper side of the transducer, as shown in Figure 5.14.

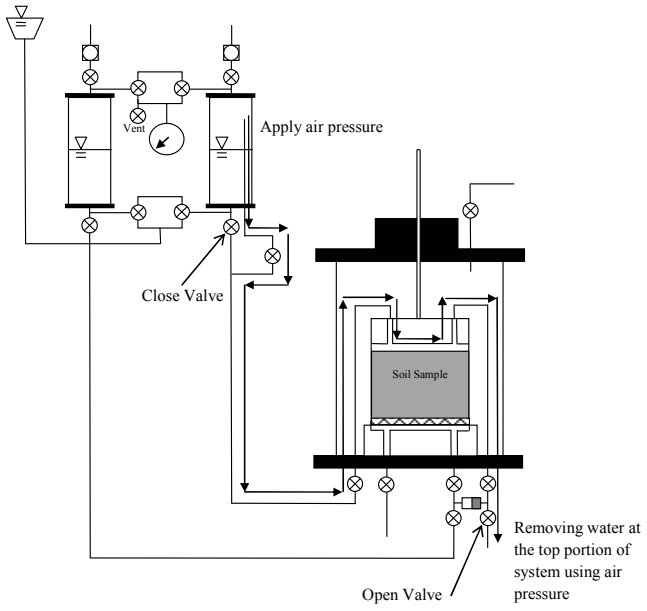

Figure 5.14. Flushing water from the top platen, top back pressure line, and upper chamber of the differential transducer

After removing water from the top portion, pore air pressure is controlled through the top porous stone, and pore water pressure is controlled through the fine filter paper or HAE ceramic plate. At this time, water pressure at the bottom portion remains the same as the air pressure at the top portion by controlling both pressures by a single regulator. Therefore, matric suction is zero before starting the flow test because matric suction is defined as the difference between the

pore water pressure and the pore air pressure. When the flow rate is applied at the bottom, the differential transducer measures the difference between the pore air pressure at the top and the pore water pressure induced by the flow pump (pore air pressure at the top is constant during the flow test, and pore water pressure decreases or increases due to withdrawal or infusion of water at the bottom by operating the flow pump).

From suction response result, transient suction-saturation curve can be obtained by using the amount of water pulled out (drying cycle) or pushed in (wetting cycle) by the flow pump operation. The following procedure explains how to convert from suction response result to transient suction-saturation or water content. First, the pressure (*volt*) corresponding to time obtained by flow pump can be converted into suction head (*mm*) or suction (*kPa*) by using the calibration coefficient of the transducer. The degree of saturation or volumetric water content can be calculated as a function of time by using the volume of water flow induced by flow pump. The SWRC can be obtained from transient suction-saturation curve. This procedure is summarized as follows:

$$\Delta V = \Delta V_W = pump\ area\ (= 792 mm^2) \times \Delta pump\ position\ (mm)$$

$$V_{V0} = V_{W0}\ (when\ \ S = 100\%)$$

$$V_W(t) = V_{W0} - \Delta V(t) \tag{5.4}$$

$$S(t) = \frac{V_W(t)}{V_{V0}} \quad \& \quad \theta = n \times S(t)$$

where V=total volume, $V_w(t)$=volume of water as a function of time, V_{w0}=initial volume of water, V_{v0}=intial volume of void, $S(t)$=saturated as a function of time, θ=volumetric water content, and n= porosity.

5.3 Test Procedures (Infiltration Test)

5.3.1. Preparation of Test

A soil specimen is compacted at the desired water content in the mold outside of the triaxial cell, and placed in a sealed plastic bag for several days to establish the equilibrium in water content. Before the placement of the soil sample inside the cell, the high air entry ceramic plate should be fully saturated using the FPS shown in Figure 4.1. Oven-dried ceramic plate is placed between the bottom and top platen. The latex rubber membrane is installed around bottom platen and top platen with O-rings. The small height of the rubber membrane is needed to cover only one-third of the top platen. Also, an additional O-ring is needed around the ceramic plate to prevent air entrance into the gap between the bottom platen and ceramic plate after removal of top platen after saturation, since the diameter of the bottom platen is larger than the ceramic plate. High vacuum is immediately applied to the ceramic plate and the triaxial cell is closed. After water fills up the triaxial cell, a vacuum must be applied to the ceramic plate for several hours. Air remaining in voids of the ceramic plate is removed by deaired water flow from bottom to top through the tubes connected to the reservoir. Sufficiently high cell pressure and back-pressure are applied for 24 hours in order to make remaining air to dissolve easily in water. After full saturation of the ceramic plate, the water in triaxial cell is drained and top platen is removed from the ceramic plate without removing the rubber membrane. The system is reconfigurated from Figure 4.1 to Figure 4.2. Any water remaining on the ceramic plate is removed quickly, and prepared soil sample is placed on the saturated ceramic plate. Top platen is placed on the soil sample, and the rubber membrane is installed around bottom platen, soil specimen, and top platen with O-rings. Right side port on the top platen is removed, and the port on the top platen is closed. Therefore, outflow from the soil sample can go only to the weighing scale through the

other tube. Triaxial chamber is filled with water. The soil specimen tends to draw water instantly from the ceramic plate, and equilibrium is reached between the soil specimen and ceramic plate after several minutes. Confining pressure is applied up to desired value gradually. While applying the confining pressure to the triaxial cell, the suction decreases, and equilibrium is reached once again after several minutes.

5.3.2. Infiltration Test

After obtaining the initial suction value, the flow pump operates in infusion mode with chosen flow rate. Water flows through the soil specimen, and then water goes to the weighing scale through the tube after water reaches the top of the soil sample. When water passes the tube length of 500 and 1000 mm, time at two positions of tube is recorded. From these, time value at the tube length of 0 mm can be obtained inversely using the change of pump position between the tube length 500 and 1000 mm. The degree of saturation of the soil specimen corresponding to zero pressure value is obtained from the flow pump position corresponding to zero pressure value during infiltration test multiplied by the flow pump area. After water reaches the scale, the outflow is measured for several minutes, and compared with the outflow volume calculated by flow pump position.

After completing the infiltration test, the hydraulic conductivity test using several flow rates is conducted and calculated by using Equations (5.1), (5.2), and (5.3).

CHAPTER 6

MAINTAINED SUCTION MEASUREMENT

Maintained suction measurement using a FPS is conducted for the measurement of suction response and SWRC and evaluation of the HCF. Three materials, Pocheon sand, Bonny silt, and F-75 Ottawa sand are chosen as the test materials. Ten different tests with three materials are conducted, and Table 6.1 shows a summary of the tests.

Table 6.1. Summary of maintained suction measurement

Test #	Soil	HAE Plate	*n* (porosity)	Purpose
MSM-P1	Pocheon sand	1-bar HAE plate	0.345	SWRC & HCF
MSM -P2	Pocheon sand	1-bar HAE Plate	0.327	SWRC
MSM -P3	Pocheon sand	1-bar HAE plate	0.327	SWRC
MSM -P4	Pocheon sand	1-bar HAE plate	0.327	SWRC
MSM -P5	Pocheon sand	1-bar HAE plate	0.344	SWRC
MSM -B1	Bonny silt	3- bar HAE plate	0.400	SWRC & HCF
MSM -B2	Bonny silt	0.22 micron filter	0.375	SWRC & HCF
MSM -F1	F-75 Ottawa sand	0.22 micron filter	0.447	SWRC & HCF
MSM -F2	F-75 Ottawa sand	0.8 micron filter	0.447	SWRC
MSM -F3	F-75 Ottawa sand	0.8 micron filter	0.443	SWRC

Five tests with Pocheon sand, two tests with Bonny silt, and three tests with F-75 Ottawa sand were conducted. In this chapter, test #MSM-P1, # MSM -B1, # MSM -B2, and # MSM -F1 are discussed. Results of the other are presented in Appendix A. Test # MSM -P1 is conducted for the measurement of the SWRC and evaluation of the HCF. 1 bar HAE ceramic plate is used

for the test, since the fine filter paper easily gets damage during testing. In case of Bonny silt, test # MSM -B1 is conducted with 3 bar HAE ceramic plate, and test # MSM -B2 is conducted with 0.22 micron filter paper. The HCF in only drying cycle is evaluated in test # MSM -B1, and the reason will be discussed later. The HCF in both drying and wetting cycles are evaluated in test # MSM -B2. Finally, test # MSM -F1 with F-75 Ottawa sand, a representative uniform sand, is conducted for the SWRC and the HCF.

Equations (5.1) to (5.3) are used for the measuring the hydraulic conductivities before drying cycle and after wetting cycle. Equation (5.4) is used for converting the suction response as a function of time to transient suction-saturation curve. From these converted values, the SWRC are obtained. HCFs in each soil are evaluated using an inverse problem solution approach (i.e., optimization process) from experimental suction response and the SWRC results. Also, the head loss of HAE ceramic plates and fine filter papers in Table 4.1 are considered in calculation of suction response and hydraulic conductivity corresponding to the applied flow rates.

6.1 Suction Response and SWRC

Each test with each soil is conducted for measurement of the suction response induced by the flow pump and the SWRC. Test # MSM -P1 with Pocheon sand, # MSM -B1 with Bonny silt, and # MSM -F1 with F-75 Ottawa sand are reviewed for the measurement of the suction response and the SWRC.

In case of Pocheon sand (#MSM -P1), the soil specimen is compacted at the water content of 9.1% with 6.75 cm diameter and 5.53 cm height. The porosity and saturated hydraulic conductivity of Pocheon sand specimen are 0.345 and 1.0E-06 m/s, respectively. Applied flow rate, 5.5E-08 m/s (pump speed=2.5E-07 m/s) in all withdrawal and infusion stages is 20 times slower than saturated hydraulic conductivity. Target suctions for the SWRC are 12.6,

24.6, 35.8, and 72.5 kPa for both drying and wetting cycles. Suction response value subtracts head loss of 1 bar HAE ceramic plate from measured suction value, since head loss of 1 bar HAE ceramic plate corresponding to applied flow pump speed is 0.5 kPa.

In case of Bonny silt (#MSM -B1), the soil specimen is compacted at the water content of 16.7% with 6.75 cm diameter and 6.04 cm height. The porosity and saturated hydraulic conductivity of Bonny silt specimen are 0.400 and 1.2E-07 m/s, respectively. 5 times slower flow rate, 2.2E-08 m/s (pump speed=1.0E-07 m/s) than saturated hydraulic conductivity is applied in all stages. In order to obtain the SWRC points, the four target suctions are 45.4, 83.5, 120.0, and 171.5 kPa for both drying and wetting cycles. Head loss, 0.95 kPa of 3 bar HAE ceramic plate corresponding to applied flow pump speed is also considered.

In case of F-75 Ottawa sand (#MSM -F1), the soil in dry condition is poured into the mold mounted on the bottom platen, and vacuum is applied to keep the shape of the soil specimen. The porosity and the saturated hydraulic conductivity of F-75 Ottawa sand specimen are 0.447and 6.22E-06 m/s, respectively. 0.22 micron filter paper instead of HAE ceramic plate is used, and the head loss of fine filter paper is ignored, since the head loss induced by applied flow pump speed is very small. Test with F-75 Ottawa sand (#MSM -F1) is carried out with three different flow rates, 3 times slower flow rate than saturated hydraulic conductivity in first suction increasing stage, 15 times slower flow rate in second stage, and 317 times slower flow rate in third stage during drying cycle. Target suctions for the SWRC are 5.5, 10.5, and 16.2 kPa for drying cycle. In case of F-75 sand, the threshold is set up about 0.1 kPa, since the SWRC of the uniform sand is in narrow suction range. Unlike other tests, the flow pump speed is exchanged in each equilibration stage, since the HCF of the uniform sand decreases

dramatically as the suction increases and the flow pump speed generally causes the overshooting of the target suction if a high flow rate is selected.

Figures 6.1 to 6.4 show the suction response results, volume change of water flow, axial displacement, transient suction-saturation curve, and SWRC of each soil. All points in Figures 6.1 to 6.4 indicate the desired target equilibrium points at each target suction value. In Figure 6.1, suction responses of each soil are presented up to each target suction. After induced suction by flow rate reaches target suction, the flow pump keeps suction at the bottom of the soil specimen constant by repeatedly stopping and starting the flow within the suction interval (i.e., from target suction to threshold suction value) during several hours in order to reach water content at equilibrium (uniform suction and water content profiles of the soil specimen). When the time interval between target suction and threshold suctions exceeds set-up target decay period, generally 5000 seconds between target and threshold suction values in each equilibration stage, the soil specimens approach the water content in equilibrium, and cumulative volume of outflow (drying cycle) or inflow (wetting cycle) at the bottom of the soil specimen ceases, as shown in Figure 6.2. Pump position is a mirror image of this curve because the cumulative volume of water flow is calculated by the amount of water pushed or pulled out by the flow pump. Figures 6.2 show that cumulative volume of inflow in wetting cycle does not reach zero at suction of 0 kPa due to air entrapment in soils. This causes the difference of water content at the suction of 0 kPa between drying and wetting cycle in SWRC.

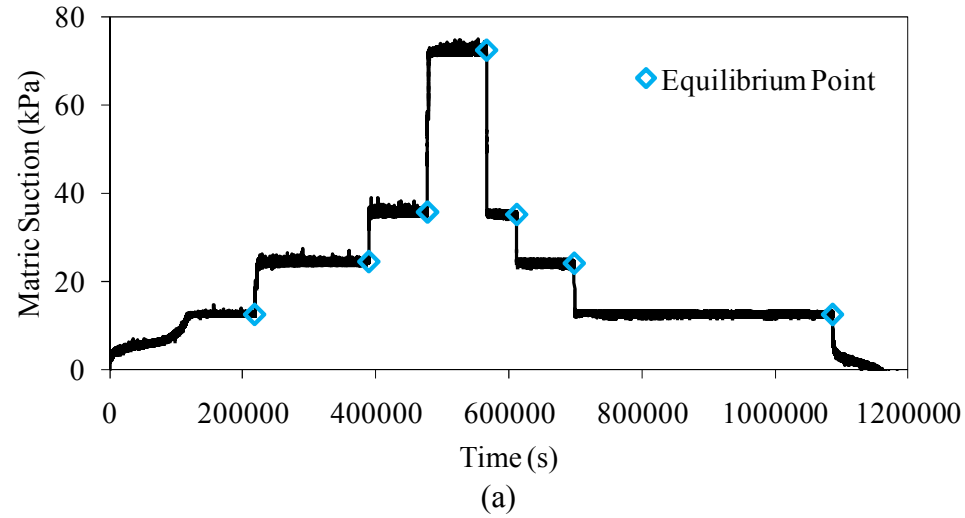

(a)

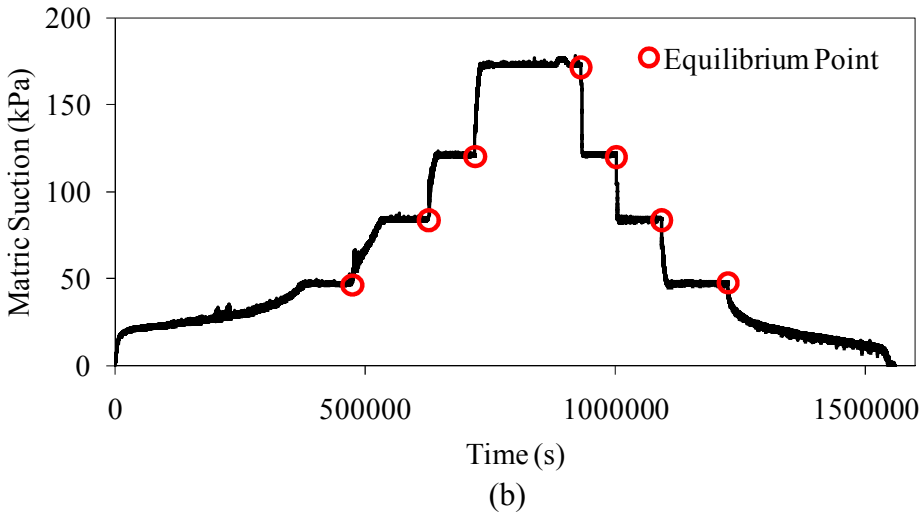

(b)

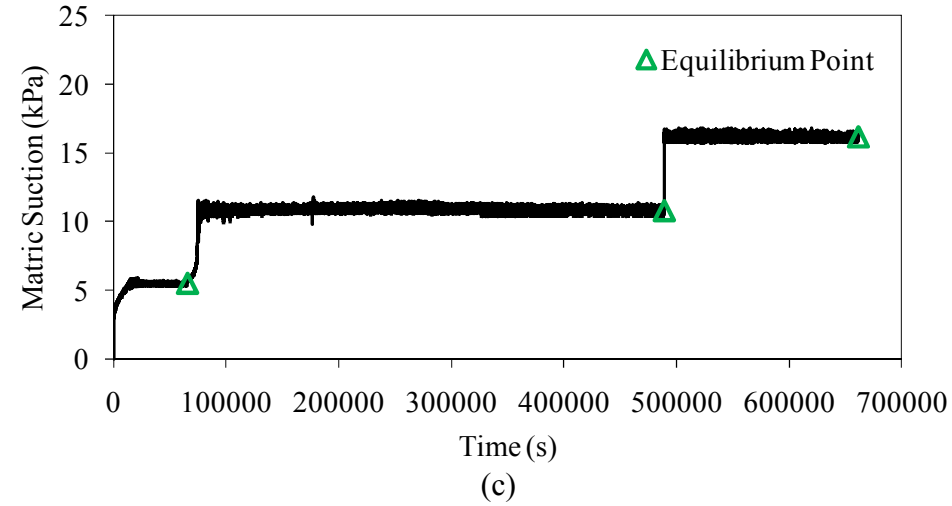

(c)

Figure 6.1. Suction responses and equilibrium points: (a) Pocheon sand, # MSM-P1;(b) Bonny silt, # MSM-B1; (c) F-75 Ottawa sand, # MSM-F1

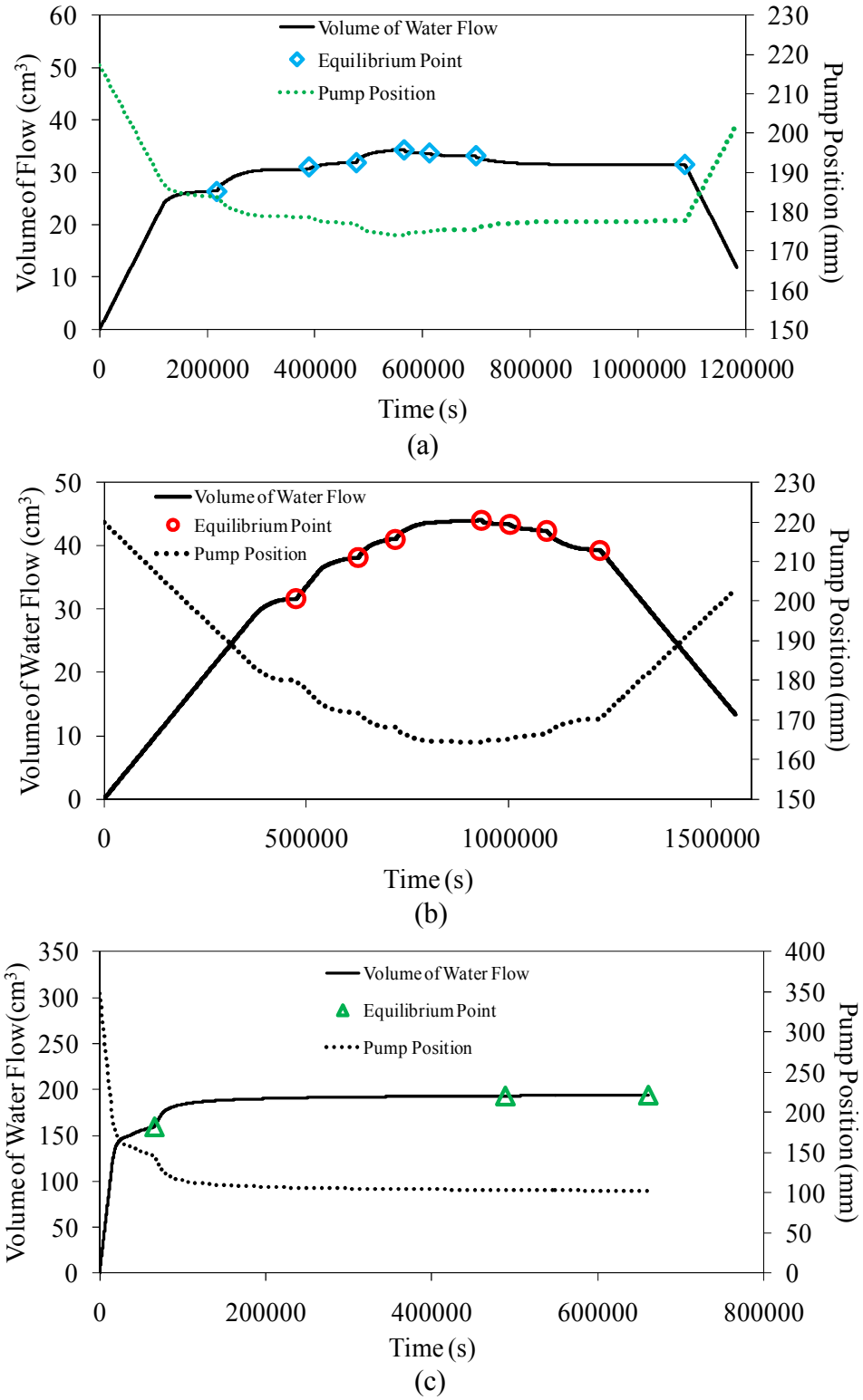

Figure 6.2. Cumulative volume of water flow during testing: (a) Pocheon sand, # MSM-P1;(b) Bonny silt, # MSM-B1; (c) F-75 Ottawa sand, # MSM-F1

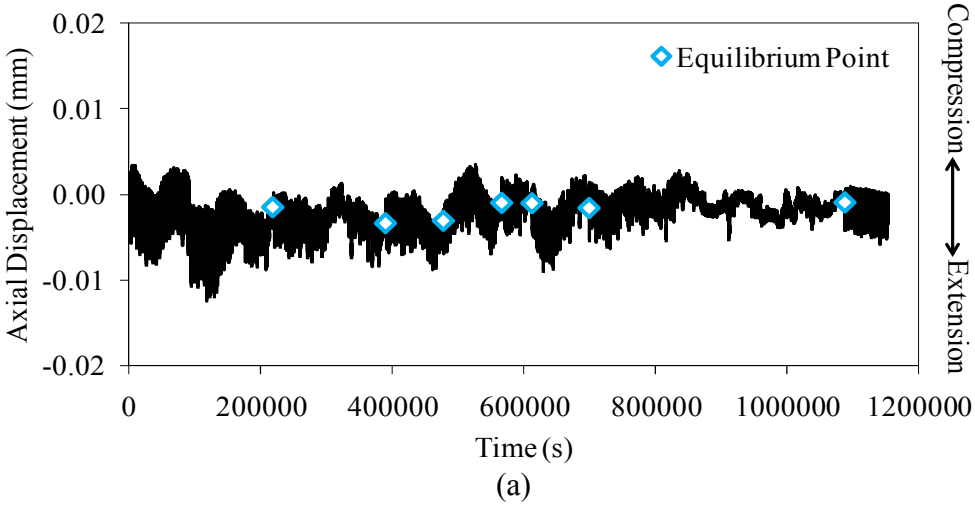

(a)

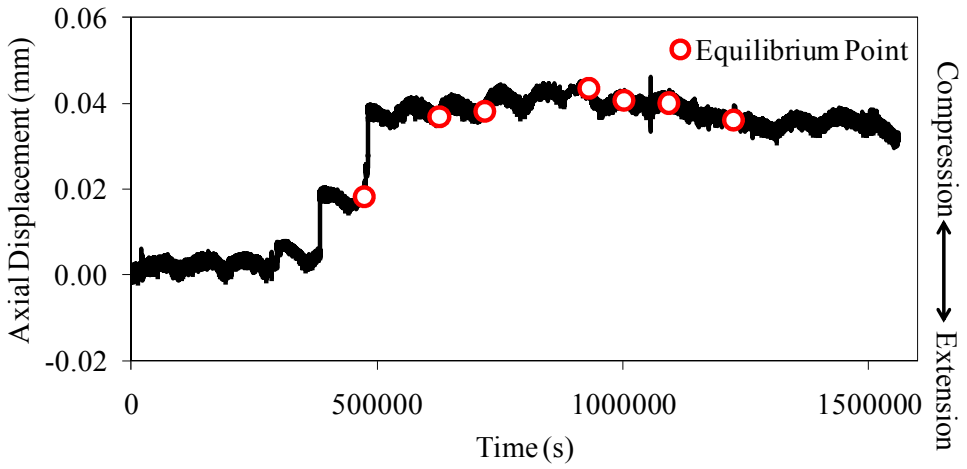

(b)

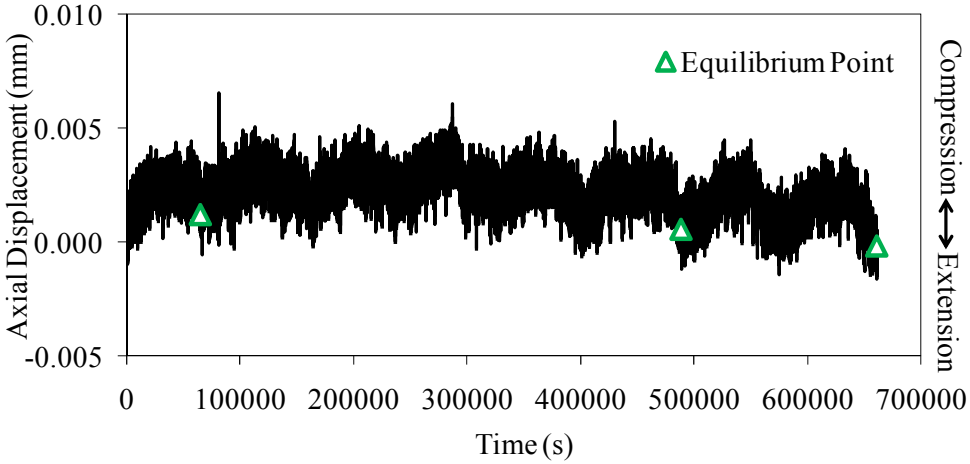

(c)

Figure 6.3. Axial displacement during testing: (a) Pocheon sand, # MSM-P1;(b) Bonny silt, # MSM-B1; (c) F-75 Ottawa sand, # MSM-F1

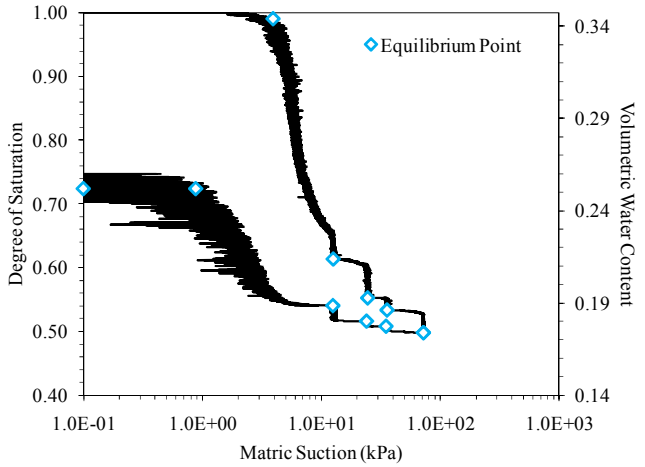

(a)

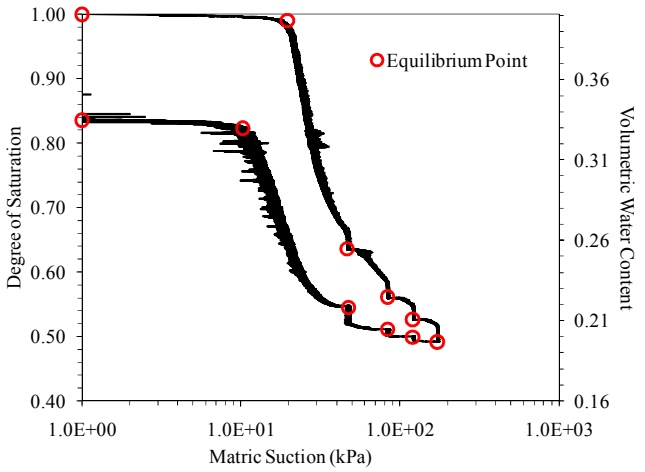

(b)

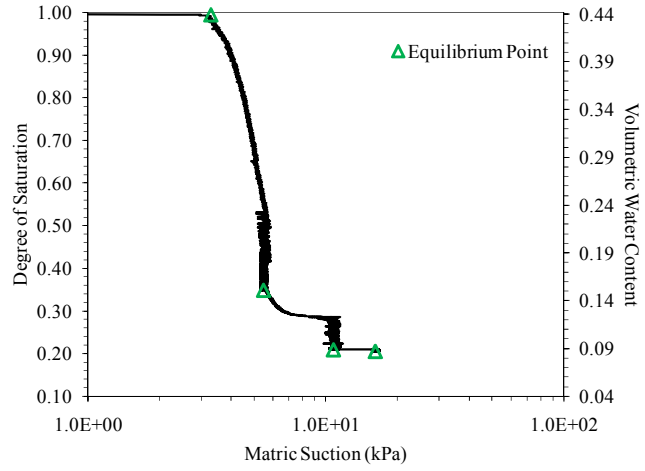

(c)

Figure 6.4. Transient suction-average saturation curve and equilibrium points: (a) Pocheon sand, # MSM-P1;(b) Bonny silt, # MSM-B1; (c) F-75 Ottawa sand, # MSM-F1

After exceeding target decay period in each equilibration stage, the suction induced by flow pump goes toward next target suction, and same procedure is repeated for water content at equilibrium. When suction reaches the final target suction in drying cycle, 24 to 48 hours is needed in order to reach target decay period of 5000 sec. After time interval reaches target decay period of 5000 sec in final suction maintaining stage, the direction of flow pump is exchanged and flow pump restarts with infusion mode for wetting cycle. In the wetting cycle, the first SWRC point is the same as the final SWRC point of drying cycle.

During each test, the axial displacement is also measured. The soil specimen expands slightly during testing for Pocheon sand, whereas the soil specimens compresses slightly during test for F-75 Ottawa sand. However, there is no significant volume change during testing, as shown in Figure 6.3. In the case of Bonny silt, the height of soil specimen decreases during the drying cycle as the suction increases, whereas the height of soil specimen increases slightly during the wetting cycle. Even though the soil specimen of Bonny silt compressed about 0.04 mm during testing, the change of the volume during testing is ignored to measure the SWRC, since this leads to only 0.004 difference of porosity.

From suction responses shown in Figure 6.1, transient suction-saturation curves are obtained by using the amount of water pulled out (drying cycle) or pushed in (wetting cycle) according to flow pump operating position, as shown in Figure 6.4.

6.2 Evaluation of HCF

In order to evaluate the proper HCF corresponding to each withdrawal stage in the drying cycle or infusion stage in the wetting cycle, an inverse problem solution approach (i.e, optimization process) is used with the experimental suction response result and the SWRC fit. In this analysis, our SWRC is assumed to each soil and represent the SWRC over the entire suction

range exactly without volume change. In order to represent the optimized HCF, HCF prediction modes such as BC HCF model and VG HCF model are used. The same bottom boundary flux as is used in each stage. Even though the HCF can be obtained in each equilibration stage with constant-head bottom boundary condition, only withdrawal and infusion stages are used for optimization of the HCF, because the suction range is overlapped between former withdrawal or infusion stage and latter equilibration stage. In this analysis, UNSAT-H is used as the system model, and PEST is connected to UNSAT-H in order to optimize curve fitting parameters of the HCF models in terms of minimizes the weighted least squares corresponding to each withdrawal stage and each infusion stage. In the first withdrawal stage of the drying cycle and the last infusion stage of the wetting cycle, only λ in BC HCF model or α and n in VG HCF model are used for optimization, because the air entry value and saturated hydraulic conductivity before drying cycle, and air entrapment value and hydraulic conductivity after wetting cycle are measured directly during testing. However, saturated hydraulic conductivity and air entry value (if wetting cycle, hydraulic conductivity and air entrapment value) are also considered as the curve fitting parameters for optimization in other withdrawal and infusion stages in order to represent the HCF corresponding to each suction range more accurately. In the first withdrawal stage of drying cycle, the initial condition of every location of the soil specimen is the suction of 0 kPa, because of full saturation before the test. In other stages, the initial condition of the soil specimen is determined by using the simulation of the suction equilibration stage with the constant suction bottom boundary condition and the optimized HCF found in former withdrawal or infusion stage. In simulating to suction equilibration stage, the suction at the bottom is kept in constant and the suction values in other locations of the soil specimen go to the suction value at

the bottom on the bases of drying material properties during drying cycle or wetting material properties during wetting cycle.

In inverse analysis for the HCF, PEST requires that upper and lower bounds be supplied for adjusted parameters. If not, UNSAT-H would produce non-sensical result or may incur a run time error if certain inputs transgress permissible domain. The upper and lower bounds of the hydraulic conductivity value are set up 100 times higher and 100 times slower hydraulic conductivity, respectively. In case of the air entry value or air entrapment value, the bound for optimization is set up between 0 kPa and 10 times higher value than measured air entry or entrapment value. The lower bound value for curve fitting parameter λ in BC HCF model is set up to be only positive without an upper bound. Curve fitting parameters, α and n in VG HCF model are set up between 10 times lower and 10 times higher values than the curve fitting parameters value from the SWRC. In addition, a proper choice of initial parameter value is needed in each optimization stage, since a proper choice of initial parameter values has a pronounced effect on optimization efficiency. If not, convergence will be slow, requiring many more optimization iterations. In each suction range, the optimization process starts with the parameter value from the SWRC and measured air entry or entrapment value and measured hydraulic conductivity at zero suction. If optimization process with our initial parameter values is not convergent, the initial parameter values are changed, and optimization process is restarted. In this case, initial parameter value is found from the trial and error method in comparison with experimental result for optimization efficiency. In this inverse analysis, optimization process continues until coefficient of determination is higher than 0.9 (coefficient of correlation higher than 0.95).

Figure 6.5 shows the SWRC BC fit of Pocheon sand for optimization. Figure 6.6 shows how to adjust the curve fitting parameters of UNSAT-H until the fit between UNSAT-H output and experimental suction response result through several iterations. Optimization process starts with the parameter λ from the SWRC fit. Seven optimization iterations are conducted for the HCF, and there is no significant difference between the simulation with λ from the SWRC fit and experimental test result in first withdrawal stage, as shown in Figure 6.6. Optimization result is represented in Appedix B.

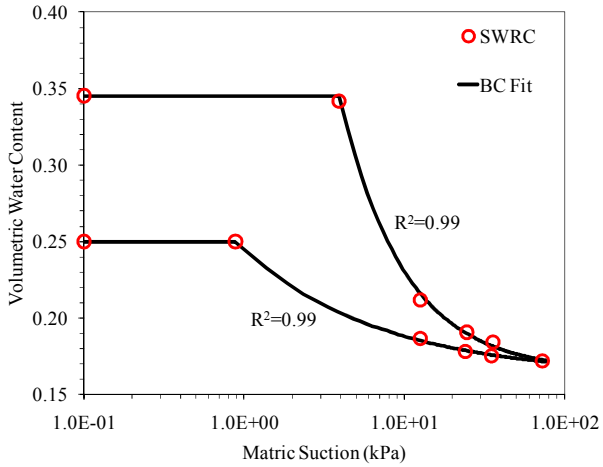

Figure 6.5. SWRC and BC fit (Pocheon Sand, # MSM-P1)

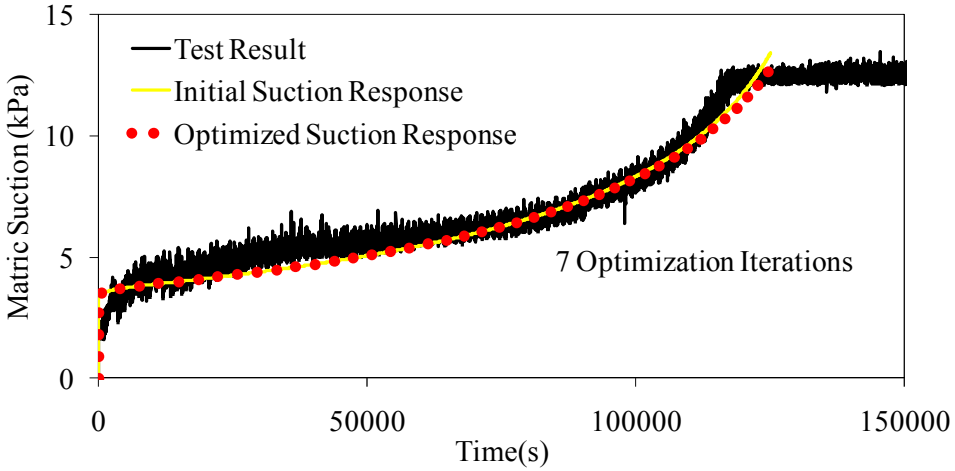

Figure 6.6. Optimization process in first withdrawal stage (Pocheon Sand, # MSM-P1)

Figure 6.7 (a) shows the suction profiles of soil specimen with the optimized HCF, and the last suction profile values of soil specimen gives the initial value to simulation for the next equilibration stage. Figure 6.7 (b) show the suction profiles in suction equilibration stage with the optimized HCF in first withdrawal stage and the initial suction value of soil specimen obtained from Figure 6.7 (a). The last suction profile values also give the initial values to optimize for the second withdrawal stage. Figure 6.8 shows the optimization process in second withdrawal stage with initial values obtained from simulation of the former equilibration stage. Optimization process starts with measured saturated hydraulic conductivity, measured air entry value, and λ from the SWRC fit, and the HCF is optimized after 17 iterations and 107 UNSAT-H calls. Figure 6.8 shows the optimization result of the HCF in comparison with BC HCF model corresponding to first and second withdrawal stages. Only λ in BC model is used for optimization in first suction increasing stage, whereas the air entry value and saturated hydraulic conductivity as well as λ are used for optimization in second withdrawal stage.

Repeating the same procedure, the optimized HCFs in each withdrawal stage and infusion stage are obtained, and simulations of each equilibration stage are also conducted in order to determine the initial conditions for next withdrawal or infusion stage for optimization. Suction profiles at different time increments in each stage are shown in Appendix C. Figure 6.10 shows the simulation with optimized HCF in comparison with experimental suction response result. Figures 6.11 to 13 show the optimized HCF corresponding to each suction range. Appendix D shows the optimized values and coefficient of determination in HCF model for drying and wetting cycles. In the case of Pocheon sand, the optimization process is not convergent until coefficient of determination becomes higher than 0.9 in some suction ranges.

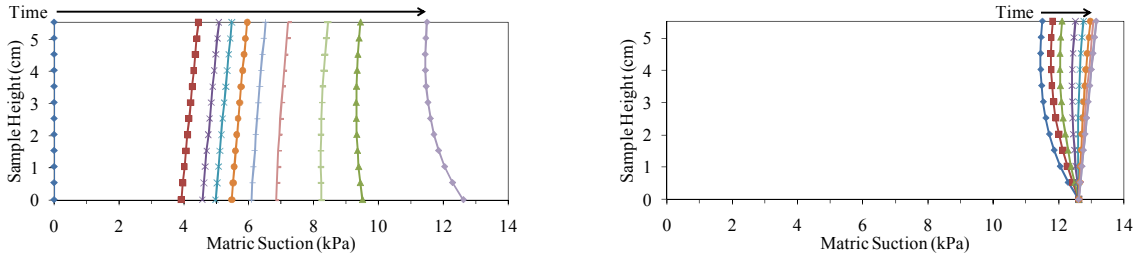

Figure 6.7. Simulation with optimized HCF in first withdrawal and equilibration stage (Pocheon Sand, # MSM-P1): (a) first withdrawal stage; (b) first suction equilibration stage

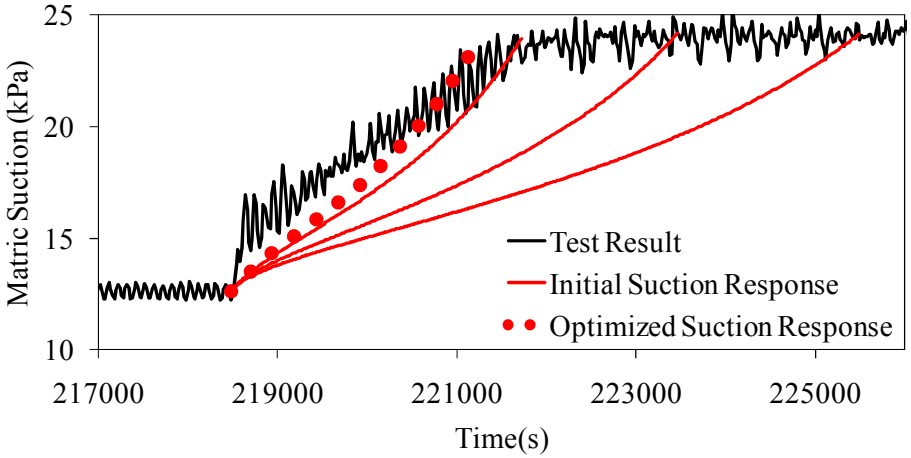

Figure 6.8. Optimization process in second withdrawal stage (Pocheon Sand, # MSM-P1)

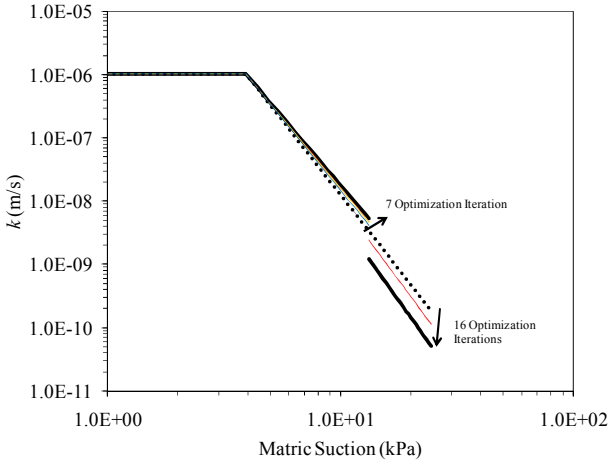

Figure 6.9. Optimization Process of the HCF corresponding to first and second withdrawal stages (Pocheon Sand, # MSM-P1)

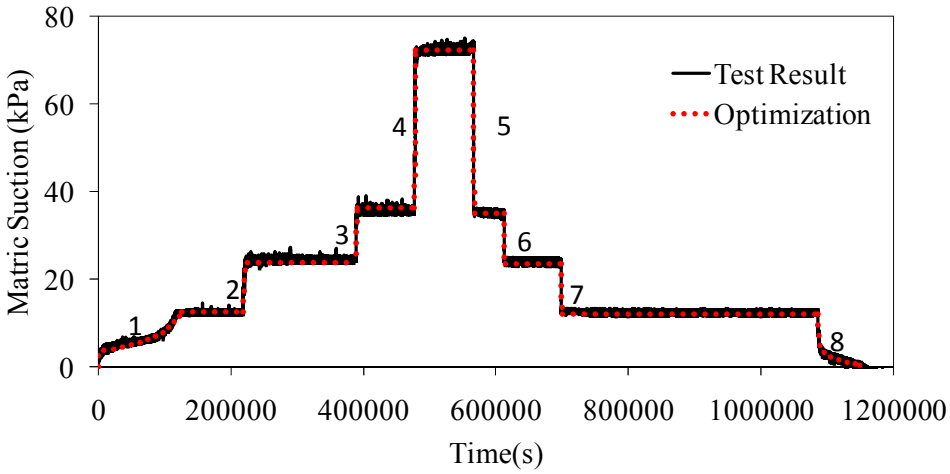

Figure 6.10. Optimization result for the HCF (Pocheon Sand, # MSM-P1)

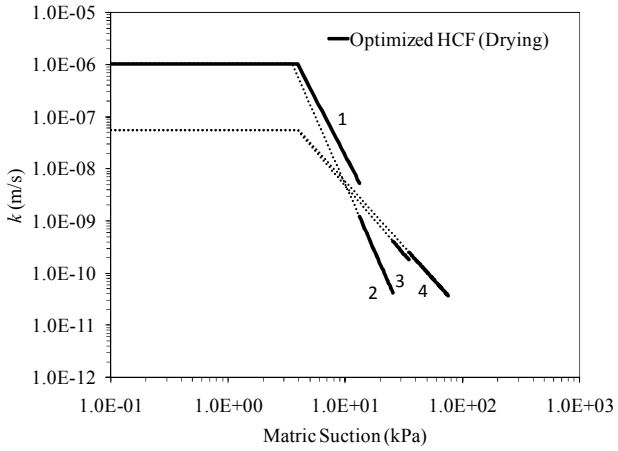

Figure 6.11. Optimized HCF during drying cycle (Pocheon Sand, # MSM-P1)

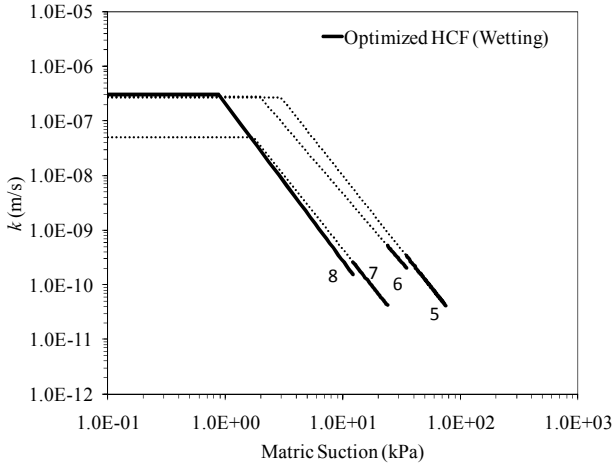

Figure 6.12. Optimized HCF during wetting cycle (Pocheon Sand, # MSM-P1)

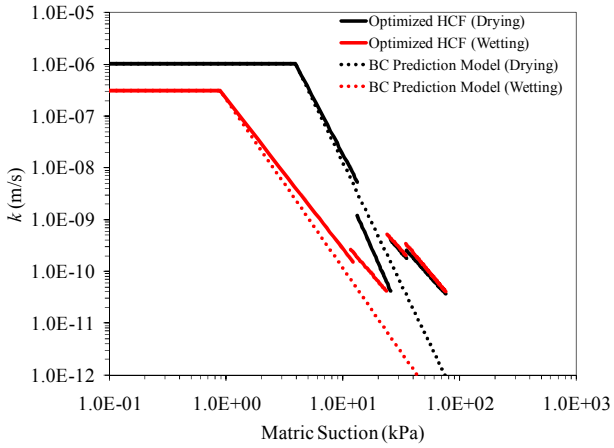

Figure 6.13. Optimized HCF corresponding to experimental suction response result (Pocheon Sand, # MSM-P1)

In same manner, the optimized HCFs of Bonny silt and F-75 Ottawa sand are obtained. Figures 6.14 to 6.17 present result for Bonny silt (#MSM-B1), and Figures 6.18 to 6.23 present result for Bonny silt (#MSM-B2). Figures 6.24 to 6.27 present result for F-75 Ottawa sand (#MSM-F1). In case of Bonny silt, optimization process of #MSM-B1 is conducted for only drying cycle because there was an error in measurement of the hydraulic conductivity value after wetting cycle due to head loss in the 3 bar HAE ceramic plate. The saturated hydraulic conductivity value measured before drying cycle is 1.2E-07 m/s, whereas the hydraulic conductivity value after wetting cycle is 1.5E-07 m/s even though the degree of saturation after wetting cycle is 84 %. This is not reasonable measurement for the hydraulic conductivity, since the hydraulic conductivity value generally decreases as the degree of saturation decreases. In test #MSM-B1, it is assumed that only saturated hydraulic conductivity value measured before drying cycle is correct. For this reason, one more analysis of the HCF for Bonny silt (#MSM-B2) is conducted. The saturated hydraulic conductivity before drying is 5.1E-08 m/s, and the hydraulic conductivity after wetting corresponding to S_r of 79% is 5.0E-09m/s, one order magnitude lower from saturated hydraulic conductivity value. This is because the hydraulic

conductivity tests before drying cycle and wetting cycle with 0.22 micron filter paper are more reasonable due to much lower head loss than in the 3 bar HAE ceramic plate, as mentioned in Chapter 4. Optimized parameter values in each analysis are presented in Appendix D.

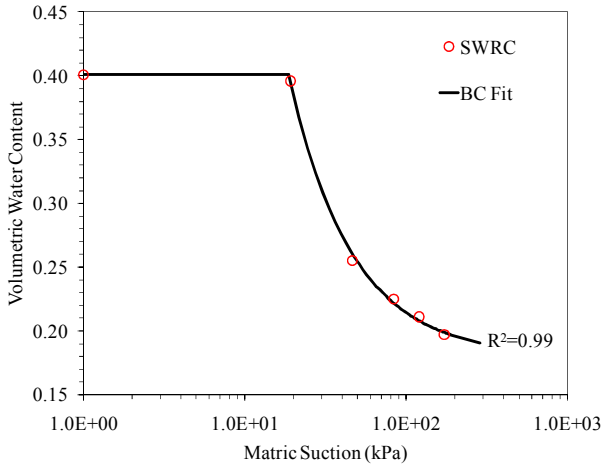

Figure 6.14. SWRC and BC fit (Bonny silt, # MSM-B1)

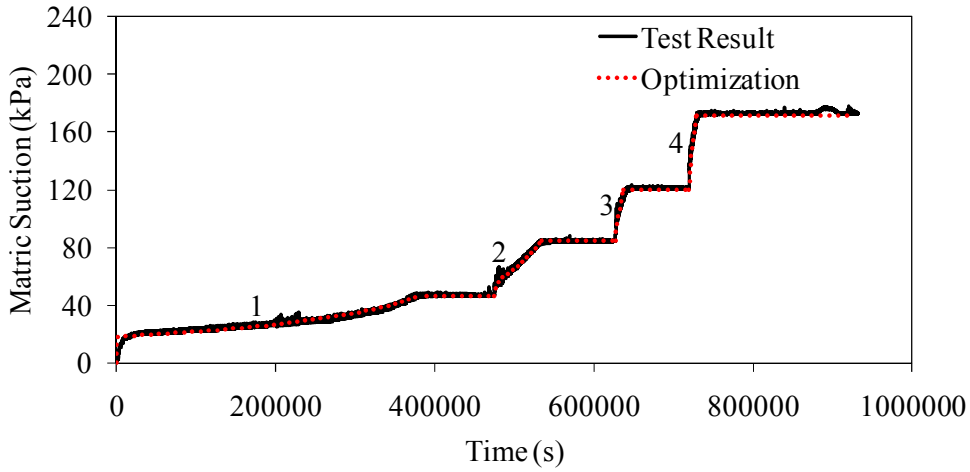

Figure 6.15. Optimization result of drying cycle for the HCF (Bonny silt, # MSM-B1)

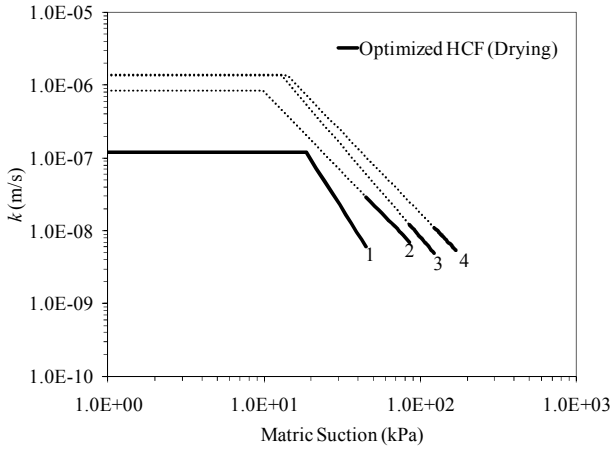

Figure 6.16. Optimized HCF during drying cycle (Bonny silt, # MSM-B1)

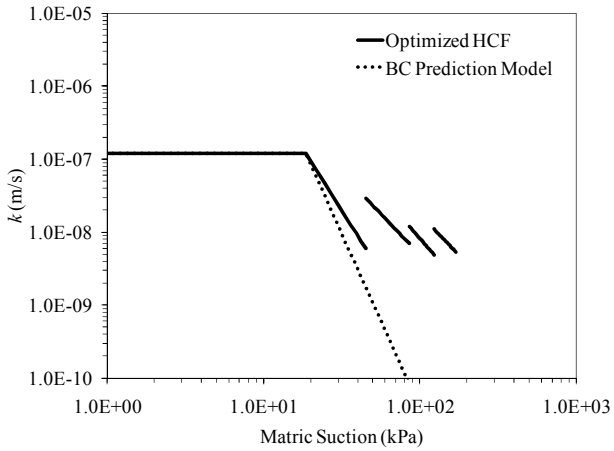

Figure 6.17. Optimized HCF corresponding to experimental suction response result (Bonny silt, # MSM-B1)

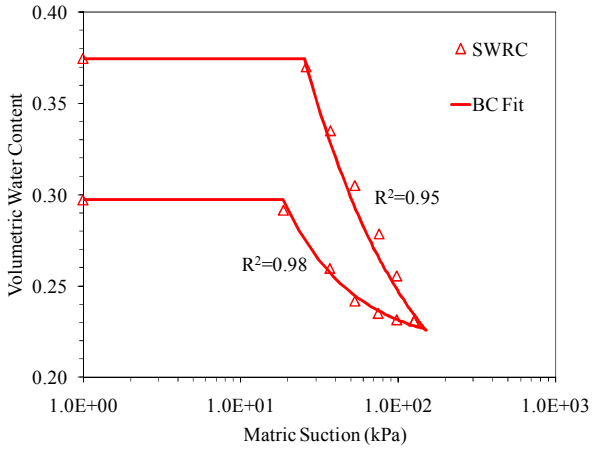

Figure 6.18. SWRC and BC fit (Bonny silt, # MSM-B2)

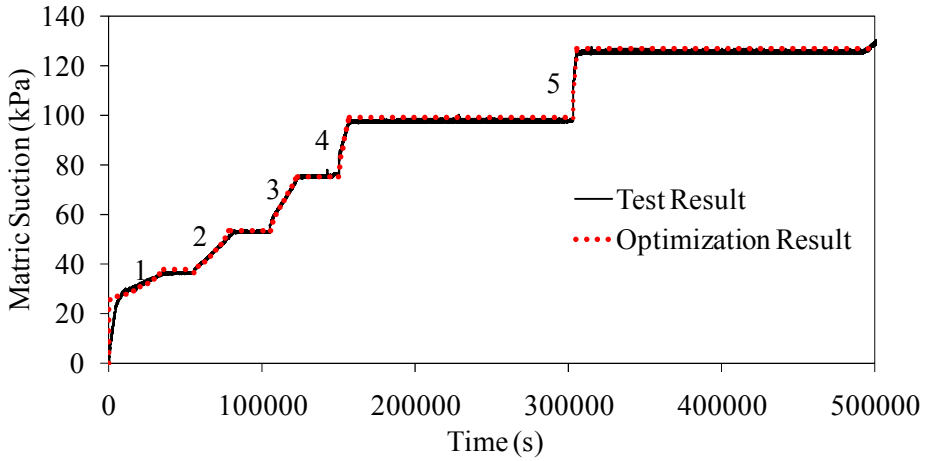

Figure 6.19. Optimization result of drying cycle for the HCF (Bonny silt, # MSM-B2)

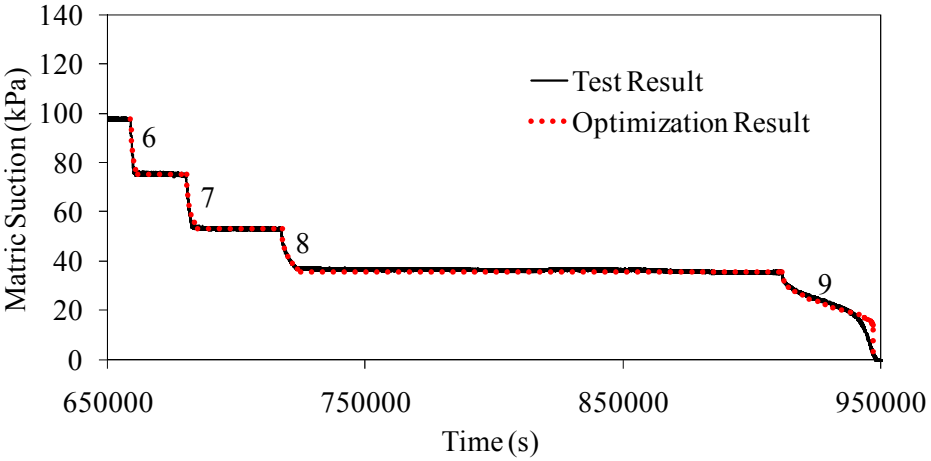

Figure 6.20. Optimization result of wetting cycle for the HCF (Bonny silt, # MSM-B2)

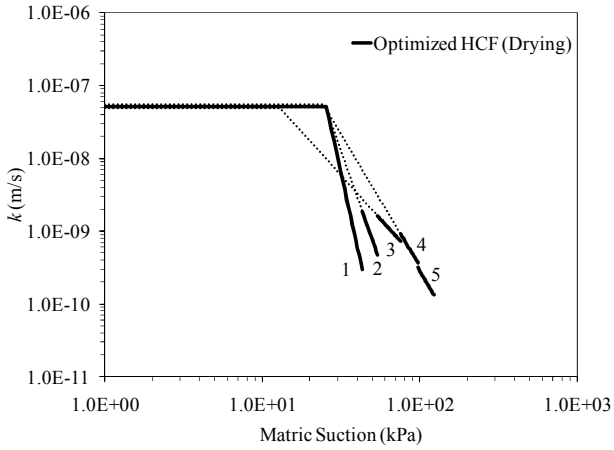

Figure 6.21. Optimized HCF during drying cycle (Bonny silt, # MSM-B2)

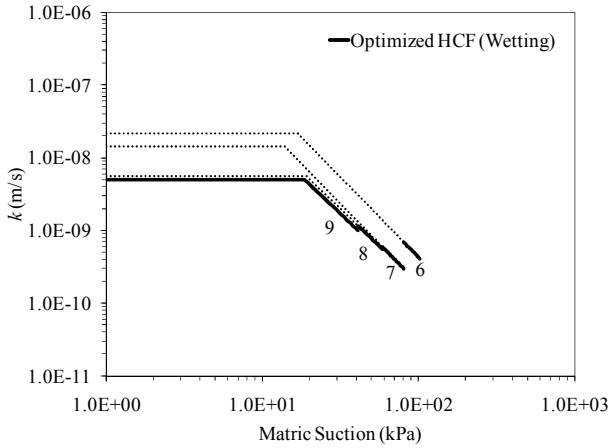

Figure 6.22. Optimized HCF during wetting cycle (Bonny silt, # MSM-B2)

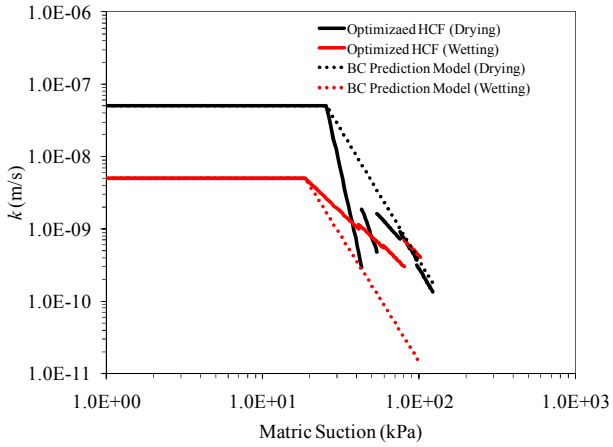

Figure 6.23. Optimized HCF corresponding to experimental suction response result (Bonny silt, # MSM-B2)

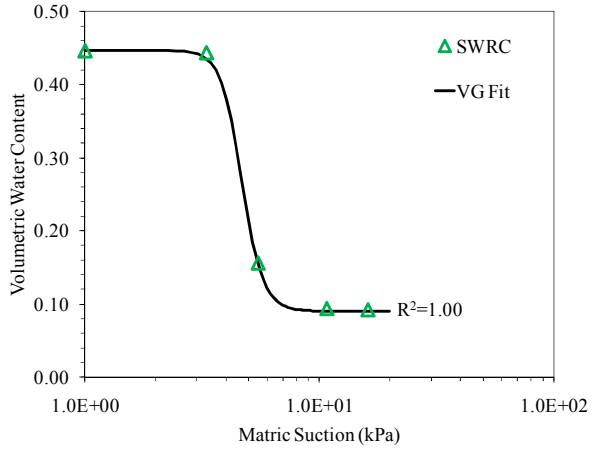

Figure 6.24. SWRC and VG fit (F-75 Ottawa Sand, # MSM-F1)

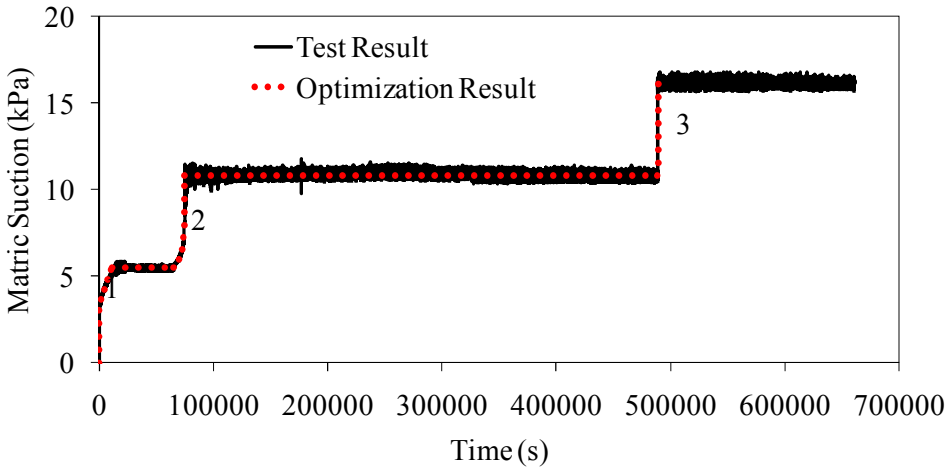

Figure 6.25. Optimization result for the HCF (F-75 Ottawa Sand, # MSM-F1)

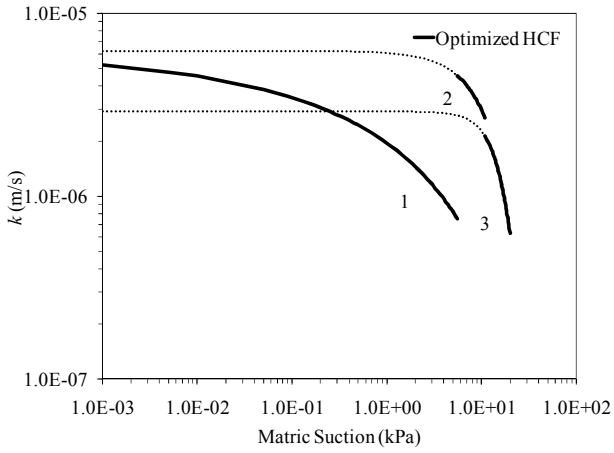

Figure 6.26. Optimized HCF during drying cycle (F-75 Ottawa Sand, # MSM-F1)

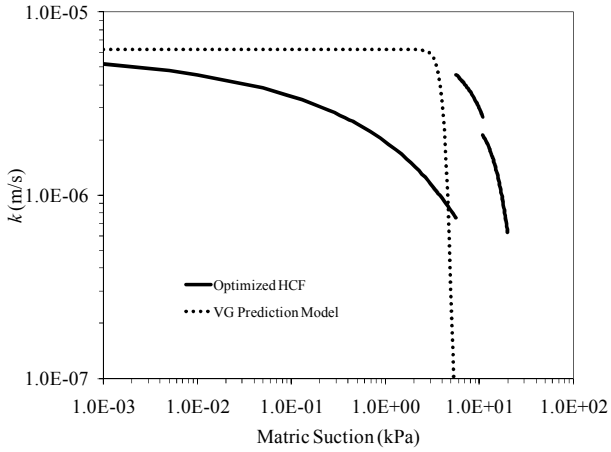

Figure 6.27. Optimized HCF corresponding to experimental suction response result (F-75 Ottawa Sand, # MSM-F1)

6.3 Discussion

6.3.1. Suction Response and SWRC

When the flow rate is applied at the bottom of the soil specimen, suction and water content profiles of soil specimen depend on the directions and the applied flow rates. In both withdrawal and infusion modes of the flow pump, the best way to measure the SWRC is applying the flow rate that is low enough with the respect to the hydraulic conductivity value at given saturation to a produce a uniform suction and water content distribution in the soil specimen. This applied flow rate is called the "*optimal flow rate*" for measurement of the SWRC using the FPS. When an optimal flow rate is applied, suction response induced by the flow pump represents the SWRC, and the suction and water content profiles of soil specimen with the optimal flow rate are uniform at different time increments, as shown in Figure 6.28. However, applying the optimal flow rate corresponding to unsaturated hydraulic conductivity is difficult for several reasons. First, the hydraulic conductivity corresponding to the given saturation is unknown before and during the test and decreases suddenly as suction increases, even though FPS allows for the change of the flow rate during testing. Also, applying the optimal flow rate at higher suction value is impossible because our FPS has a lower limit of the flow rate to apply. Recommended flow rate is saturated hydraulic conductivity at the beginning, and slower flow rate is applied as the suction increases until the lower limit of the FPS is reached. This helps to avoid the highly non-uniform water content profiles of the soil specimen during test and save time to reach the water content in equilibrium. However, this also causes prolonged testing because the suction response is very slow due to the slower flow rate, although the water content in equilibrium is reached faster in suction maintaining stage.

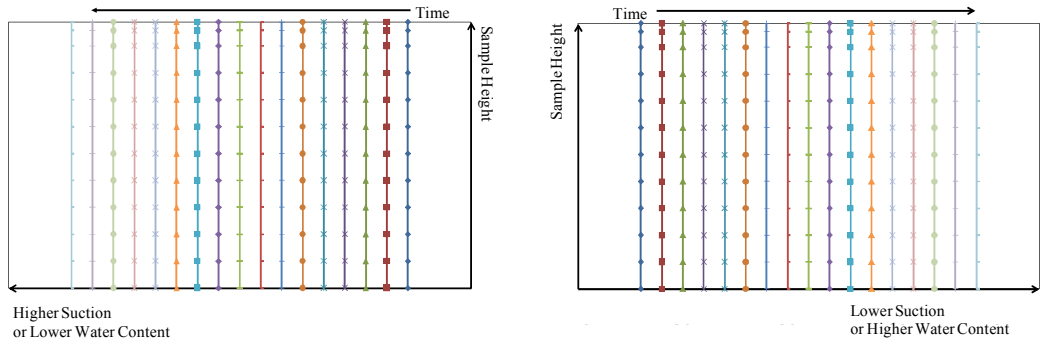

(a) (b)

Figure 6.28. Suction and water content profiles of the soil specimen in drying and wetting cycle when the optimal flow rate is applied: (a) Drying cycle; (b) Wetting cycle

In the wetting cycle, the soil is filled with water from the bottom of the soil, and the air is moved at the top of the soil. During the wetting cycle, the air entrapment suction in the SWRC of the wetting cycle is generally smaller than the air entry suction value in the SWRC of drying cycle. Also, water retained by soil during the drying process is greater than water absorbed by the soil during the wetting process at the same suction. The air entrapment suction in the wetting curve does not develop the same shape as air entry suction in the drying curve, because larger pore spaces located at the middle of the soil prevents the capillary rise from fully developing in areas of a larger radius, *R*, as shown in Figure 6.29 (a). Appendix E shows the difference between air entry suction and air entrapment suction. Also, the SWRC cannot reach full saturation, in general, because the water bypasses the smaller pore space due to a bigger pressure difference, and the smaller pores cannot be filled with water as shown in Figure 6.29 (b). In this case, air is trapped and isolated by pore water and soil skeleton, air could not move from top portion of the soil specimen. However, water can outflow from the top boundary. This phenomenon can affect the slope between zero suction and air entrapment suction in the SWRC and this slope of the SWRC becomes more horizontal, as much more air is entrapped. After water outflows from the top of the soil sample during wetting cycle (i.e. zero suction in the

wetting cycle), the degree of saturation can not be obtained and other measurement technique is needed for calculation of degree of saturation after zero suction.

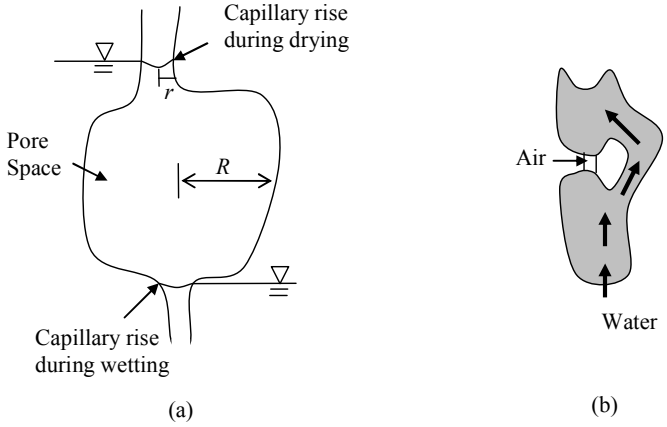

Figure 6.29. (a) Different capillary rises due to heterogeneity of the pore space distribution; (b) Drawing how air entrapment occurs in pore space after water entry value

6.3.2. HCF

From the optimization result, it is clear that the previous HCF prediction models with the parameters obtained from the SWRC equation are not valid for either the drying or the wetting cycles. Use of existing prediction models can lead to errors of several orders of magnitude, as the suction increases.

Even though the optimized HCF in the entire suction range cannot be represented with only one HCF equation, every analysis result shows that optimized HCF shows a constant tendency of hydraulic conductivity decrease with increasing suction until a certain minimal value of hydraulic conductivity is reached. In case of Pocheon sand (#MSM-P1), a minimal hydraulic conductivity is 4.2E-11 m/s with corresponding degree of saturation of 54% and suction of 25 kPa. For suctions beyond that value the optimized HCF does not show further decreases. In case of Bonny silt (#MSM-B1), a minimal hydraulic conductivity is 6.0E-09 m/s with corresponding degree of saturation of 65% and suction of 45 kPa, whereas a minimal hydraulic conductivity is

3.0E-10 m/s with corresponding degree of saturation of 82% and suction of 44 kPa in case of Bonny silt (#MSM-B2). The two soil specimens of the same material have significantly different SWRC as shown in Figure A.2. This lead to different degree of saturation values corresponding to a minimal hydraulic conductivity value. This observation of variability of SWRC and HCF requires further investigations.

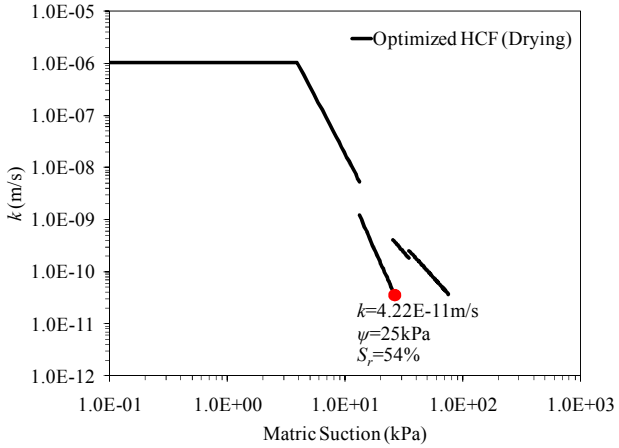

Figure 6.30. Optimized HCF during drying cycle (Pocheon sand, # MSM-P1)

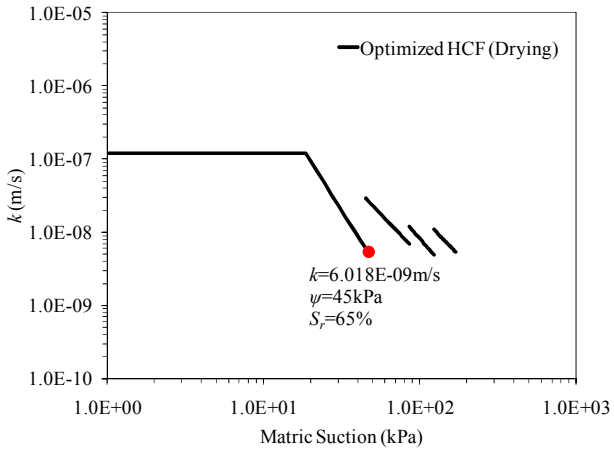

Figure 6.31. Optimized HCF during drying cycle (Bonny silt, # MSM-B1)

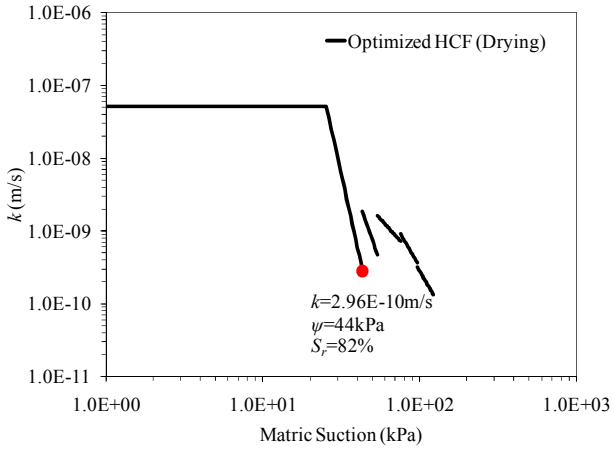

Figure 6.32. Optimized HCF during drying cycle (Bonny silt, # MSM-B2)

In case of F-75 Ottawa sand, similar pattern to Pocheon sand and Bonny silt is also observed. The hydraulic conductivity decreases until a minimal hydraulic conductivity is reached at 7.5E-07 m/s with corresponding degree of saturation of 32% and suction of 5.6 kPa. During wetting cycle in case of Pocheon sand (#MSM-P1) and Bonny silt (#MSM-B2), optimized HCFs show similar patterns to optimized HCF during drying cycle.

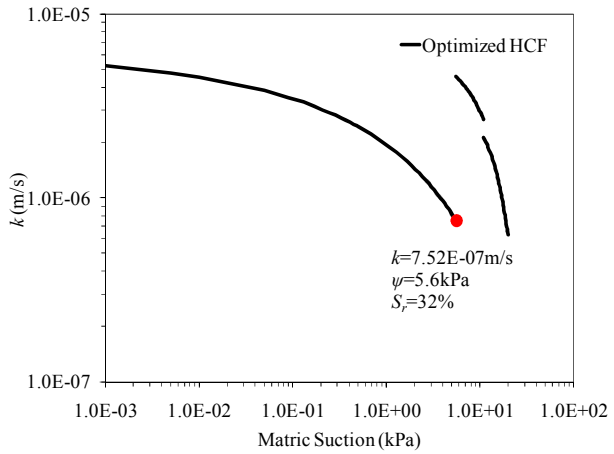

Figure 6.33. Optimized HCF during drying cycle (F-75 Ottawa sand, # MSM-F1)

Two possible explanations for such a behavior can be given. One is that our FPS is not sensitive enough to reliably control the flow and measure the suction response below certain hydraulic conductivity value. However, this is unlikely, since each soil has a different lowest

value of hydraulic conductivity such as 4.2E-11m/s for Pocheon sand, 6.0E-9 m/s for Bonny silt with higher porosity, 3.0E-10 m/s for Bonny silt with lower porosity, and 7.5E-7 m/s for F-75 Ottawa sand.

Another possibility is that water in soil does not flow as a liquid below certain hydraulic conductivity, but that the vapor-phase water flow is the primary mechanism of moisture transport at the certain hydraulic conductivity value. In general, it is known that the moisture transport change from liquid-phase water flow to vapor-phase water flow is near at the residual state (i.e., the residual water content and the residual suction of the soil). As mentioned in Chapter 2, the residual water content is defined as the water content at which suction reaches infinity (Brooks and Corey, 1964), whereas it is defined as the water content at which the slope of the SWRC and coefficient of permeability go to zero when the suction becomes large (van Genuchten, 1980). The residual water content is defined by Fredlund and Xing (1994) as the intersection of two lines, a line tangent from the inflection point of SWRC and a residual line passing through a point with suction of 10^6 kPa and zero volumetric water content, and tangent to the SWRC. The residual state suggested by Fredlund and Xing is lower than those suggested by Brooks and Corey and van Genuchten. Our analysis results show moisture transport change to vapor-phase water flow at a relatively low suction, high degree of saturation, and high hydraulic conductivity which appears to be consistent with residual state definition by Fredlund and Xing rather than those corresponding to the residual state suggested by Brooks and Corey and van Genuchten. Even though our results do not provide a definite answer to the question of transfer from liquid-water flow to vapor-phase water flow, the proposed test technique is a promising tool to address this issue in future research.

CHAPTER 7

SUCTION DROP MEASUREMENT

This chapter will review "*the method of the suction drop measurement*" developed by Hwang (2002). With the same procedure proposed in 2002 and improved flow pump capable of controlling the flow rate more precisely than in 2002, the suction response and the SWRC are obtained for both drying and wetting cycles. The SWRC from suction drop measurement is compared with the SWRC from maintained suction measurement mentioned in chapter 6. Three different materials, Pocheon sand, Bonny silt, and F-75 Ottawa sand are also used. Table 7.1 shows the porosities of each soil.

Table 7.1. Summary of materials

Test #	Soil	HAE Plate	*n* (porosity)	Purpose
SDM-P1	Pocheon sand	1-bar HAE plate	0.343	SWRC & HCF
SDM-B1	Bonny silt	3-bar HAE plate	0.406	SWRC & HCF
SDM-F1	F-75 Ottawa sand	0.8 micron filter	0.436	SWRC & HCF

7.1 Suction Response and SWRC

Pocheon sand specimen is compacted at the water content of 9.1% with 6.75 cm diameter and 5.51 cm height for #SDM-P1. Bonny silt specimen is compacted at the water content of 14% with 6.75 cm diameter and 7.71 cm height for SDM-B1. In case of F-75 Ottawa sand for SDM-F1, the soil in dry condition is poured into the mold mounted on the bottom platen, and vacuum

is applied to keep the shape of the soil specimen in the same manner as for the suction maintaining measurement.

Before beginning the suction drop measurement, every procedure is the same as the maintained suction measurement. First, the whole FPS is deaired, and, the soil specimen is fully saturated. After the fully saturated condition is accomplished, saturated hydraulic conductivity is measured by using the constant flow rate method with the head loss of HAE ceramic plate corresponding to applied flow rate. The values of saturated hydraulic conductivity in Pocheon sand, Bonny silt and F-75 Ottawa sand are 1.02E-06 m/s, 6.00E-08m/s, and 4.04E-05 m/s, respectively.

After measuring saturated hydraulic conductivity, water at top portion of equipment is replaced to air as shown in Figure 5.14. And, the flow rate is applied to the soil specimen in order to obtain the suction response and the SWRC. In order to measure the SWRC for both drying and wetting cycle, five withdrawal stages and five infusion stages are used in both cases of Pocheon sand and Bonny silt. Decreasing flow rates are applied during drying cycle as the suction increases in each stage. This is because the hydraulic conductivity in unsaturated soils becomes lower dramatically in drying cycle as the suction increases. In other words, this causes the big difference between bottom and top of the soil specimen if applied flow rate is much faster than the hydraulic conductivity corresponding to suction. Therefore, long time is needed to reach the steady state when flow pump stops, and the desired SWRC point becomes lower due to highly non-uniform suction and water content profiles of the soil specimen, even though the flow pump induces high suction response at the bottom of the soil specimen. Therefore, in order to obtain SWRC points in wide range of suction, one should be careful in choosing the appropriate flow rate in suction increasing and pressure increasing stage.

Table 7.2 and Figures 7.1 to 7.4 shows the suction drop measurement of Pocheon sand. In case of Pochen sand, the 15 times slower flow rate than saturated hydraulic conductivity is applied up to 10 kPa, and flow pump stops in order to reach the steady state. After several hours, steady state is reached at the suction of 5kPa, and this suction value and water content calculated by the volume of water pushed by the pump position is first desired SWRC point. After steady state is reached at suction of 5 kPa, flow pump restarts with 20 times slower flow rate than saturated hydraulic conductivity up to 14 kPa, and then flow pump stops. After reaching the steady state, second desired SWRC at suction 7 kPa is obtained. With same procedure, third, fourth, and fifth SWRC points are obtained at the suction of 11, 21, and 58 kPa during drying cycle, respectively. After completing drying cycle at suction of 58 kPa, the wetting cycle starts with the same procedure as the drying cycle. In wetting cycle, faster flow rate is applied as the pressure increases. Table 7.2 shows the applied flow rates corresponding to suction and pressure increasing stages. Figures 7.1, 7.2 and 7.3 show the suction response result, cumulative volume of water, and axial displacement, respectively. Figure 7.4 is the transient suction-saturation curve and SWRC converted from Figure 7.1 using Equation (5.4).

Table 7.2. Applied flow rates (#SDM-P1)

Drying Cycle Suction Range (kPa)	Pump Speed (m/s)	Flow rate (m/s)	Wetting Cycle Suction Range (kPa)	Pump Speed (m/s)	Flow rate (m/s)
0→10	2.5E-07	6.4E-08	8→1	2.5E-07	6.4E-08
5→14	2.0E-07	5.26E-08	12→3	2.5E-07	6.4E-08
7→25	1.0E-07	2.6E-08	30→5	2.0E-07	5.2E-08
11→42	1.0E-07	2.6E-08	42→11	1.5E-07	3.97E-08
21→82	8.0E-08	2.1E-08	58→30	1.0E-07	2.6E-08

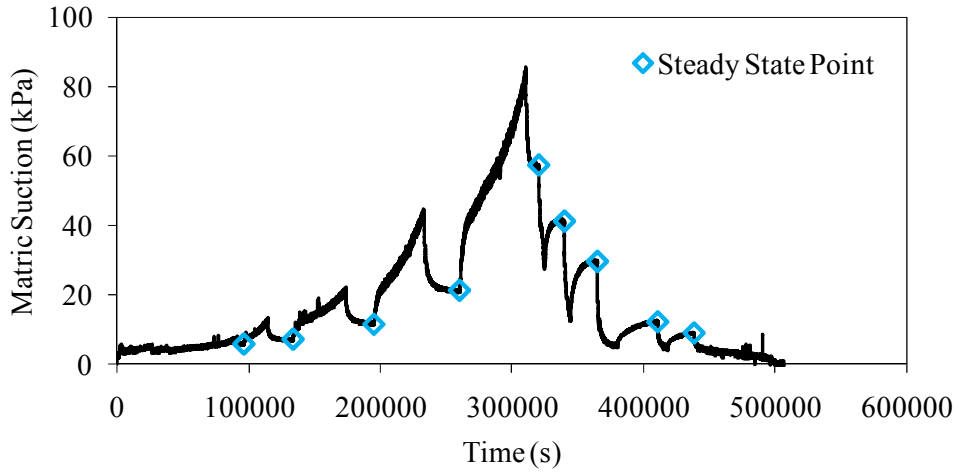

Figure 7.1. Suction response and steady state points (Pocheon Sand, #SDM-P1)

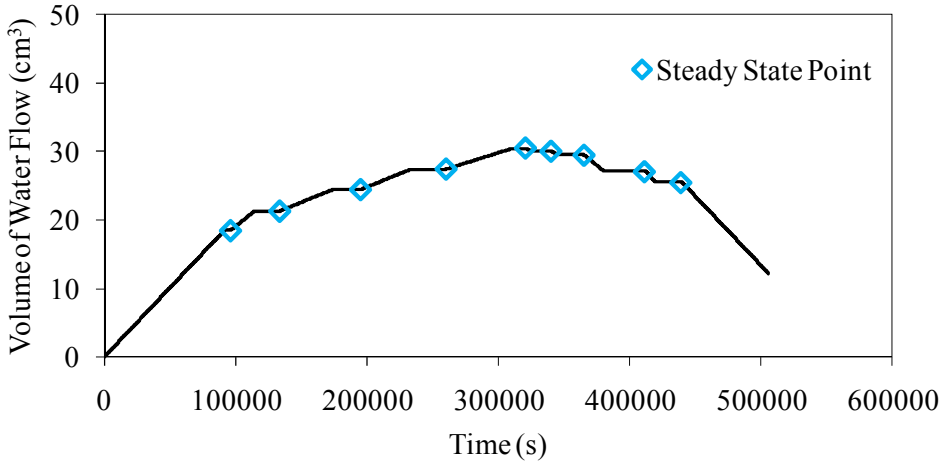

Figure 7.2. Volume of out flow during testing (Pocheon Sand, #SDM-P1)

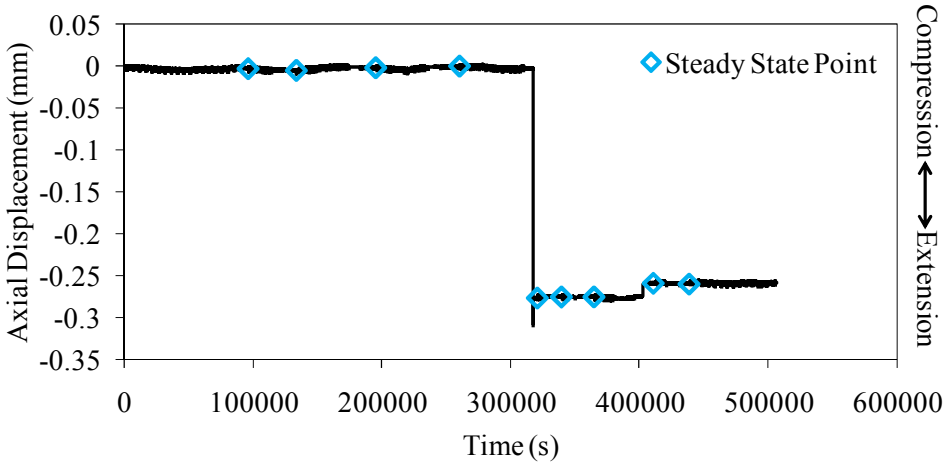

Figure 7.3. Axial displacement during testing (Pocheon Sand, #SDM-P1)

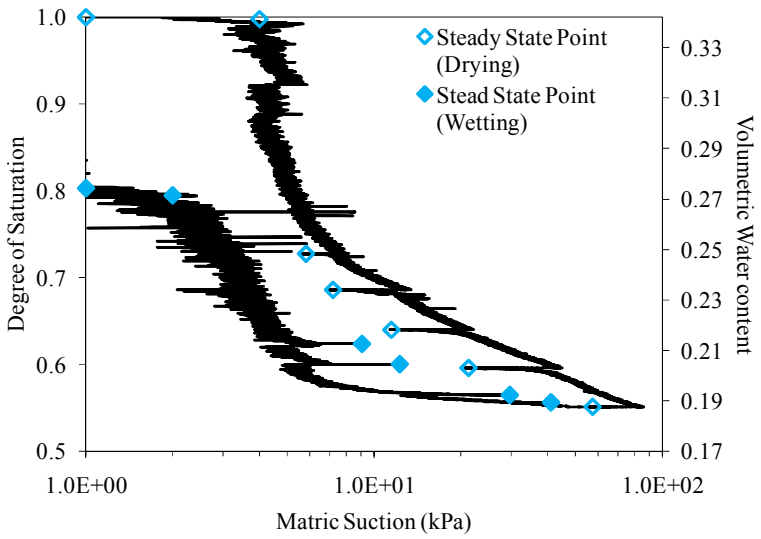

Figure 7.4. Transient suction saturation curve and steady state points (Pocheon Sand, #SDM-P1)

Table 7.3 and Figures 7.5 to 7.8 show the suction drop measurement of Bonny silt. Like Pocheon sand test, five withdrawal stages in drying cycle and five infusion stages in wetting cycle are used in case of Bonny silt. Ten times faster flow rate than saturated hydraulic conductivity is applied up to 100 kPa in first suction increasing stage, and first SWRC point is obtained at suction of 44 kPa after reaching the steady state. Other SWRC points in drying and wetting cycle are obtained in the same manner as the test of Pocheon sand. Table 7.3 shows the applied flow rates during test, and Figures from 7.5 to 7.8 show the suction response, cumulative volume change, axial displacement and transient suction-saturation curve with nine SWRC points, respectively.

Table 7.3. Applied flow rate (Bonny Silt, SDM-B2)

Drying Cycle Suction Range (kPa)	Pump Speed (m/s)	Flow rate (m/s)	Wetting Cycle Suction Range (kPa)	Pump Speed (m/s)	Flow rate (m/s)
0→100	6.0E-07	1.3E-07	46→0	6.0E-07	1.3E-07
44→150	3.0E-07	6.6E-08	62→24	4.0E-07	8.8E-08
48→172	1.5E-07	3.3E-08	90→32	2.0E-07	4.4E-08
84→184	1.0E-07	2.2E-08	120→50	1.0E-07	2.2E-08
112→194	5.0E-08	1.1E-08	134→98	5.0E-08	1.1E-08

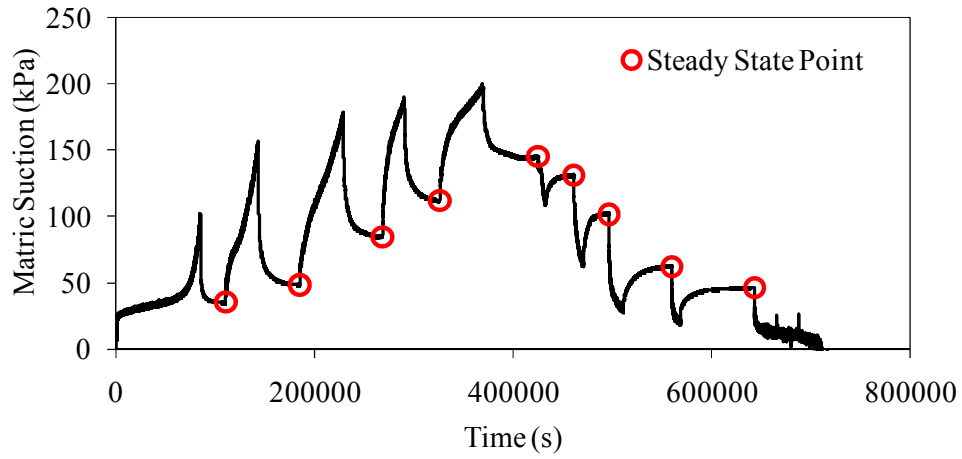

Figure 7.5. Suction response and steady state points (Bonny Silt, #SDM-B1)

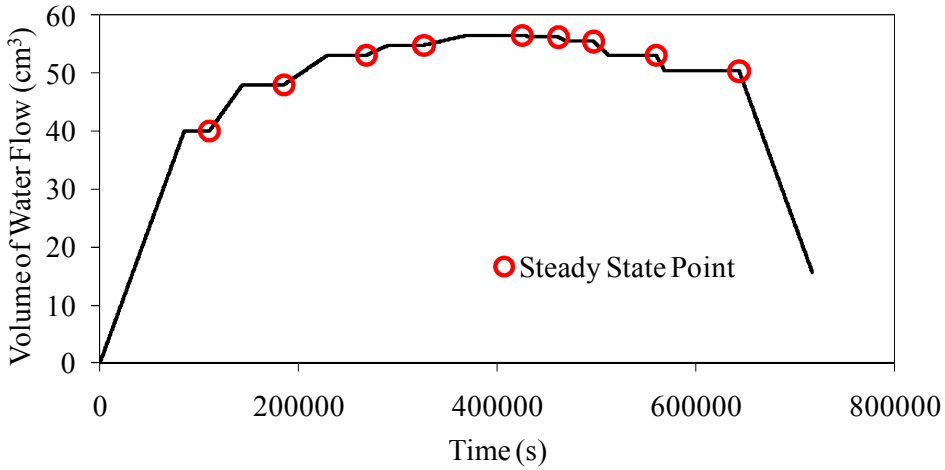

Figure 7.6. Volume of water flow during testing (Bonny Silt, #SDM-B1)

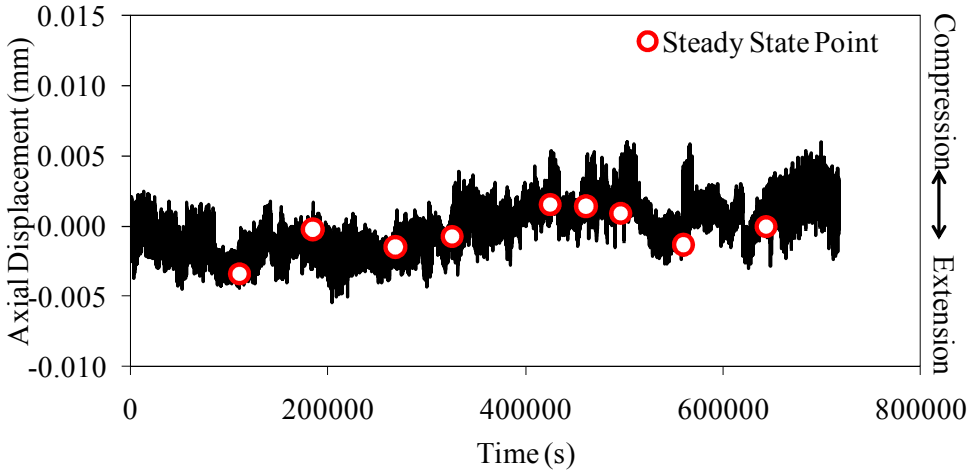

Figure 7.7. Axial Displacement during testing (Bonny Silt, #SDM-B1)

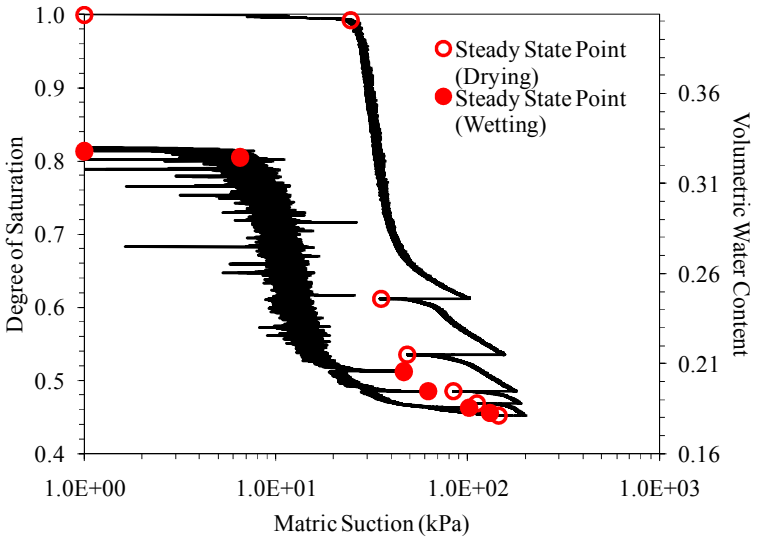

Figure 7.8. Transient suction saturation curve and steady state points (Bonny Silt, #SDM-B1)

Table 7.4 and Figures 7.9 to 7.12 show the suction drop measurement of F-75 sand Ottawa sand. In case of F-75 Ottawa sand, three withdrawal stages in drying cycle and three infusion stages in wetting cycle are conducted. Ten times slower flow rate than saturated hydraulic conductivity is applied up to 4.5 kPa in first suction increasing stage, and first SWRC point is obtained at suction of 2.67 kPa after reaching the steady state. Other SWRC points in drying and wetting cycle are obtained in the same manner. Table 7.4 shows the applied flow rates during test, and Figures from 7.9 to 7.12 show the suction response, cumulative volume change, axial displacement and transient suction-saturation curve with six SWRC points, respectively. In case of soil having a relatively uniform pore size distribution like F-75 Ottawa sand, it is difficult to obtain the SWRC from the suction drop measurement at the residual state. In general, overall slope and the shape after air entry pressure in suction response and the SWRC are relatively flatter than for well graded sand because the drainage is more rapid and the more of the pores are drained over a relatively narrow range of suction. The suction increases rapidly soon after water content reaches the residual state. However, the suction for the SWRC after

third suction withdrawal stage suddenly drops even though water content almost reaches the residual state, as shown in Figure 7.9.

Table 7.4. Applied flow rate (F-75 Ottawa Sand, #SDM-F1)

Drying Cycle Suction Range (kPa)	Pump Speed (m/s)	Flow rate (m/s)	Wetting Cycle Suction Range (kPa)	Pump Speed (m/s)	Flow rate (m/s)
0→4.5	2.0E-05	4.4E-06	2.29→0	1.0E-05	2.2E-06
2.67→5.6	1.0E-05	2.2E-06	3.61→1.72	2.0E-05	4.4E-06
2.87→26.23	5.0E-06	1.1E-06	6.24→3.3	4.0E-05	8.8E-06

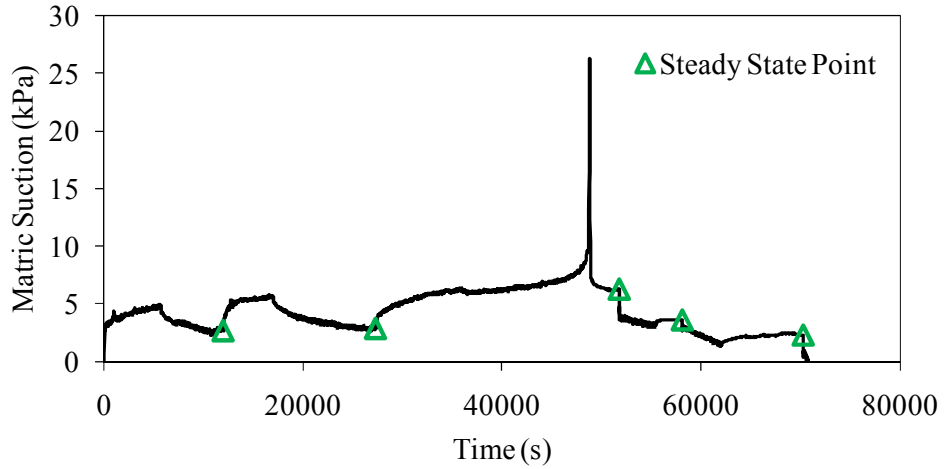

Figure 7.9. Suction response and steady state points (F-75 Ottawa Sand, #SDM-F1)

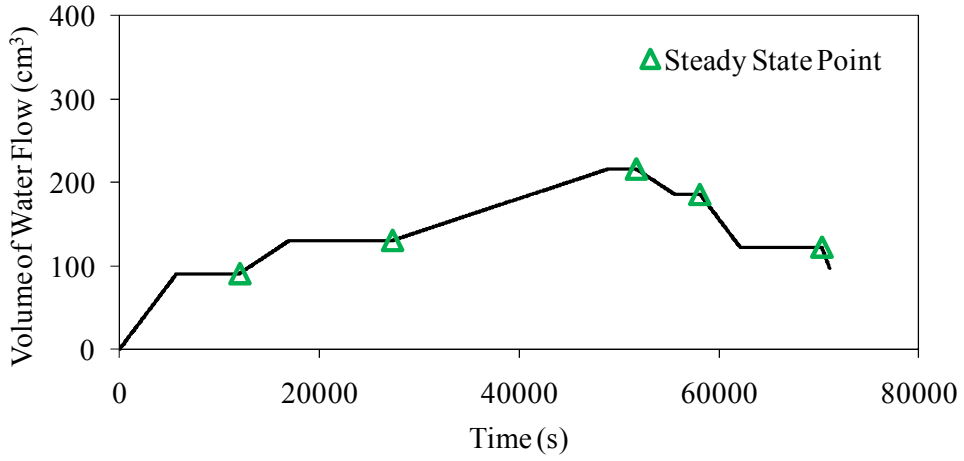

Figure 7.10. Volume of out flow during testing (F-75 Ottawa Sand, #SDM-F1)

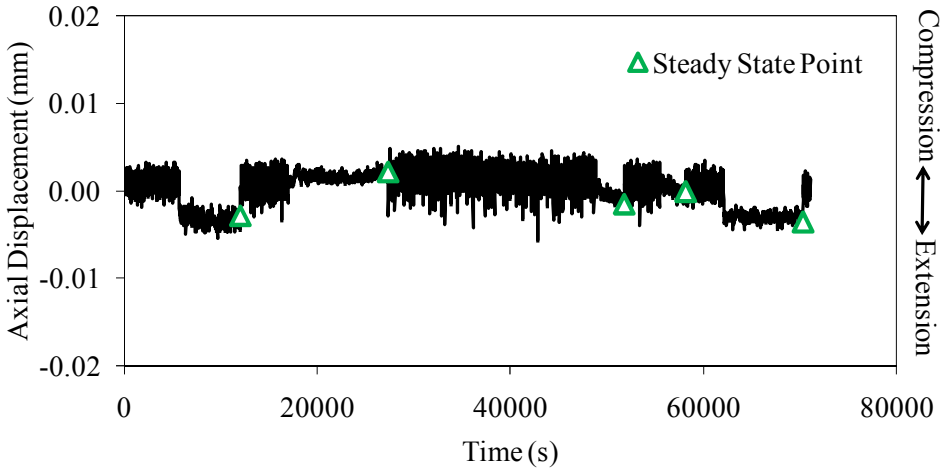

Figure 7.11. Axial Displacement during testing (F-75 Ottawa Sand, #SDM-F1)

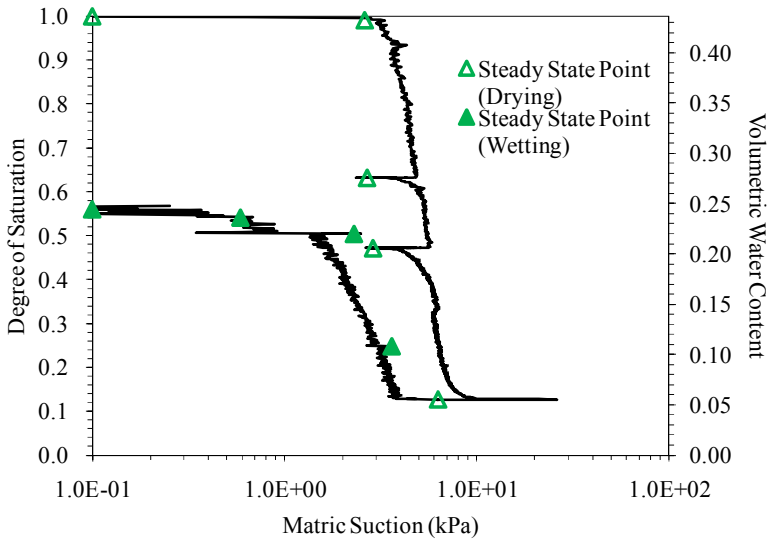

Figure 7.12. Transient suction saturation curve and steady state points (F-75 Ottawa Sand, #SDM-F1)

7.2 Discussion

Figures 7.13 to 7.18 show comparisons of experimental results between suction drop measurement and maintained suction measurement in each soil. SWRCs in each soil from two measurement techniques show discrepancy between two measurement techniques. There are several kinds of reasons. Even though porosities of two soil specimens in each soil are similar to each other and the same net confining stress is used for tests, it is guessed that each soil

specimen has a different soil structure. In addition, two different equilibration methods in two measurement techniques also cause the difference between two SWRCs from two measurement techniques. In suction drop measurement, hysteretic process exists during suction drop and pressure drop stage when the flow pump stops. For example, wetting process is dominated at the bottom of the soil specimen, whereas drying process is dominated at bottom during suction drop stage. This can affect the determination of the SWRC, since hydraulic characteristics between drying and wetting cycles are significantly different from each other. This also leads to different axial displacement results during testing, even though axial displacement during testing is negligible in measured SWRC. In case of Bonny silt, the height of soil specimen decreases with increasing suction during drying cycle, whereas the height increases slightly during wetting cycle in maintained suction measurement, as shown in Figure 6.3 (b). However, the height of soil specimen increases slightly during test in suction drop measurement, as shown in Figure 7.7. Other cases with Pocheon sand and F-75 Ottawa sand also show different axial displacements between two measurement techniques during testing.

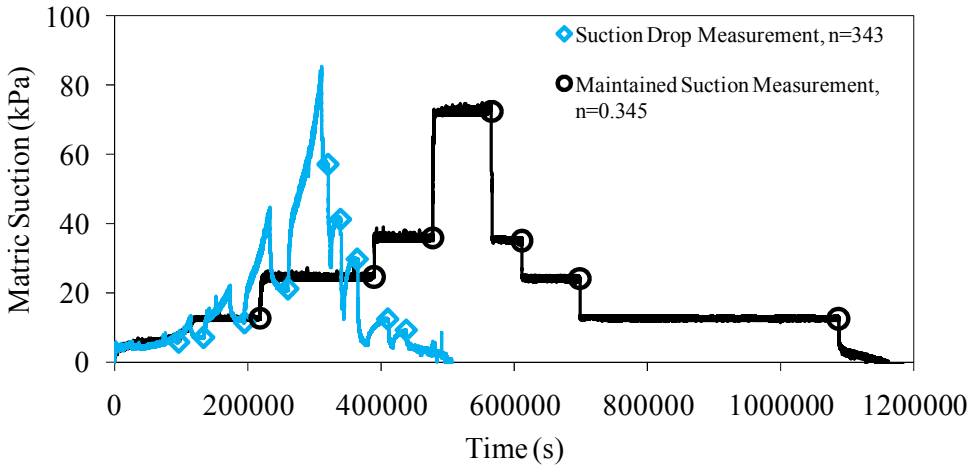

Figure 7.13. Comparison of suction response between suction drop measurement and maintained suction measurement (Pocheon sand)

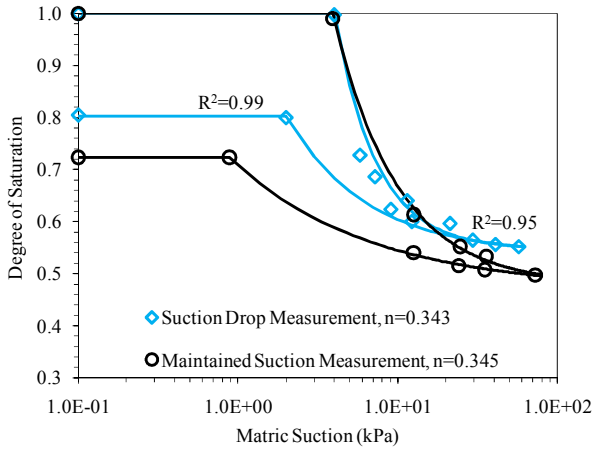

Figure 7.14. Comparison of SWRC between suction drop measurement and maintained suction measurement (Pocheon Sand)

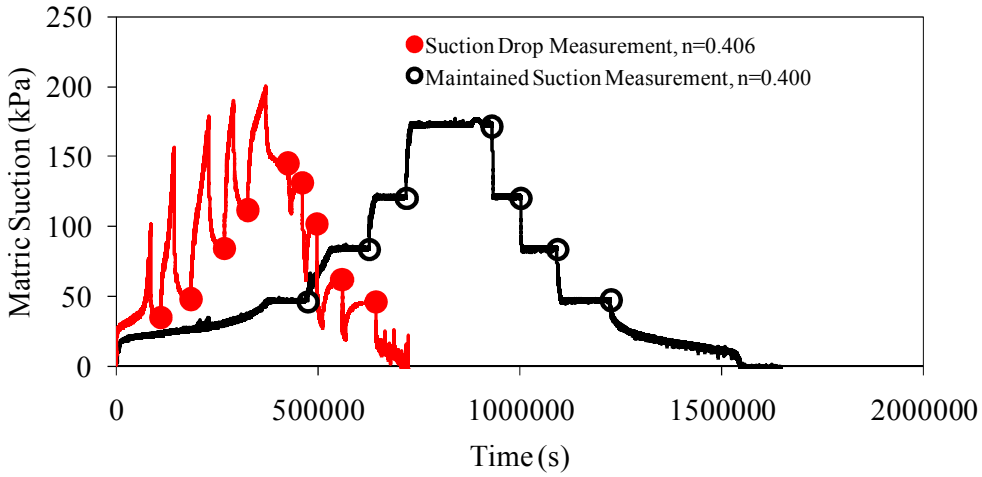

Figure 7.15. Comparison of suction response between suction drop measurement and maintained suction measurement (Bonny Silt)

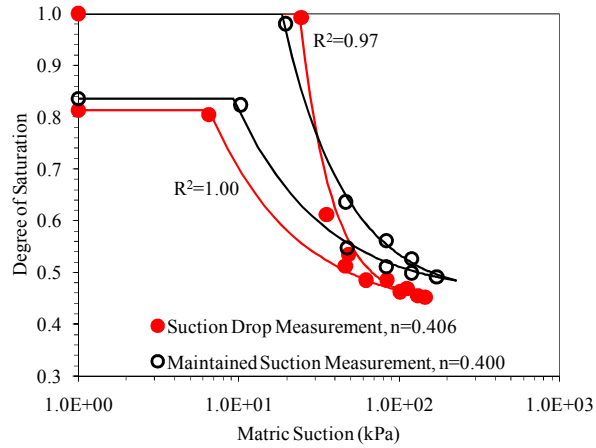

Figure 7.16. Comparison of SWRC between suction drop measurement and maintained suction measurement (Bonny Silt)

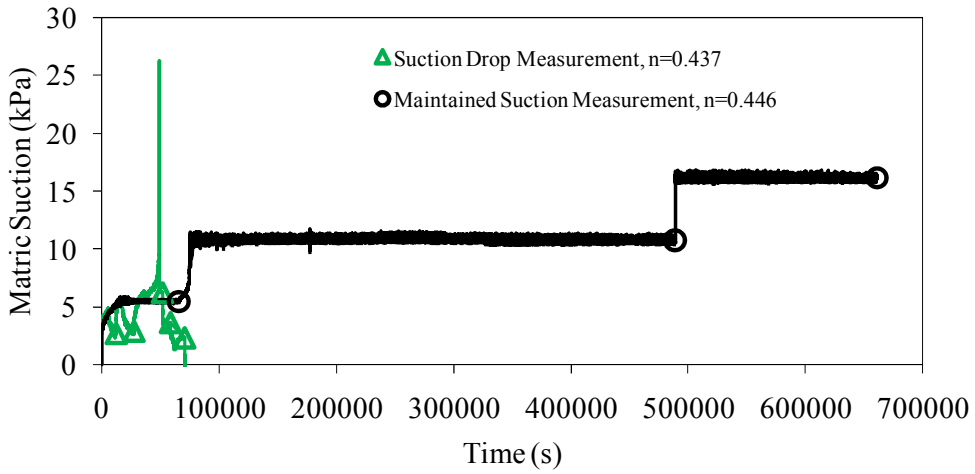

Figure 7.17. Comparison of suction response between suction drop measurement and maintained suction measurement (F-75 Ottawa sand)

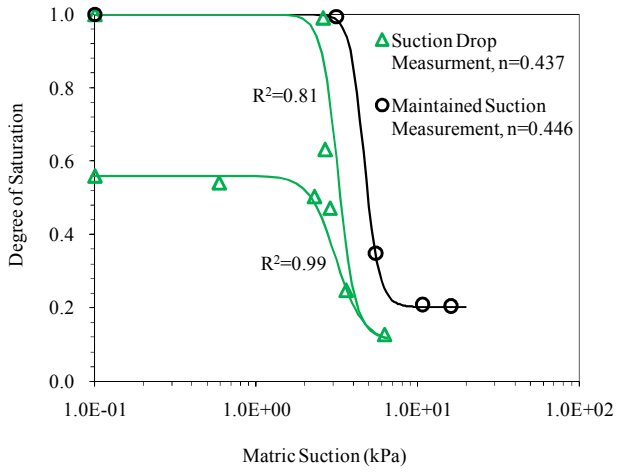

Figure 7.18. Comparison of SWRC between suction drop measurement and maintained suction measurement (F-75 Ottawa sand)

In Chapter 6, it was expected that the limit of moisture transport between liquid-phase water flow and vapor-phase water flow takes place at certain hydraulic conductivity value from inverse analysis for the HCF. The values of suction and degree of saturation corresponding to the limit in each soil were 25 kPa and 54% for Pocheon sand 45 kPa 65% for Bonny silt, and 5.6 kPa and 32% for F-75 Ottawa sand in maintained suction measurement, respectively. The suction increase induced by the flow pump during drying cycle in suction drop measurement exceeded these limits. As shown in Figures 7.1 and 7.5, the slopes of suction response after fourth

withdrawal stage of Pocheon sand and second withdrawal stage of Bonny silt show gradual decreases in the rate of suction increases. This means that the hydraulic conductivity does not decrease with increasing suction. Therefore, it is expected that the hydraulic connection between top and bottom of the soil specimen is broken and vapor-phase water flow is dominated in fourth withdrawal stage of Pocheon sand and second withdrawal stage of Bonny silt in suction drop measurement. For these reasons, suction drop measurement is not appropriate for determination of the SWRC, since our test analysis uses only liquid-phase water flow and measurement of the suction response. In addition, it is difficult to simulate suction drop stage numerically due to existing hydraulic hysteresis during suction drop stage.

CHAPTER 8

INFILTRATION TEST IN UNSATURATED SOILS

In order to simulate the infiltration phenomenon in the laboratory, the FPS is modified form Figures 4.1 to 4.2. In infiltration test with unsaturated soil specimen, the atmospheric air pressure and negative water pressure are used instead of the pore air pressure and pore water pressure. Before the infiltration test with unsaturated soil sample, several initial suction tests are conducted to obtain the SWRC with high air entry ceramic plate. Tensiometer is also used to measure the initial suction in order to validate the initial suction test result. Table 8.1 shows the summary of the soil specimens used for infiltration test.

Table 8.1. Summary of infiltration test

Test #	Soil	HAE Plate	*n* (porosity)	Purpose
IT-B1	Bonny silt	0.5-bar HAE plate	0.393	SWRC & HCF
IT-B2	Bonny silt	0.5-bar HAE plate	0.401	Pressure response

8.1 Initial Suction Test

Before the infiltration test with unsaturated soil sample, several initial suction tests are conducted using the basic apparatus of initial suction, as shown in Figure 4.3. Figures 8.1 and 8.2 show the initial suction test results with nine different water content soil specimens. Figure 8.1 presents four initial suction test result using bottom platen including its own high air entry value ceramic plate which has small pores of relatively uniform size. Figure 8.2 shows the initial

suction test result with five different water content soil specimen using the saturated 0.5 bar HAE ceramic plate. Figure 8.3 shows the initial suction test result with three different water content soil specimens using the tensiometer. Each height of soil sample is between 6 cm and 7 cm, and the time required to reach equilibrium becomes longer, as the initial volumetric water content becomes lower, as shown in Figures 8.1 and 8.2.

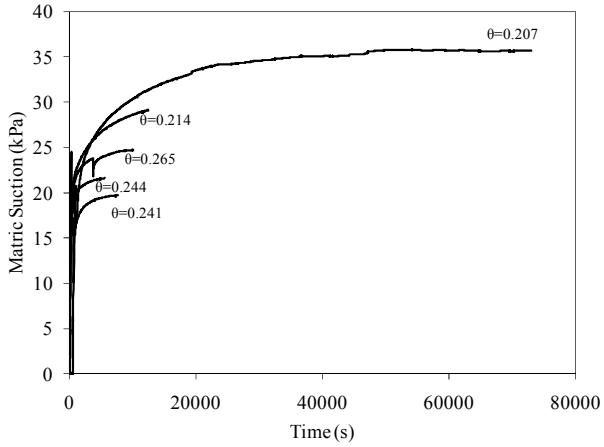

Figure 8.1. Initial suction test

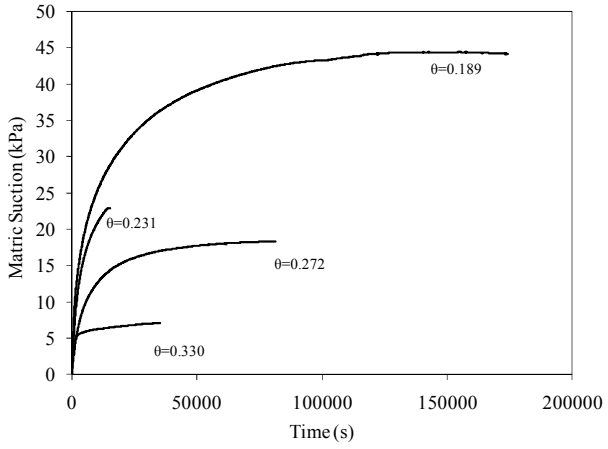

Figure 8.2. Initial suction test before infiltration test

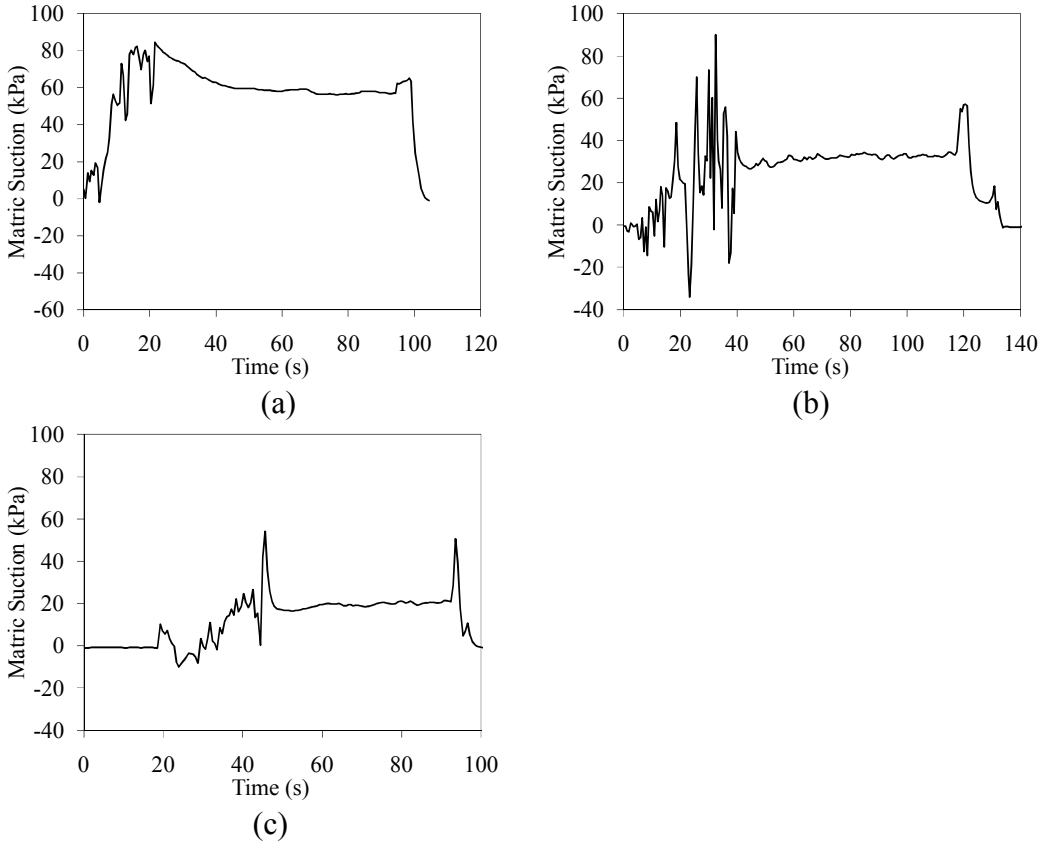

Figure 8.3. Tensiometer test with three different water contents: (a) θ=0.202; (b) θ=0.255; (c) θ=0.313

Figure 8.3 shows tensiometer test result with three different water content soil specimens, and Figure 8.4 shows the SWRC from the initial suction values with different water contents in comparison with previous initial suction test result (Bicalho, 1999) and tensiometer test result. In case of the tensiometer test, the initial suction values corresponding to the water contents are a little higher than the other initial suction tests. This is because soil specimens are exposed to air and not prevented to loose the water content from evaporating when tensiometer is placed in the soil specimen. Also, when the tensiometer inserted into the soil specimen, it was very difficult to screw deep into soil specimen because the soil specimens were already compacted before putting tensiometer into soil specimen. These lead to less reliable suction measurements. Therefore, the initial suction result by using the tensiometer is neglected in later analysis.

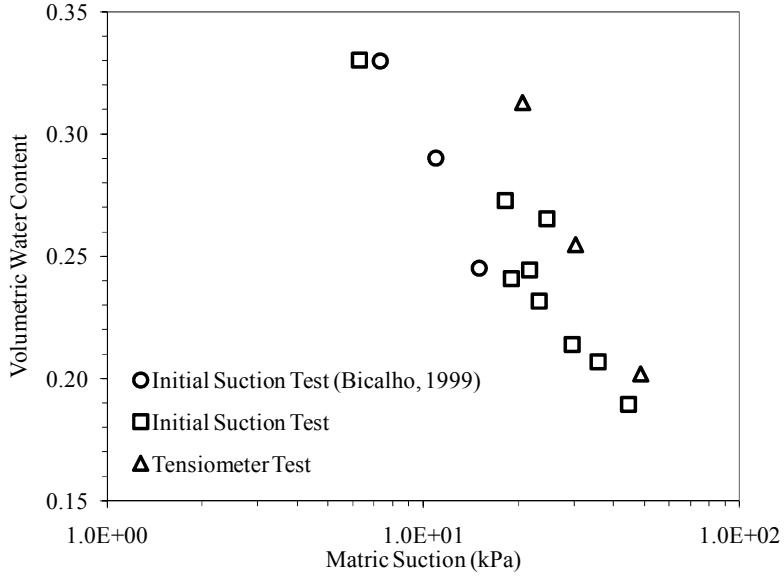

Figure 8.4. SWRC (Initial Suction Test)

8.2 Infiltration Test in Unsaturated Soils

Two soil specimens are compacted at water content of 15% with 6.38 cm height and 6.75 cm diameter for test #IT-B1 and with 6.44 cm height and 6.75 cm diameter for test #IT-B2. Figure 8.5 shows two infiltration test results. After each soil sample is placed on the saturated ceramic plate, equilibrium is reached at the suction of 21.7kPa between the sample and ceramic plate at 8100 seconds for #IT-B1 and 18.63 kPa at 8680 seconds. In #IT-B1, infiltration test begins at suction of 21.7 kPa with the flow rate of 2.2E-07 m/s (pump speed=1E-06 m/s). In test #IT-B2, infiltration test starts with the flow rate of 2.2E-07 m/s at suction of 18.63 kPa and twice faster flow rate, 4.4E-07 m/s is applied at suction of 12.11 kPa.

Figures 8.5 and 8.6 show the infiltration test result. In #IT-B1, water reaches the top of the soil sample at about 29150 seconds. The pump position at this time is 20.03 mm, and the volume of water pushed by flow pump is 15.86 cm^2. The degree of the saturation at this time is 79.9% when water reaches the top of the soil sample. From 29150 seconds, top porous stone begins saturation and water begins to flow out from top platen at 35830 seconds when top porous stone is saturated. At 39000 seconds, water reaches the empty bottle on the scale. After

completing infiltration test, the hydraulic conductivity value, 7.62E-08 m/s corresponding to degree of the saturation of 79.9% was obtained with three different constant flow rates. In #IT-B2, water reaches the top of the soil sample at about 19000 seconds. The pump position at this time is 16.33mm, and the volume of water pushed by flow pump is 12.93 cm^2. Due to twice faster flow rate, suction response in #IT-B2 reaches zero at 18500 seconds faster than test #IT-B1. The degree of saturation at this time is 74.0% when water reaches the top of the soil sample. From 19000 seconds, top porous stone begins saturation and water begins to flow out from top platen at 22350 seconds when top porous stone is saturated. At time of 24330 seconds, water reaches the empty bottle on the scale. After completing infiltration test, the hydraulic conductivity value, 7.32E-08 m/s corresponding to degree of the saturation of 74.0% was obtained with seven different constant flow rates. The comparison between the measured volume of outflow on the scale and the volume of water induced by flow pump is shown in Figure 8.7.

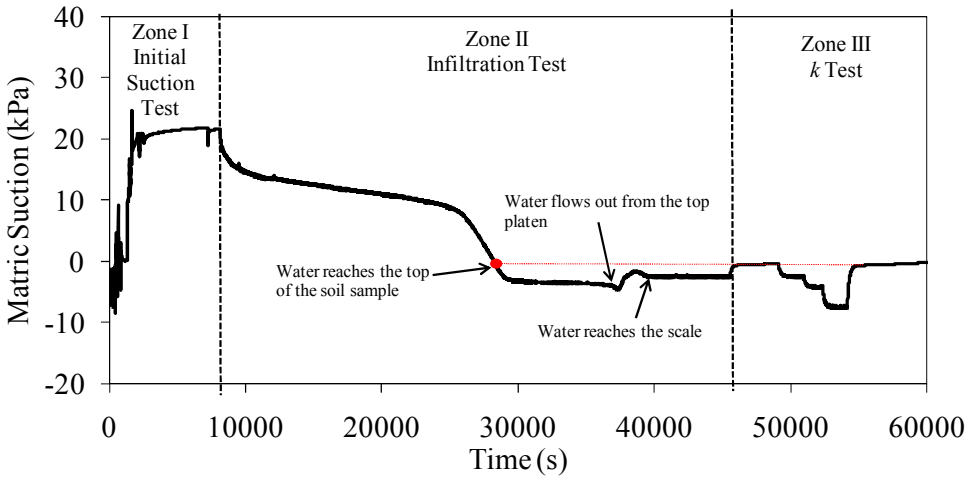

Figure 8.5. Infiltration test results in unsaturated soils (#IT-B1, n=0.393 and infiltration rate=2.2E-07 m/s)

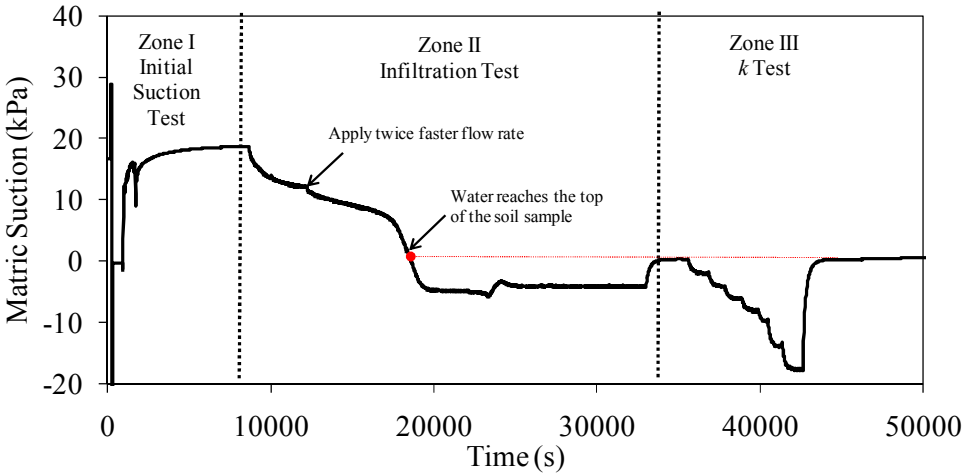

Figure 8.6. Infiltration test results in unsaturated soils (#IT-B2, n=0.40 and infiltration rate=2.2E-07 m/s and 4.4E-07 m/s)

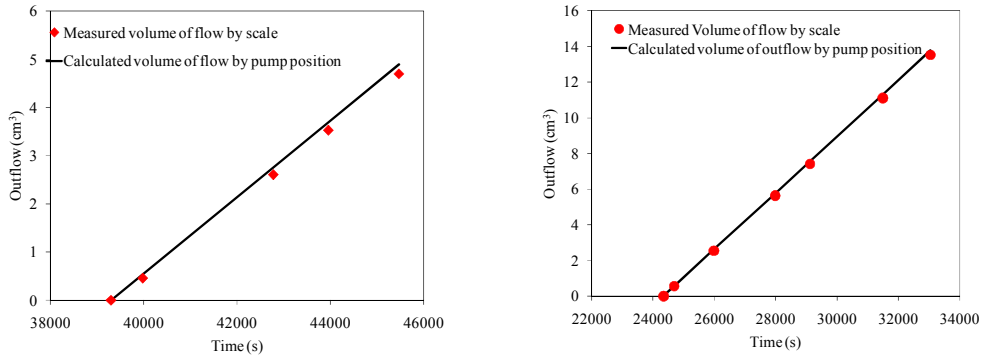

(a) (b)

Figure 8.7. Volume of outflow: (a) #IT-B1; (b) #IT-B2

8.3 Analysis for SWRC and HCF

The goal of this approach is to find the SWRC and HCF corresponding to the infiltration test result. For analysis, test #IT-B1 result is used. In test #IT-B1, water started flowing from top of the soil specimen at degree of the saturation of 79.9%. Volumetric water content and hydraulic conductivity corresponding to degree of the saturation of 79.9% are 0.314 and 7.62E-08 m/s, respectively. Therefore, SWRC in test #IT-B1 starts at the volumetric water content of 0.31 at suction of 0 kPa. Even though air entrapment pressure of about 10 kPa is observed from the infiltration test, air entrapment pressures in both SWRC and HCF models are considered as the curve fitting parameter for more precise optimization. In this analysis, the SWRC and the

HCF are optimized simultaneously, and BC model and VG model are used for representation of the optimized SWRC and HCF. In this analysis with UNSAT-H and PEST, experimental result for optimization is used only between flow pump starting point (i.e., initial suction value) to air occlusion pressure, since UNSAT-H leads to sudden drop of matric suction after air entrapment pressure. Also, the lower limit and upper limit for the optimization of SWRC with BC fit or VG fit are set up on the basis of initial suction test result, as shown in Figure 8.8 and 8.9. This is because PEST leads to lower residual water content value and flatter slope in the SWRC than the initial suction test result and different pressure response from the experimental pressure response, since the air entrapment pressure is considered as the curve fitting parameter and the experimental pressure response is used only from initial suction value to air entrapment pressure for optimization. Trial and error method is also used with SEEP/W in order to obtain the SWRC and HCF data corresponding to infiltration results.

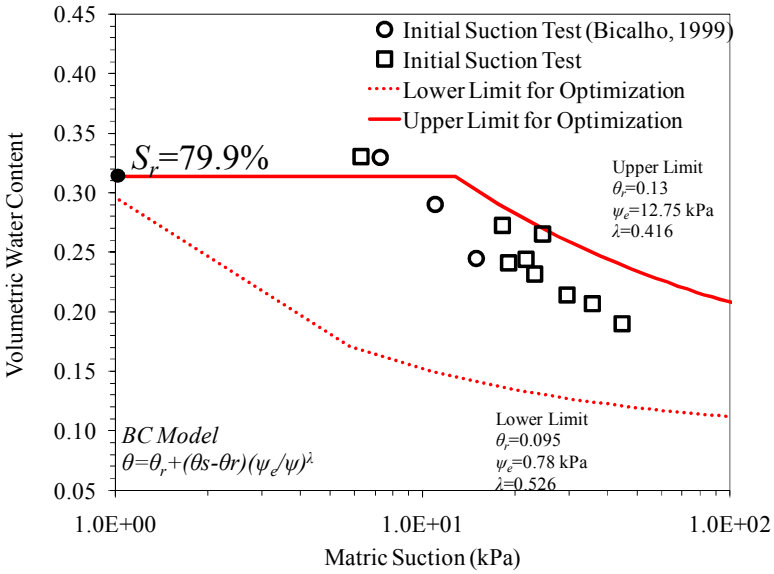

Figure 8.8. Lower and upper parameter limits for the optimization of SWRC BC fit

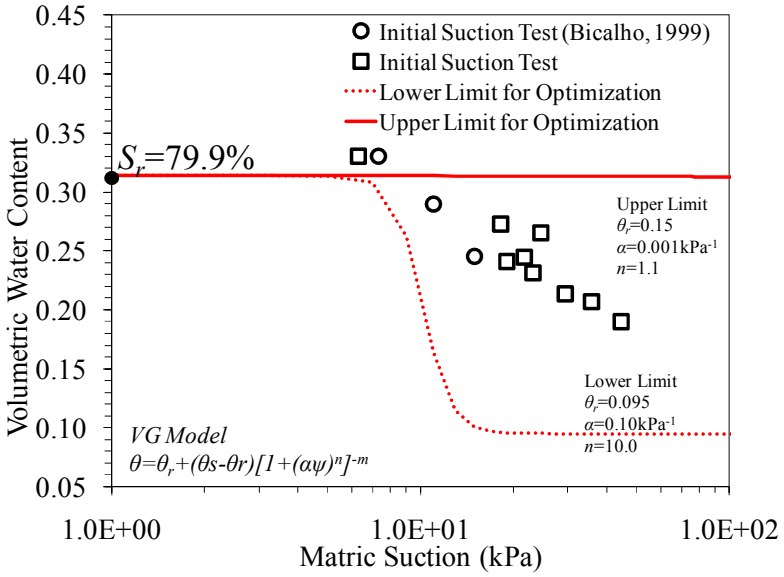

Figure 8.9. Lower and upper parameter limits for the optimization of SWRC VG fit

Figures 8.10 and 8.11 show the optimization result using BC model and Figure 8.12 and 8.13 show the optimization result using VG model. The optimized curve fitting parameters in each model are presented in Appendix D. Figures 8.14 and 8.15 show the result using a trial and error with SEEP/W until data points of the SWRC and the HCF matches the infiltration test result. Figure 8.16 shows the proper SWRCs of each analysis in comparison with the initial suction test, and Figure 8.17 shows the proper HCFs of each analysis. Even though there are little discrepancy between each SWRC and initial suction result, the HCFs in each analysis show some discrepancy among one another, as shown in Figure 8.17. This leads to the different matric suction and water content profiles of soil specimen at different time increments.

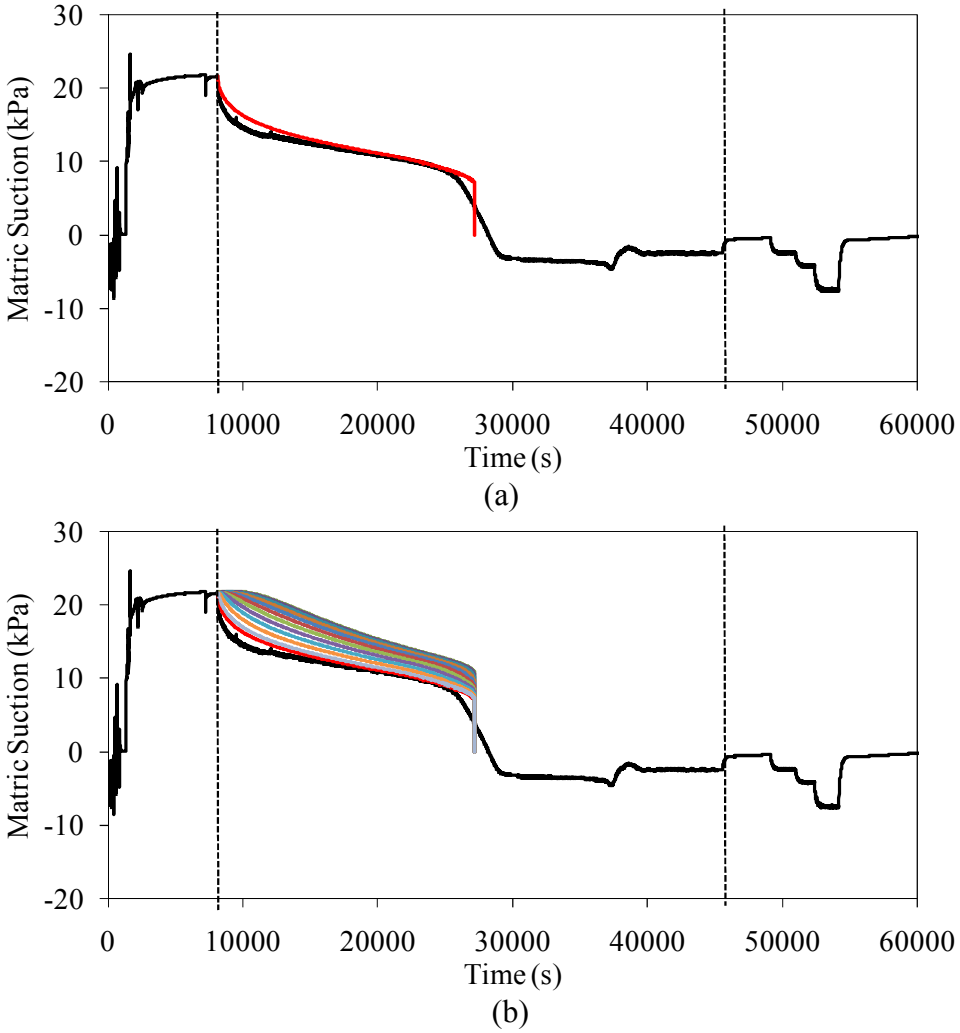

Figure 8.10. Optimization result using BC model (Bonny silt, #IT-B1): (a) Result at the bottom of the soil specimen; (b) Result at each layer of the soil specimen

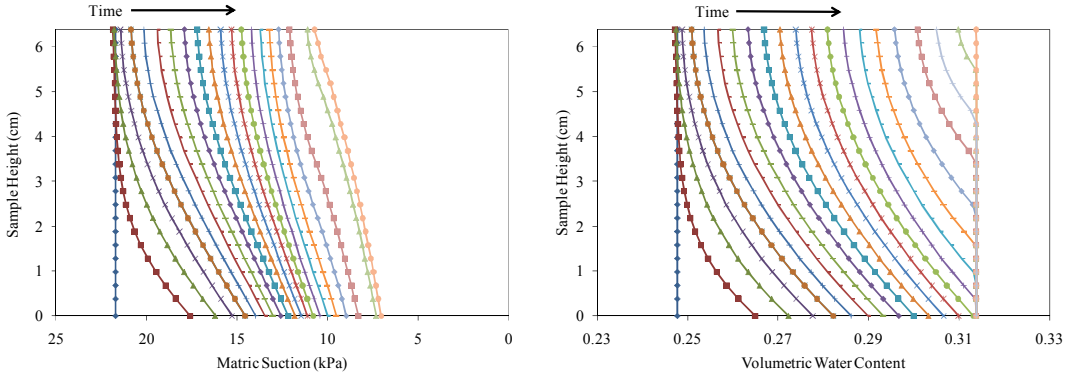

Figure 8.11. Matric suction and volumetric water content profiles at different time increments with BC model corresponding to infiltration test result (Bonny silt, #IT-B1)

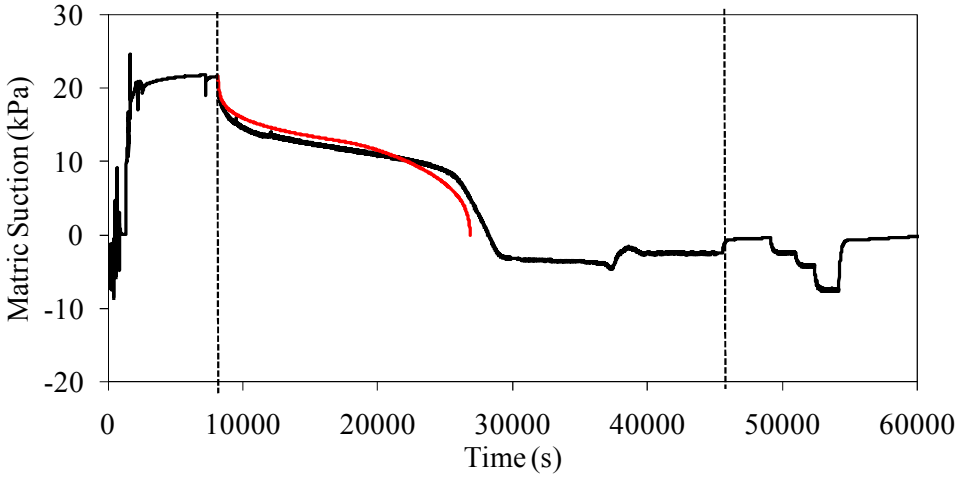

(a)

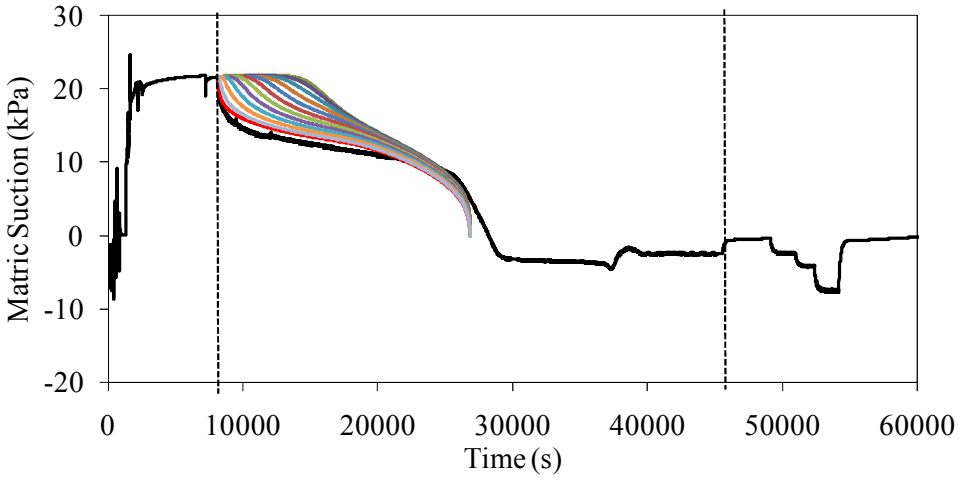

(b)

Figure 8.12. Optimization result using VG model (Bonny silt, #IT-B1): Result at the bottom of the soil specimen; (b) Result at each layer of the soil specimen

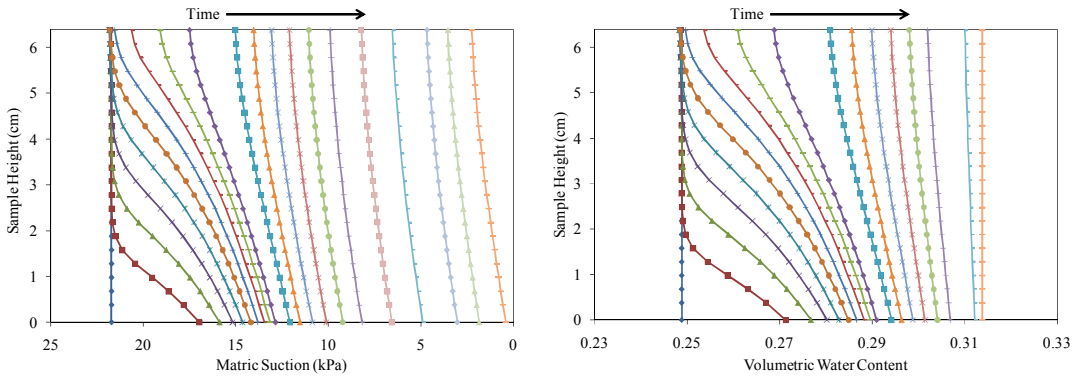

Figure 8.13. Matric suction and volumetric water content profiles at different time increments with VG model corresponding to infiltration test result (Bonny silt, #IT-B1)

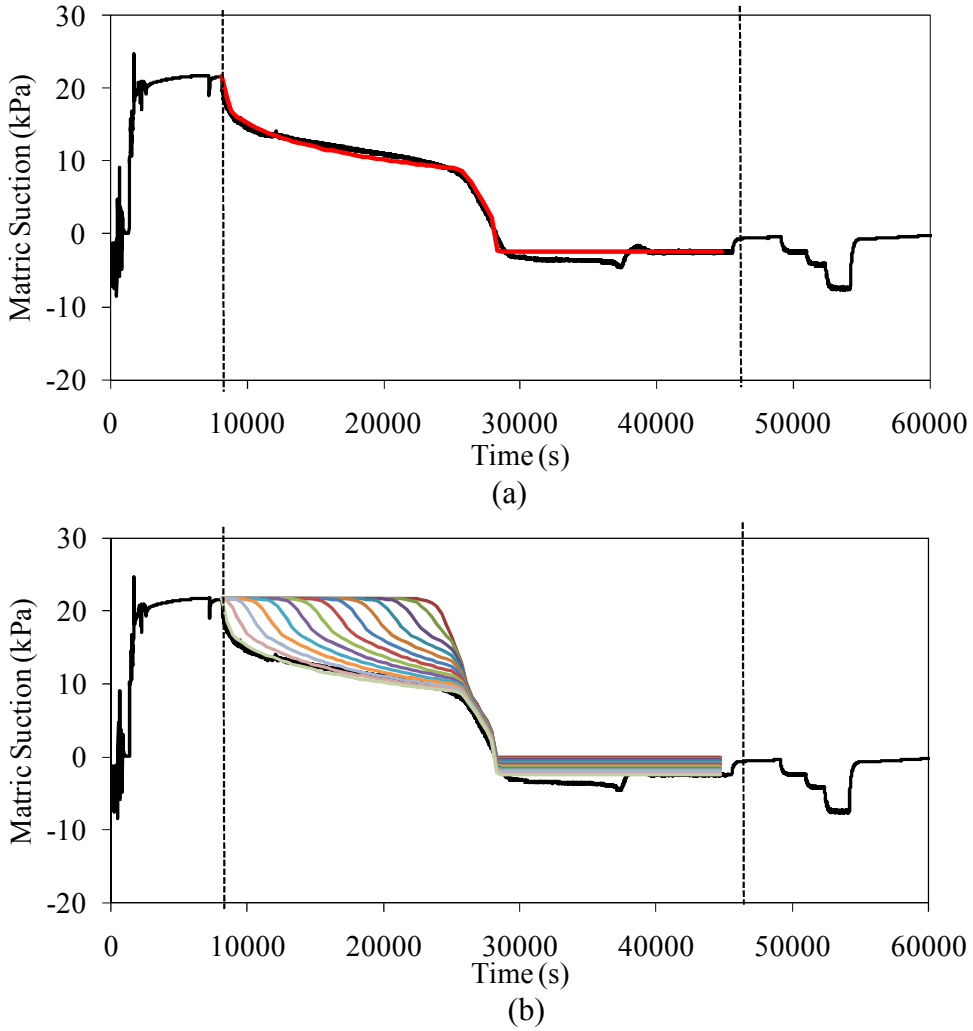

Figure 8.14. Trial and error method for the proper SWRC and HCF using SEEP/W (Bonny silt, #IT-B1) : Result at the bottom of the soil specimen; (b) Result at each layer of the soil specimen

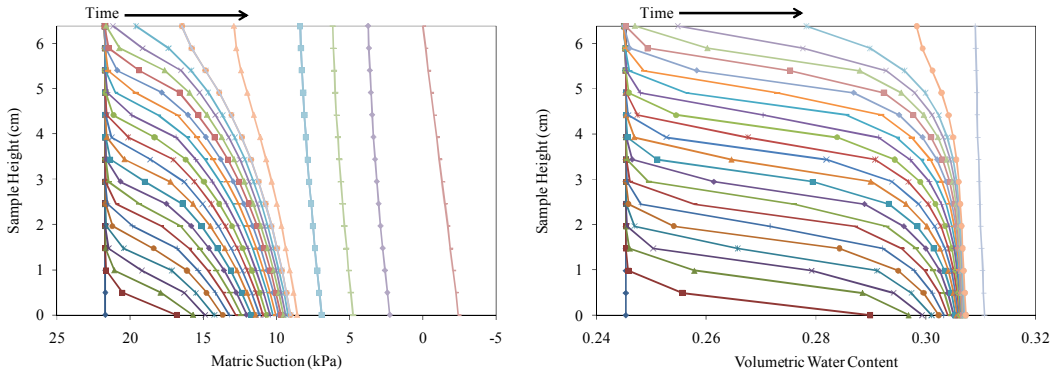

Figure 8.15. Matric suction and volumetric water content profiles at different time increments with the proper SWRC and HCF data points corresponding to infiltration test result (Bonny silt, #IT-B1)

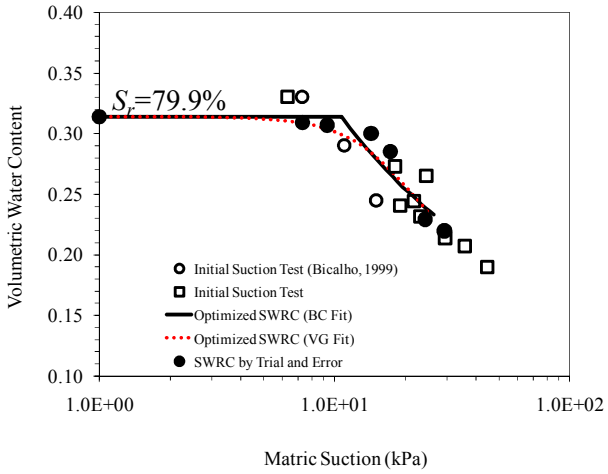

Figure 8.16. Proper SWRC using optimization (Bonny silt, #IT-B1)

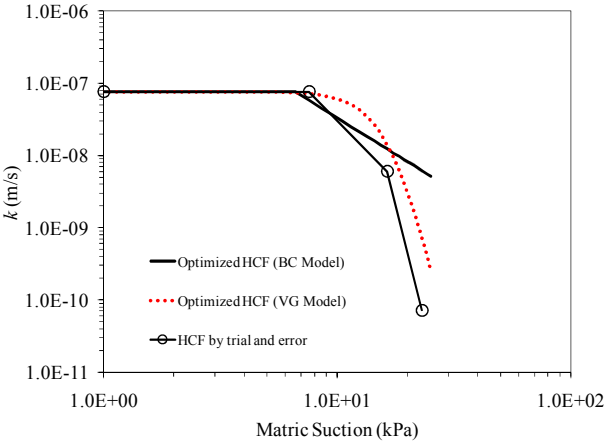

Figure 8.17. Proper HCF using optimization (Bonny silt, #IT-B1)

8.4 Discussion

From test result, it is concluded that our FPS is also appropriate for infiltration test without the proceeding of drying cycle. The optimized SWRC in infiltration test is based on the initial suction test result. This is because the initial suction test is also based on the wetting cycle. In other words, the soil specimen is placed on the saturated HAE ceramic plate, and then the soil specimen leads to draw water from the saturated HAE ceramic plate to soil specimen. In order to validate the optimized SWRC, optimized SWRC from infiltration test is compared with the SWRC of wetting cycle from the suction feedback control loop measurement (Test #MSM-B1)

due to the similar porosity. Even though the degree of saturation corresponding to suction of 0 kPa is different from each other by about 4 %, the air occlusion value of optimized SWRC is the same as for the SWRC of wetting cycle in test #MSM-B1, as shown in Figure 8.18. Also, optimized SWRC shows the similar tendency to SWRC of maintained suction measurement up to initial suction value of 21.7 kPa of test #IT-B1. Since test #MSM-B1 used 3 bar HAE ceramic plate and the hydraulic conductivity value is not available, the optimized HCF of infiltration test is compared with the HCF of wetting cycle from test #MSM-B2 which has porosity of 0.375. Figure 8.19 shows the comparison of the HCF between test #IT-B1 and #MSM-B2. Figure 8.19 shows a significant difference in hydraulic conductivity for two bonny silt specimens at similar degree of saturation. As it was shown in Figure 4.10, different Bonny silt specimens show high sensitivity of the hydraulic conductivity value due to minor changes in porosity, which may explain difference observed in Figure 8.19.

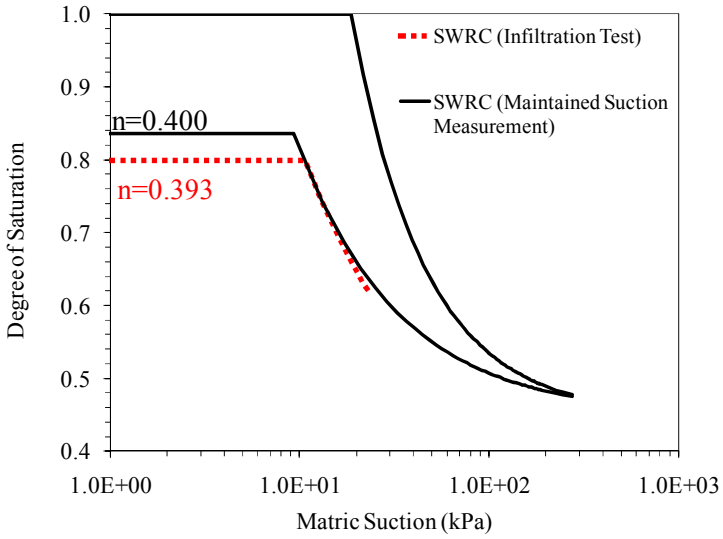

Figure 8.18. Comparison of optimized SWRC BC fits between infiltration test (#IT-B1) and maintained suction measurement (#MSM-B1)

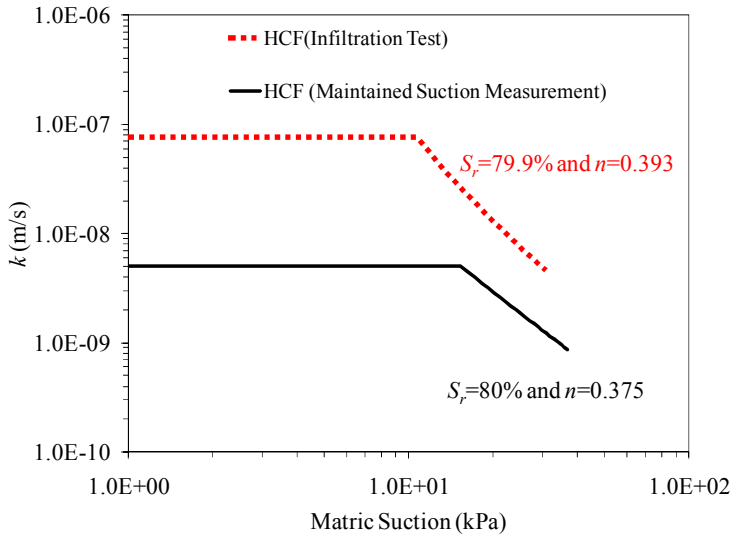

Figure 8.19. Comparison of optimized HCF BC fit between infiltration test(#IT-B1) and maintained suction measurement (#MSM-B2)

CHAPTER 9

SUMMARY, CONCLUSIONS, AND RECOMMENDATIONS

9.1 Summary

The goals of this research were to observe water flow in unsaturated soils, to measure the SWRC by using a new FPS technique with suction-feedback control loop, and to evaluate the proper HCF corresponding to suction response using an inverse problem solution approach. The summary of this research is as follows.

- Three types of soils such as, two well graded sands, and a uniform sand were chosen as the test materials.
- The head loss of fine filter papers and HAE ceramic plates are considered in measuring the suction response, the SWRC, and hydraulic conductivity.
- A new experimental methodology, "*Maintained Suction Measurement*" was developed to measure the suction response and the SWRC using a conventional triaxial equipment and axis translation technique.
- A previous experimental methodology, "*Suction Drop Measurement*" developed by Hwang in 2002 was reviewed and used for measuring the suction response and the SWRC in order to compare with the results from maintained suction measurement.
- The proper HCF in each soil was evaluated by using an inverse problem solution approach with measured suction response and the SWRC. UNSAT-H and PEST

programs were used for optimization process, and the BC and VG HCF prediction models were used to represent the proper HCF.

- One more experimental methodology, "*Infiltration Test*" was developed to measure the pressure response without precedence of drying cycle and to evaluate the SWRC and the HCF. The proper SWRC and HCF were evaluated simultaneously by using an optimization process and trial error method. In order to validate the SWRC evaluated from the infiltration test, the SWRC, obtained from initial suction test is used. Also, the evaluated SWRC and HCF were compared with the SWRC and HCF from the maintained suction measurement.

9.2 Conclusions

It is important to characterize the SWRC and the HCF in geotechnical engineering applications, and a reliable and convenient methodology is needed to characterize the flow phenomena in unsaturated soils. This research shows that a new FPS technique is suitable for measuring the suction response to obtain the SWRC and evaluating the HCF during hydraulic hysteresis. The following specific conclusions were drawn from the result in this study:

1. A new FPS technique (maintained suction measurement) with a suction-feedback control loop is appropriate for measuring the suction response and the SWRC during drying and wetting cycles.
2. The FPS and the developed testing methodology provided experimental data from which both SWRC and HCF are readily obtained. The HCF is obtained through an optimization process. The optimized HCF is expressed with curve fitting parameters unrelated to the SWRC. Our results showed that the commonly used prediction models cannot represent the hydraulic conductivity reliably over a wide suction range. Also, HCF prediction

models, from the SWRC models lead to several order of magnitude difference from the proper HCF obtained in the optimization process.

3. The optimized HCF corresponding to suction response showed limit of the hydraulic conductivity where its value does not decrease with increasing suction. It is suggested that the vapor-phase water flow is a primary mechanism of moisture transport below that hydraulic conductivity value. However, corresponding suction and degree of saturation at which this limit is reached, are quite different from the residual state suggested by Brooks and Corey (1964) and van Genuchten (1980), but are similar to residual state suggested by Fredlund and Xing (1994).
4. Based on the result from maintained suction measurement, the suction drop measurement developed in 2002 was reviewed, and the suction drop measurement is found not to be appropriate for measuring the SWRC.
5. The developed FPS is also suitable for characterizing hydraulic properties of initially unsaturated soil specimens provided that initial suction measured in each specimen. Using an infiltration result, the SWRC and the HCF were evaluated concurrently by using an inverse problem solution approach. The proper SWRC for infiltration test were similar to the SWRC of wetting cycle from maintained suction measurement and the initial suction test result.

9.3 Recommendations

In continuation of this research, the following recommendations are envisioned.

- Mathematical equation is needed for describing the HCF over a range of suction where liquid water flow dominates the process. This equation should be able to describe the HCF in vicinity of the residual state.

- The proper HCF obtained from an inverse problem approach showed the different suction and water content profiles of the soil specimen at different time increments due to different shapes for each HCF model corresponding to suction range. In this research, it cannot be concluded which optimized HCF is correct, because suction response result induced by flow pump can be only represented at the bottom boundary of the soil specimen. In order to improve our analysis, the methodology or technique considering the suction or water content value in each layer of the soil specimen is needed during testing. In addition, our results should be compared with results from other measurement technique such as centrifuge permeameter.
- The determination of hydraulic characteristics such as the SWRC and the HCF are affected by soil structure variables such as pore structure, compaction conditions, volume changes, stress state, and so on. More studies are needed to quantify these effects.

References

Abu-Hejkeh, A. N., Znidarcic, D., and Illangasekare, T. (1993). "Parameter Estimation of Hydraulic Conductivity in Unsaturated Soils using the Flow Pump Technique." Unsaturated Soil. Geotechnical Special Publication No. 39 : 163-174.

Aiban,S. A. and Znidarcic, D. (1989). "Evaluation of the Flow Pump and Constant Head Techniques for Permeability Measurements." Geotechnique 39 (4): 655-666.

Bicalho, K. V, (1999). "Modeling Water Flow in an Unsaturated Compacted Soil," Ph.D. Thesis, University of Colorado at Boulder, Boulder, Colorado.

Briggs, L. J., and McLane, J. W. (1907), "The Moisture Equivalent of Soils." *U.S. Dept.Agr.Bur.Soils, Bulletin 45*: 23

Brooks, R. H., and Corey, A. T. (1964), "Hydraulic Properties of Porous Media," Colorado State University, Hydrology Paper, 3, March.

Burdine, N. T. (1953) "Relative permeability calculations from pore-size distribution data." Petr. Trans., Am. Inst. Mining Metall. Eng. 198:71-77

Childs, E. C., and Collis-George, N., (1950). "The Permeability of Porous Materials," *Proceedings, Royal Society, London,* Series A, 210: 392-405.

Chiu, T.-F., and Shackelford, C. (1998). "Unsaturated Hydraulic Conductivity of Compacted Sand-Kaolin Mixes," *Journal of Geotechnical and Geoenvironnental Engineering,* 124(2): 160-170.

Chiu, T.-F., and Shackelford, C. (2001). "Laboratory Evaluation of Sand undrains," *Journal of Geotechnical and Geoenvironnental Engineering,* 126(1): 990-1001.

Celia, M.A., Bouloutas, E.T. and Zarba, R. L., (1990). "A General Mass-Conservative Numerical Solution for the Unsaturated Flow Equation," *Water Resour. Res*., 26:1483-1496

Craig, R. F. ((2004). *Craig's Soil Mechanics 7th edition*, New York, Spon Press.

Daniel, D.E. (1883). "Permeability Test for Unsaturated Soils," *Canadian Geotechnical Journal*, 33: 150-158.

Duncan, J. M., and Wright, S. G.. (2005), *Soil Strength and Slope Stability*, New Jersey, John Wiley & Sons, Inc.

Ebrahimi-B, N., Gitirana, G. F. N., Jr., Fredlund, D. G., Fredlund, M. D., and Samarasekera, L. (2004). "A lower limit for the water premebility coefficient." *Proc., 57th Canadian Geotechnical Conf.*, Vol. 1, Quebec City, Que., Canada, 12-19.

Edlefsen, N. E., and Anderson, A. B. C. (1943). "Thermodynamics of soil moisture," Hilgardia, 15: 31-298.

Farrel, D.G., and Larson, W. E. (1972). "Modelling the pore structure of porous media." *Water Resource, Res.*, 3: 699-706.

Fawcett, R.G., and Collis-George, N. (1967). "A Filter Paper Method for Determining the Moisture Characteristics of Soils," *Australian Journal of Experimental Agriculture and Animal Husbandry*, 7: 162-167.

Fayer, M. J. (2000). *Unsat-H version 3.01:Unsaturated Soil Water and Heat Flow Model:Theory, User manual, and Examples*, Pacific Northwest National Laboratory, Richland, Washington.

Fredlund, D. G. (2006). "Unsaturated Soil Mechanics in Engineering Practice," *Journal of Geotechnical and Geoenvironnental Engineering*, 132(3): 286-321.

Fredlund, D. G., and Rahardjo, H. (1993). *Soil Mechanics for Unsaturated Soils*, New Jersey, John Wiley & Sons, Inc.

Fredlund, D. G., and Xing, A (1994). "Equations for the Soil-Water Characteristic Curve," *Canadian Geotechnical Journal*, 31: 521-532.

Fredlund, D. G., Xing, A., and Huang, S. (1994). "Prediction the Permeability Function for Unsaturated Soil using the Soil-Water Characteristic Curve," *Canadian Geotechnical Journal*, 31: 533-546.

Gardner, R (1937). "The Method of Measuring the Capillary Tension of Soil Moisture over A Wide Moisture Range," *Soil Science,* 43: 277-283

Gardner, W. R. (1958). "Some Steady State Solutions of the Unsaturated Moisture Flow equation with Application to Evaporation from a Water Table," *Soil Science,* 85(4): 228-232.

Ghayoomi, M., (2011). "Seismically Induced Settlement of Partially-Saturated Sand," Ph.D. Thesis, University of Colorado at Boulder, Boulder, Colorado.

Hamilton, J. M., Daniel, D.E. and Olson, R. E.(1981). "Measurement of Hydraulic Conductivity of Partially Saturated Soils" *Permeability and Groundwater Contaminant Transport*. ASTM, STP, 746: 182-196.

Hilf, J. W. (1956). "An Investigation of Pore-Water Pressure in Compacted Cohesive Soils" Ph.D. Dissertation, Technical Memo No. 654, U.S. Department of Interior, Bureau of Reclamation, Design and Construction Division, Denver, Colorado.

Huang, K., Mohanty, B.P., and van Genuchten, M.Th. (1996). "A New Convergence Criterion for the Modified Picard Iteration Method to Solve the Variably Saturated Flow Equation," *Journal of Hydrology* 178 :69-91

Hwang, C. (2002). "Determination of Material Functions for Unsaturated Flow," Ph.D. Thesis, University of Colorado at Boulder, Boulder, Colorado.

Khanzode, R. M., Vanapali, S.K., and Fredlund, D.G., (2002). "Measurement of soil-water characteristic curves for fine-grained soils using a small-scale centrifuge." *Can. Geotech. Jour*., 39: 1209-1217.

Khosravi, A., (2011). "Small Strain Shear Modulus of Unsaturated, Compacted Soils During Hydraulic Hysteresis," Ph.D. Thesis, University of Colorado at Boulder, Boulder, Colorado.

Lee, J., (2007). "Parameter Estimation for Unsaturated Flow," M.S. Thesis, University of Colorado at Boulder, Boulder, Colorado.

Likos, W. J., and Lu, N. (2001). "Automated Measurement of Total Suction Characteristics in the High Suction Range : Application to Assessment of Swelling Potential," *Transportation Research Record: Journal of the Transportation Research Board*, 1786, TRB, Washington, 119-128.

Lu, N., Kwicklis, E. M., and Rousseau, J. P. (2001). "Determining Fault Permeability from Subsurface barometer pressure at Yucca Mountain, Nevada," *Journal of Geotechnical and Geoenvironnental Engineering,* 127: 801-809.

Lu, N., and Likos, W. J. (2004). *Unsaturated Soil Mechanics*, Hoboken, New Jersey : John Willey & Sons, Inc.

Lu, N., Wallyace, A., Carrera, J., and Likos, W. J. (2006). "Constant flow method for concurrently measuring soi-water characteristic curve and hydraulic conductivity function. *ASTM Geotechnical Testing Journal,* 29(3): 1-12.

McCartney, J. S. (2007). "Determination of the Hydraulic Characteristics of Unsaturated Soils using a Centrifuge Permeameter," Ph.D. Thesis, University of Texas at Austin, Austin, Texas.

McCartney, J. S and Parks, J. (2009). "Uncertainty in Predicted Hydraulic Conductivity Functions of Unsaturated Soils," 17th ICSMGE Conference, Alexandria, Egypt.

McCartney, J. S and Znidarcic, D. (2010). "Test System for Hydraulic Properties of Unsaturated Nonwoven Geotextiles," *Geosynthetics International*, 17(5): 10.

McCartney, J. S and Zornberg, J.G. (2005). "The Centrifuge Permeameter for Unsaturated Soils (CPUS)," Tarantino, A., Romero, E., and Cui, Y.J. (eds). Trento. Italy, 27-29 June 2005. Balkema, Rotterdam.

McCartney, J. S and Zornberg, J.G. (2010). "Centrifuge Permeameter for Unsaturated Soils I: Theoretical Basis and Experimental Developments," *Journal of Geotechnical and Geoenvironnental Engineering*, 136(8): 1051-1063.

McCartney, J. S and Zornberg, J.G. (2010). "Centrifuge Permeameter for Unsaturated Soils II: Measurement of The Hydraulic Characteristics of an Unsaturated Clay," *Journal of Geotechnical and Geoenvironnental Engineering,*136(8): 1064-1076.

Meerdink, J. Benson, C., and Khire, M. (1996). "Unsaturated Hydraulic Conductivity of Two Compacted Barrier Soils," *J.Getech. Eng.,* ASCE, 122(7): 565-576.

Moore, R. (1939). "Water Conduction from Shallow Water Tables," Hilgardia, 12: 383-426.

Mualem, Y. (1976a) "A New Model for Prediction the Hydraulic Conductivity of Unsaturated Porous media," Water Resour. Res., 12: 513-522.

Mualem, Y. (1976b) "A Catalogue of the Hydraulic Properties of Unsaturated Soils," Research Project no.442, Technion, Israel Institute of Technology, Haifa, Israel.

Olsen, H. W., Morin, R. H., and Nichols, R. W. (1988). "Flow pump application in triaxial testing," Donaghe, R. T., Cahney, R.c., and Silver, M. L., eds., *Advanced Triaxial Testing of Soil and Rock*, ASTM STP 977, ASTM, Philadelphia, 482-504.

Parks, J. M., (2010). "Investigation of Infiltration and Drainage Flow Processes in Unsaturated Soil Using a Centrifuge Permeameter," M.S. Thesis, University of Colorado at Boulder, Boulder, Colorado.

Pham, H. Q., Fredlund, D. G., and Barbour, S. L. (2003a). "Estimation of the hysteretic soil-water characteristic curves from the drying boundary curve." *Proc., 56th Canadian Geotechnical Conf.*, 2: 115-121.

Pham, H. Q., Fredlund, D. G., and Barbour, S. L. (2003b). "A practical hysteresis model for the soil-water characteristic curve for the soils with negligible volume change." *Can. Geotech. J.*, 40(4): 293-298.

Rad, N. S. and Clough, G. W. (1984). "New Procedure for Saturating Sand Specimens" *Journal of Geotechnical Engineering*, 110(9): 1205-1218.

Resnick, G. S., (1988). "Centrifugal modeling of seepage, slope stability, and the influence of horizontal drains**,"** M.S. Thesis, University of Colorado at Boulder, Boulder, Colorado.

Richards, B. G. (1965). "Measurement of the Free Energy of Soil Moisture by the Psychrometric Technique Using Thermistors," *Moisture Equilibria and Moisture Changes in Soils Beneath Covered Areas, A Symp. in Print*. Australia: Butterworths, 39-46.

Richards, L. (1952). "Water Conducting and Retaining Properties of Soils in Relation to irrigation," *Proc. Int. Symp*. On Desert Res. 523-426.

Sigda, J. M. , and Wilson, J. L. (2005). "Are Faults Preferential Flow Paths thorugh Semiarid and Arid Vadose Zones," *Water Resour.Res*.39(8): 1225-1239.

Spanner, D. C. (1951). "The Peltier Effect and Its Use in the Measurement of Suction Pressure." *J.Exp.Bot*., 11: 145-168.

Tami, D., Rahardjo, H., and Leong, E. C. (2004a). "Effects of Hysteresis on Steady-State Infiltration in Unsaturated Slopes.." *Journal of Geotechnical and Geoenvironnental Engineering*, 130(9): 956-967.

Thomson, W., (1871), *Philosophical Magazine*, 42: 448.

van Genuchten, M. TH.(1980). "A Closed-Form for Predicting the Hydraulic Conductivity of Unsaturated Soils," *Soil Science Society of America Journal*, 44: 892-898.

Vanapalli, S. K., Fredlund, D.G., and Sillers, W. S. (1998) "The Meaning and Relevance of Residual State to Unsaturated soils." *51st Canadian Geotechnical Conference*, Edmonton, Alberta, October 4-7, 1998.

Vogel, T., and Cislerova, M.(1988). "On the reliability of unsaturated hydraulic conductivity calculated from the moisture retention curve," *Transport in Porous Media,* 3:1-15

Wildenschild, D., Hopmans, J..W, and Simunek, J. (2001). "Flow Rate Dependence of Soil Hydraulic Characteristics," *Soil Science Society of America Journal*, 65(1): 35-48.

Wildenschild, D., and Jensen, K. H.(1999). "Laboratory Investigations of Effective Flow Behavior in Unsaturated Heterogeneous Sands," *Water Resour. Res*., 35:17-27.

Wildenschild, D., and Jensen, K. H.(1999). "Numerical Modeling of Observed Effective Flow Behavior in Unsaturated Heterogeneous Sands," *Water Resour. Res*., 35:29-42.

Williams, J., Prebble, R. E., Williams, W. T., and Hignett, C. T.,(1983). "The Influence of Texture, Structure, and Clay Mineralogy on the Soil Moisture Characteristics," *Australian. J. of Soil Res.,* 21: 15-32.

Young, M., Karagunduz, A., Simunekm J., and Pennell, K. (2002). "A modified Upward Infiltration Method for Characterizing Soil Hydraulic Properties," *Soil Science Society of America Journal,*66: 57-64.

Znidarcic, D., Illangasekare, T., and Manna, M. (1991). Laboratory Testing and Paramter Estimation for Two-Phase Flow Problems. In Mclean et al (ed.) *Proc. of the Geotechnical Engineering Congress*. Boulder CO. 1991. ASCE, New York.

Znidarcic, D., and Lee, J. (2009). "Critical Rainfall Infiltration Issues in Landslides," The First Italian Workshop on Landslides, Napoli, Italy.

Appendix A

SWRC of Soil Specimens at Different Porosities and Different Net Confining Pressures

The determination of the SWRC is affected by soil structure variables such as net confining pressure, pore size distribution, compaction conditions, and so on. This chapter represents two impact variables such as porosity and net confining pressure in determination of the SWRC.

Figures from A.1 to A.2 show the comparison of suction responses, transient suction-saturation curves, SWRCs and BC fits of Pocheon sand and Bonny silt with different porosities. In case of Pocheon sand, # MSM-P1(n=0.345) and ## MSM-P2 (n=0.327) are used. Twenty times slower flow rate as saturated hydraulic conductivity is applied in #MSM-P1, whereas twice faster flow rate is applied in SMM-P2. In case of Bonny silt, test # MSM-B1(n=0.400) and # MSM-B2 (n=0.375) are used for comparison. Five times slower flow rate is applied in MSM-B1, whereas the same flow rate as saturated hydraulic conductivity is applied in MSM-B2. In both cases, the overall slope and shape of the SWRCs after air entry value are not significantly different from each other as shown in figure A.1 and A.2. Larger porosity leads to lower air entry pressure value in both cases because soil specimen with smaller porosity has a better retention ability. Also, the hysteresis loops in case of lower porosity are smaller than larger porosity.

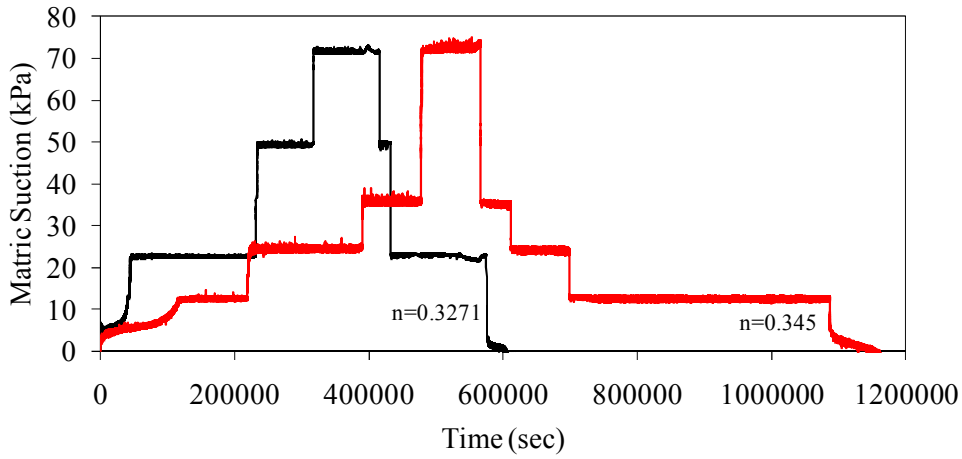

(a)

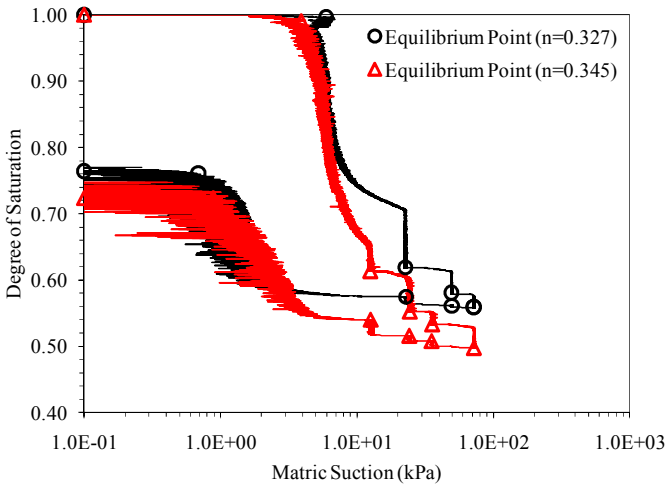

(b)

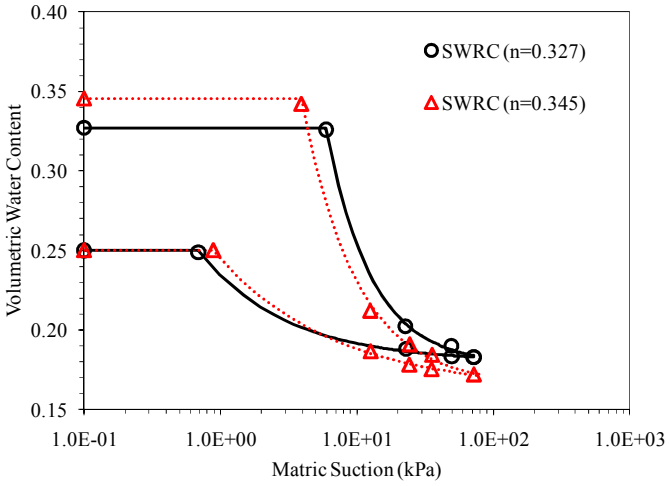

(c)

Figure A.1. Comparisons with different porosities (Pocheon sand, #MSM-P1 and #MSM-P2): (a) suction response; (b) transient suction-saturation curve; (c) SWRC

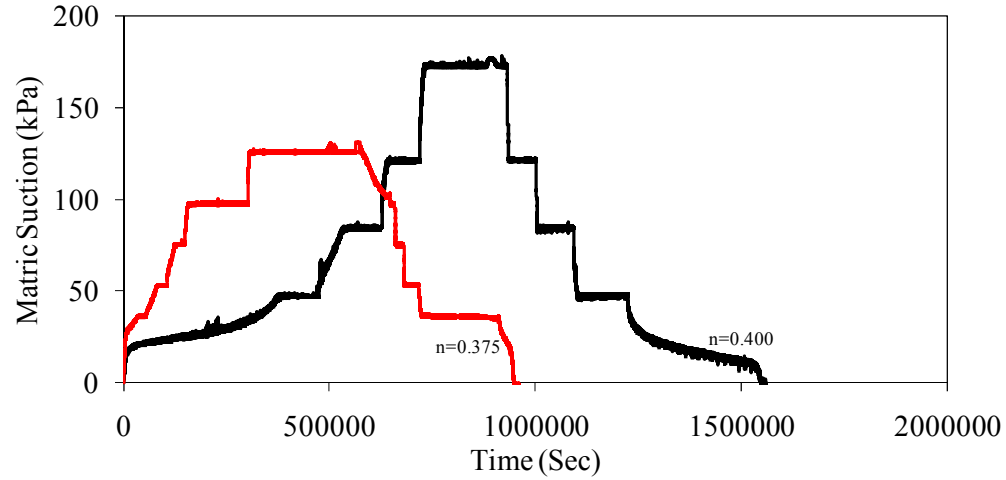

(a)

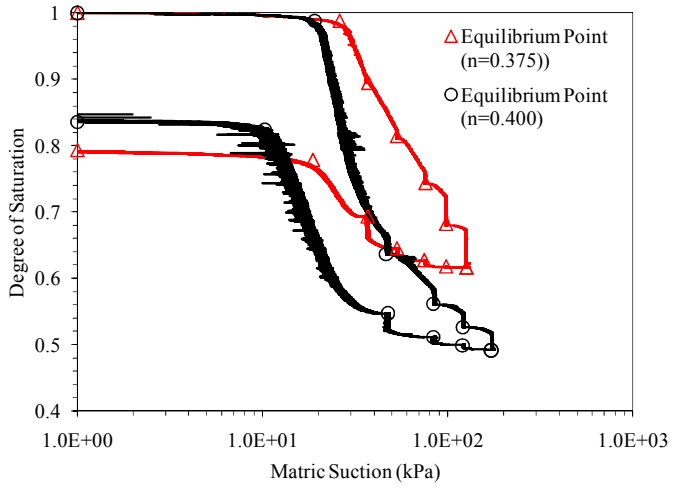

(b)

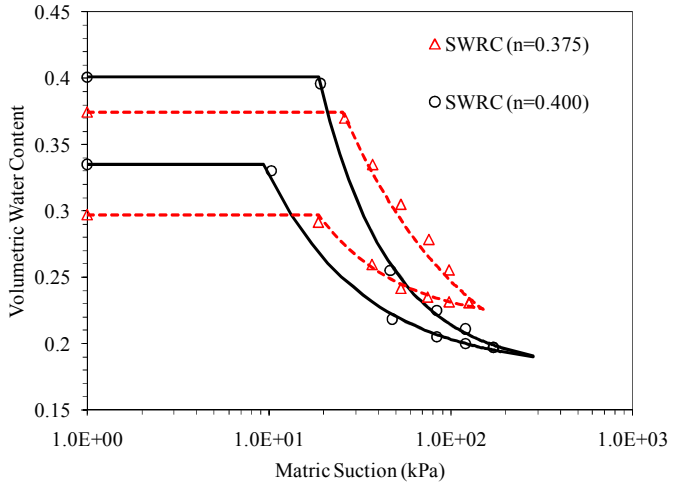

(c)

Figure A.2. Comparisons with different porosities (Bonny silt, #MSM-B1 and #MSM-B2): (a) suction response; (b) transient suction-saturation curve; (c) SWRC

Khosravi (2011) found that the net confining stress has an influence on measuring SWRC of Bonny silt in the FPS due to the rearrangement between the particles with the different net confining pressure. As a net confining pressure increases, the soil specimen has a better retention ability and higher air entry pressure. Also, the size of hysteresis loop is affected by the net confining pressure. The hysteresis loops of the SWRC subjected to the higher net confining stresses are smaller (Khosravi, 2011). Pocheon sand and F-75 Ottawa sand are used for comparisons of different net confining pressures.

Before testing with different net confining pressure, three tests of Pocheon sand with three different confining pressures (σ) and same net confining pressure (σ-u_a), 100 kPa are conducted. Confining pressures of 300 kPa, 500 kPa, and 700 kPa are used for #MSM-P2 #MSM-P3, and #MSM-P4 with the same net confining pressure, 100 kPa, respectively. Figure A.3 shows the comparison of three suction responses and SWRCs. Even though the air entry pressure is higher as confining pressure increases, the entire trends of each SWRC is not significantly different from each other. In order to compare different net confining pressures, 100 kPa, #MSM-P5 is conducted with the net confining pressure of 200 kPa after completing #MSM-P1. The height of the soil specimen in #MSM-P5 decreases 55.30 cm to 55.16 cm. This leads to smaller porosity, 0.344 and 10% slower saturated hydraulic conductivity than # MSM-P1. Figures A.4 and A.5 show results of Pocheon sand and F-75 Ottawa sand. In cases of Pocheon sand and F-75 Ottawa sand , higher net confining pressure does not lead to higher air entry pressure unlike Bonny silt test results by Khosravi (2011). However, higher net confining pressure leads to smaller hysteresis loop and higher degree of saturation after wetting cycle.

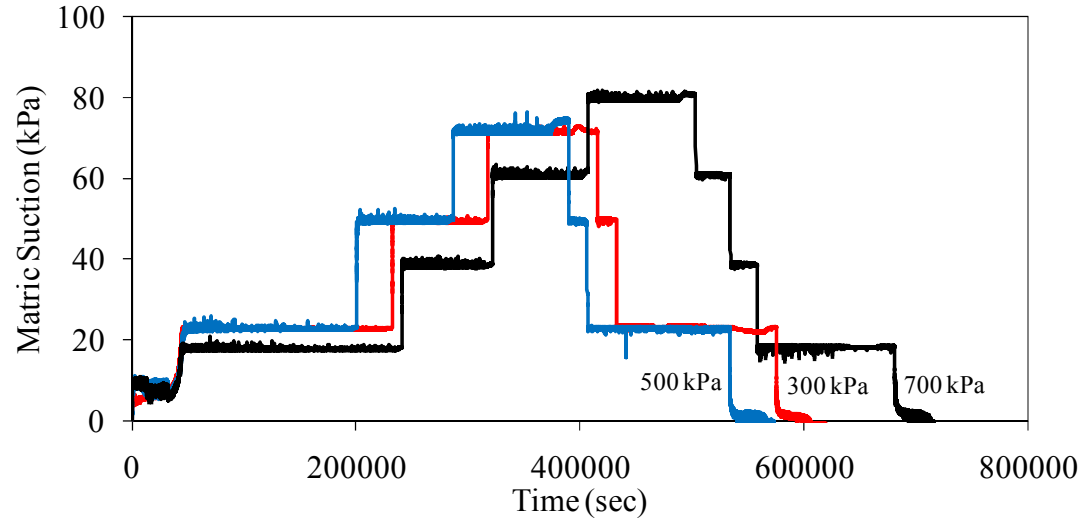

(a)

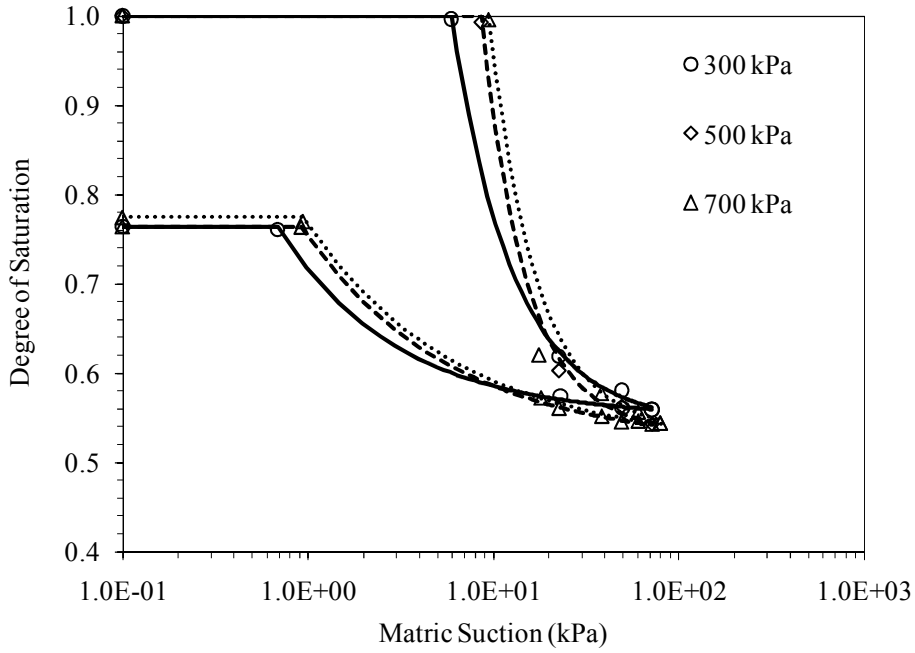

(b)

Figure A.3. Comparisons with different confining pressure and the same net pressure, 100kPa (Pocheon sand, #MSM-P2, #MSM-P3, and #MSM-P4): (a) suction response; (b) SWRC

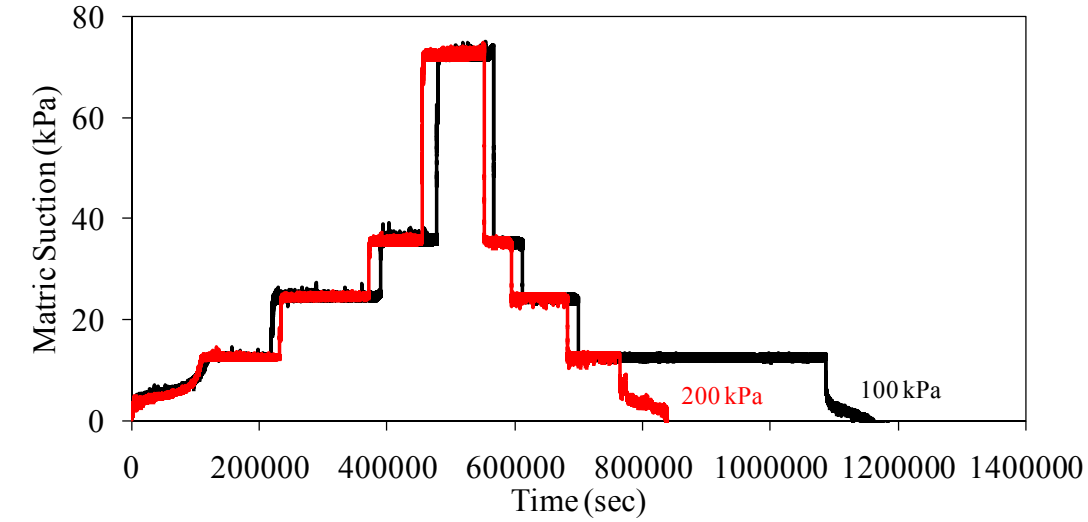

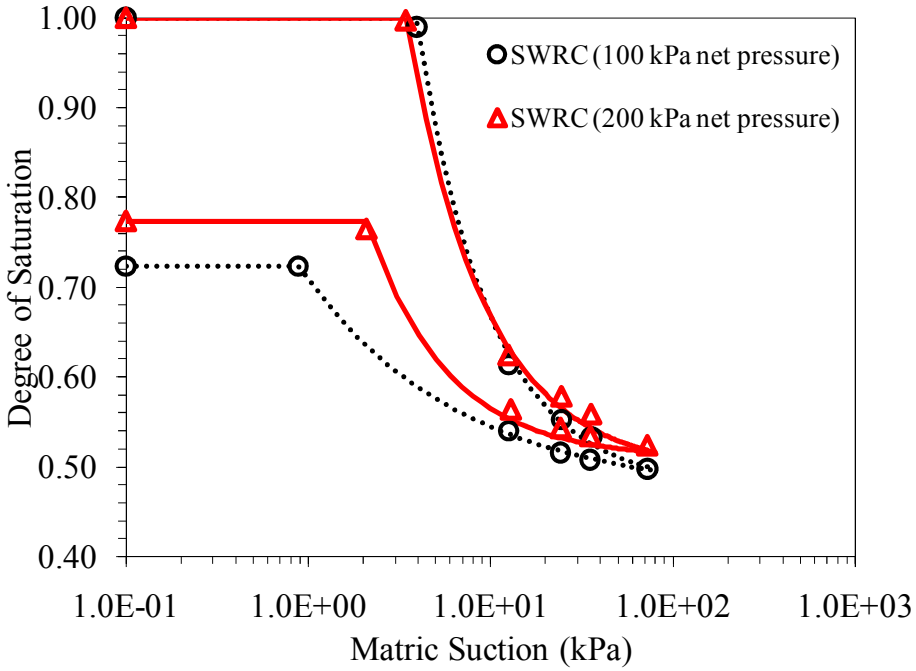

(b)

Figure A.4. Comparisons of SWRC and BC fits between 100 kPa and 200 kPa of net pressures (Pocheon Sand, #MSM-P1 and #MSM-P5): (a) suction response; (b) SWRC

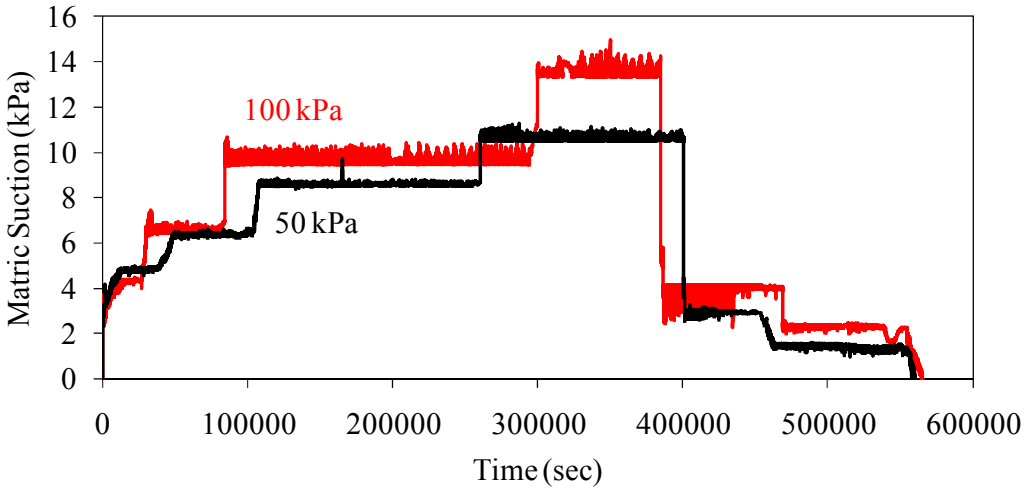

(a)

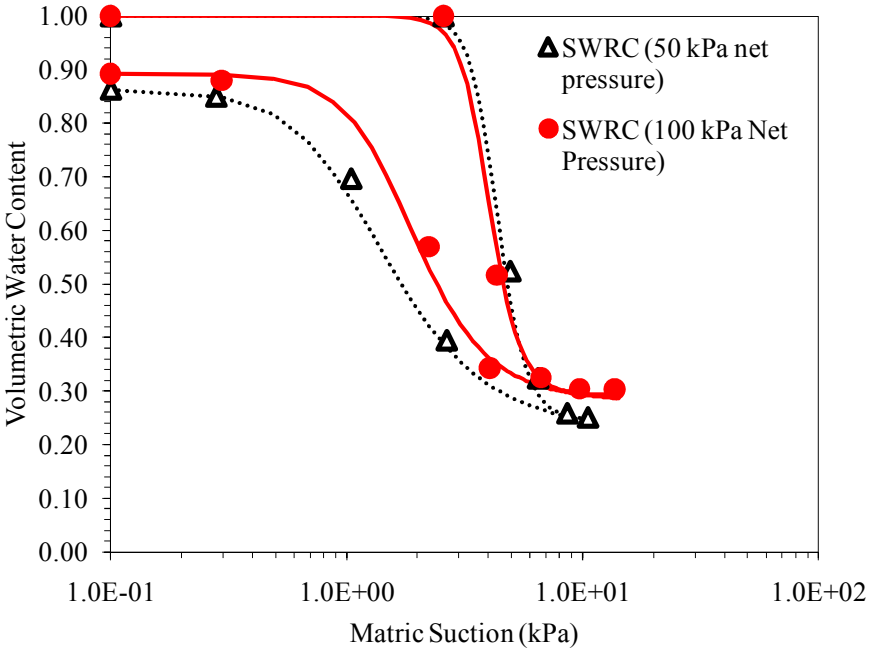

(b)

Figure A.5. Comparisons of SWRC and BC fits between 50 kPa and 100 kPa of net confining pressures (F-75 Ottawa sand, #MSM-F2 and #MSM-F3): (a) suction response; (b) SWRC

Appendix B

Example of PEST Result (First Withdrawal Stage of Test #MSM-P1)

OPTIMISATION RECORD

INITIAL CONDITIONS:
Sum of squared weighted residuals (ie phi) = 3.08180E+05

Current parameter values
a 0.925200

OPTIMISATION ITERATION NO. : 1
Model calls so far : 1
Starting phi for this iteration: 3.08180E+05

Lambda = 5.0000 ----->
Phi = 2.99534E+05 (0.972 of starting phi)

Lambda = 2.5000 ----->
Phi = 2.99534E+05 (0.972 of starting phi)

No more lambdas: relative phi reduction between lambdas less than 0.0300
Lowest phi this iteration: 2.99534E+05
Relative phi reduction between optimisation iterations less than 0.1000
Switch to central derivatives calculation

Current parameter values Previous parameter values
a 0.933492 a 0.925200
Maximum relative change: 8.9625E-03 ["a"]

OPTIMISATION ITERATION NO. : 2
Model calls so far : 4
Starting phi for this iteration: 2.99534E+05

Lambda = 2.5000 ----->
Phi = 2.77481E+05 (0.926 of starting phi)

Lambda = 1.2500 ----->
Phi = 2.77481E+05 (0.926 of starting phi)

No more lambdas: relative phi reduction between lambdas less than 0.0300

Lowest phi this iteration: 2.77481E+05

Current parameter values		Previous parameter values	
a	0.963462	a	0.933492

Maximum relative change: 3.2105E-02 ["a"]

OPTIMISATION ITERATION NO. : 3
Model calls so far : 8
Starting phi for this iteration: 2.77481E+05

Lambda = 1.2500 ----->
Phi = 2.66337E+05 (0.960 of starting phi)

Lambda = 0.62500 ----->
Phi = 2.66337E+05 (0.960 of starting phi)

No more lambdas: relative phi reduction between lambdas less than 0.0300
Lowest phi this iteration: 2.66337E+05

Current parameter values		Previous parameter values	
a	0.989532	a	0.963462

Maximum relative change: 2.7059E-02 ["a"]

OPTIMISATION ITERATION NO. : 4
Model calls so far : 12
Starting phi for this iteration: 2.66337E+05

Lambda = 0.62500 ----->
Phi = 2.60948E+05 (0.980 of starting phi)

Lambda = 0.31250 ----->
Phi = 2.60948E+05 (0.980 of starting phi)

No more lambdas: relative phi reduction between lambdas less than 0.0300
Lowest phi this iteration: 2.60948E+05

Current parameter values		Previous parameter values	
a	1.01005	a	0.989532

Maximum relative change: 2.0732E-02 ["a"]

OPTIMISATION ITERATION NO. : 5
Model calls so far : 16
Starting phi for this iteration: 2.60948E+05

```
   Lambda =  0.31250     ----->
     Phi =  2.58229E+05  (  0.990 of starting phi)

   Lambda =  0.15625     ----->
     Phi =  2.58229E+05  (  0.990 of starting phi)

 No more lambdas: relative phi reduction between lambdas less than 0.0300
 Lowest phi this iteration:  2.58229E+05

   Current parameter values              Previous parameter values
   a             1.02586             a             1.01005
 Maximum relative change: 1.5655E-02 ["a"]


OPTIMISATION ITERATION NO.       :   6
 Model calls so far           :   20
 Starting phi for this iteration:  2.58229E+05

   Lambda =  0.15625     ----->
     Phi =  2.57416E+05  (  0.997 of starting phi)

   Lambda =  7.81250E-02 ----->
     Phi =  2.57416E+05  (  0.997 of starting phi)

 No more lambdas: relative phi reduction between lambdas less than 0.0300
 Lowest phi this iteration:  2.57416E+05

   Current parameter values              Previous parameter values
   a             1.03224             a             1.02586
 Maximum relative change: 6.2252E-03 ["a"]


OPTIMISATION ITERATION NO.       :   7
 Model calls so far           :   24
 Starting phi for this iteration:  2.57416E+05

   Lambda =  7.81250E-02 ----->
     Phi =  2.56732E+05  (  0.997 of starting phi)

   Lambda =  3.90625E-02 ----->
     Phi =  2.56732E+05  (  0.997 of starting phi)

 No more lambdas: relative phi reduction between lambdas less than 0.0300
 Lowest phi this iteration:  2.56732E+05
```

Current parameter values Previous parameter values
a 1.03872 a 1.03224
Maximum relative change: 6.2770E-03 ["a"]

Optimisation complete: the 3 lowest phi's are within a relative distance
of eachother of 1.000E-02
Total model calls: 28

The model has been run one final time using best parameters.
Thus all model input files contain best parameter values, and model
output files contain model results based on these parameters.

OPTIMISATION RESULTS

Parameters ----->

Parameter	Estimated value	95% percent confidence limits lower limit	upper limit
a	1.03872	1.03403	1.04342

Note: confidence limits provide only an indication of parameter uncertainty.
They rely on a linearity assumption which may not extend as far in
parameter space as the confidence limits themselves - see PEST manual.

See file twofit.sen for parameter sensitivities.

Observations ----->

Observation	Measured value	Calculated value	Residual	Weight	Group
0001	0.100000	0.00000	0.100000	1.000	obsgroup
0002	16.9480	34.8610	-17.9130	1.000	obsgroup
0003	17.2620	34.9520	-17.6900	1.000	obsgroup
0004	19.3190	35.0440	-15.7250	1.000	obsgroup
0005	24.2690	35.1370	-10.8680	1.000	obsgroup
0006	19.5830	35.2290	-15.6460	1.000	obsgroup
0007	17.3740	35.2630	-17.8890	1.000	obsgroup
0008	18.0620	35.2930	-17.2310	1.000	obsgroup
0009	17.1120	35.3240	-18.2120	1.000	obsgroup
0010	22.9520	35.3550	-12.4030	1.000	obsgroup
0011	24.0840	35.3860	-11.3020	1.000	obsgroup
0012	18.1350	35.4160	-17.2810	1.000	obsgroup
0013	18.1280	35.4470	-17.3190	1.000	obsgroup

0014	19.7400	35.4780	-15.7380	1.000	obsgroup
0015	19.6140	35.5090	-15.8950	1.000	obsgroup
0016	22.6440	35.5400	-12.8960	1.000	obsgroup
0017	19.8990	35.5710	-15.6720	1.000	obsgroup
0018	17.6390	35.6020	-17.9630	1.000	obsgroup
0019	21.2730	35.6340	-14.3610	1.000	obsgroup
0020	19.3930	35.6650	-16.2720	1.000	obsgroup
0021	20.1680	35.6960	-15.5280	1.000	obsgroup
0022	21.7260	35.7200	-13.9940	1.000	obsgroup
0023	18.8530	35.7330	-16.8800	1.000	obsgroup
0024	21.2240	35.7520	-14.5280	1.000	obsgroup
0025	19.4810	35.7710	-16.2900	1.000	obsgroup
0026	18.0910	35.7900	-17.6990	1.000	obsgroup
0027	22.5240	35.8080	-13.2840	1.000	obsgroup
0028	19.3400	35.8270	-16.4870	1.000	obsgroup
0029	21.6630	35.8460	-14.1830	1.000	obsgroup
0030	21.1950	35.8640	-14.6690	1.000	obsgroup
0031	16.7950	35.8830	-19.0880	1.000	obsgroup
0032	19.1050	35.9020	-16.7970	1.000	obsgroup
0033	23.7150	35.9210	-12.2060	1.000	obsgroup
0034	23.6540	35.9390	-12.2850	1.000	obsgroup
0035	20.8200	35.9580	-15.1380	1.000	obsgroup
0036	17.4580	35.9770	-18.5190	1.000	obsgroup
0037	17.6500	35.9960	-18.3460	1.000	obsgroup
0038	23.1040	36.0150	-12.9110	1.000	obsgroup
0039	25.2740	36.0330	-10.7590	1.000	obsgroup
0040	21.2000	36.0520	-14.8520	1.000	obsgroup
---	---	---	---	---	---
6453	130.526	144.700	-14.1740	1.000	obsgroup
6454	129.034	144.780	-15.7460	1.000	obsgroup
6455	130.195	144.870	-14.6750	1.000	obsgroup
6456	125.351	144.950	-19.5990	1.000	obsgroup
6457	125.766	145.040	-19.2740	1.000	obsgroup
6458	125.850	145.120	-19.2700	1.000	obsgroup
6459	129.317	145.210	-15.8930	1.000	obsgroup
6460	129.577	145.290	-15.7130	1.000	obsgroup
6461	125.512	145.370	-19.8580	1.000	obsgroup
6462	126.869	145.460	-18.5910	1.000	obsgroup
6463	128.085	145.550	-17.4650	1.000	obsgroup
6464	124.818	145.630	-20.8120	1.000	obsgroup
6465	126.871	145.720	-18.8490	1.000	obsgroup
6466	126.645	145.800	-19.1550	1.000	obsgroup
6467	129.530	145.890	-16.3600	1.000	obsgroup
6468	128.455	145.970	-17.5150	1.000	obsgroup
6469	124.527	146.060	-21.5330	1.000	obsgroup
6470	129.397	146.150	-16.7530	1.000	obsgroup
6471	130.594	146.230	-15.6360	1.000	obsgroup

6472	125.857	146.320	-20.4630	1.000	obsgroup
6473	125.224	146.400	-21.1760	1.000	obsgroup
6474	126.007	146.490	-20.4830	1.000	obsgroup
6475	128.322	146.580	-18.2580	1.000	obsgroup
6476	130.552	146.660	-16.1080	1.000	obsgroup
6477	126.905	146.750	-19.8450	1.000	obsgroup
6478	126.704	146.840	-20.1360	1.000	obsgroup
6479	126.544	146.930	-20.3860	1.000	obsgroup
6480	125.844	147.010	-21.1660	1.000	obsgroup
6481	126.482	147.100	-20.6180	1.000	obsgroup

See file twofit.res for more details of residuals in graph-ready format.

See file twofit.seo for composite observation sensitivities.

Objective function ----->

Sum of squared weighted residuals (ie phi) = 2.5673E+05

Correlation Coefficient ----->

Correlation coefficient = 0.9760

Analysis of residuals ----->

All residuals:-
Number of residuals with non-zero weight = 6481
Mean value of non-zero weighted residuals = 2.340
Maximum weighted residual [observation "1798"] = 23.69
Minimum weighted residual [observation "6469"] = -21.53
Standard variance of weighted residuals = 39.62
Standard error of weighted residuals = 6.294

Note: the above variance was obtained by dividing the objective function by the number of system degrees of freedom (ie. number of observations with non-zero weight plus number of prior information articles with non-zero weight minus the number of adjustable parameters.) If the degrees of freedom is negative the divisor becomes the number of observations with non-zero weight plus the number of prior information items with non-zero weight.

Parameter covariance matrix ----->

	a
a	5.7289E-06

Parameter correlation coefficient matrix ----->

	a
a	1.000

Normalized eigenvectors of parameter covariance matrix ----->

	Vector_1
a	1.000

Eigenvalues ----->

5.7289E-06

Appendix C

Suction Profiles at Different Time Increments with Optimized HCF in Maintained Suction Measurement

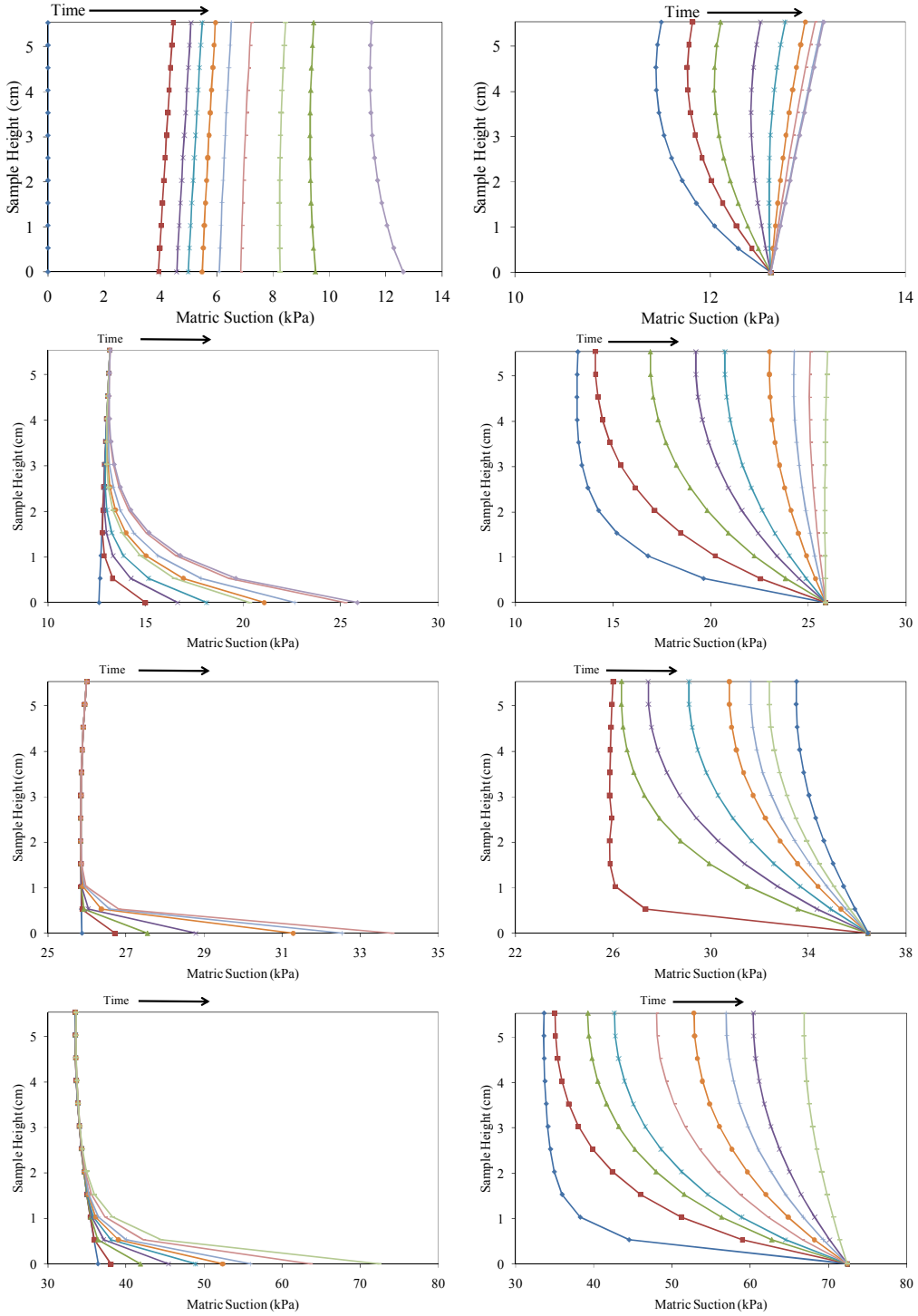

-continued-

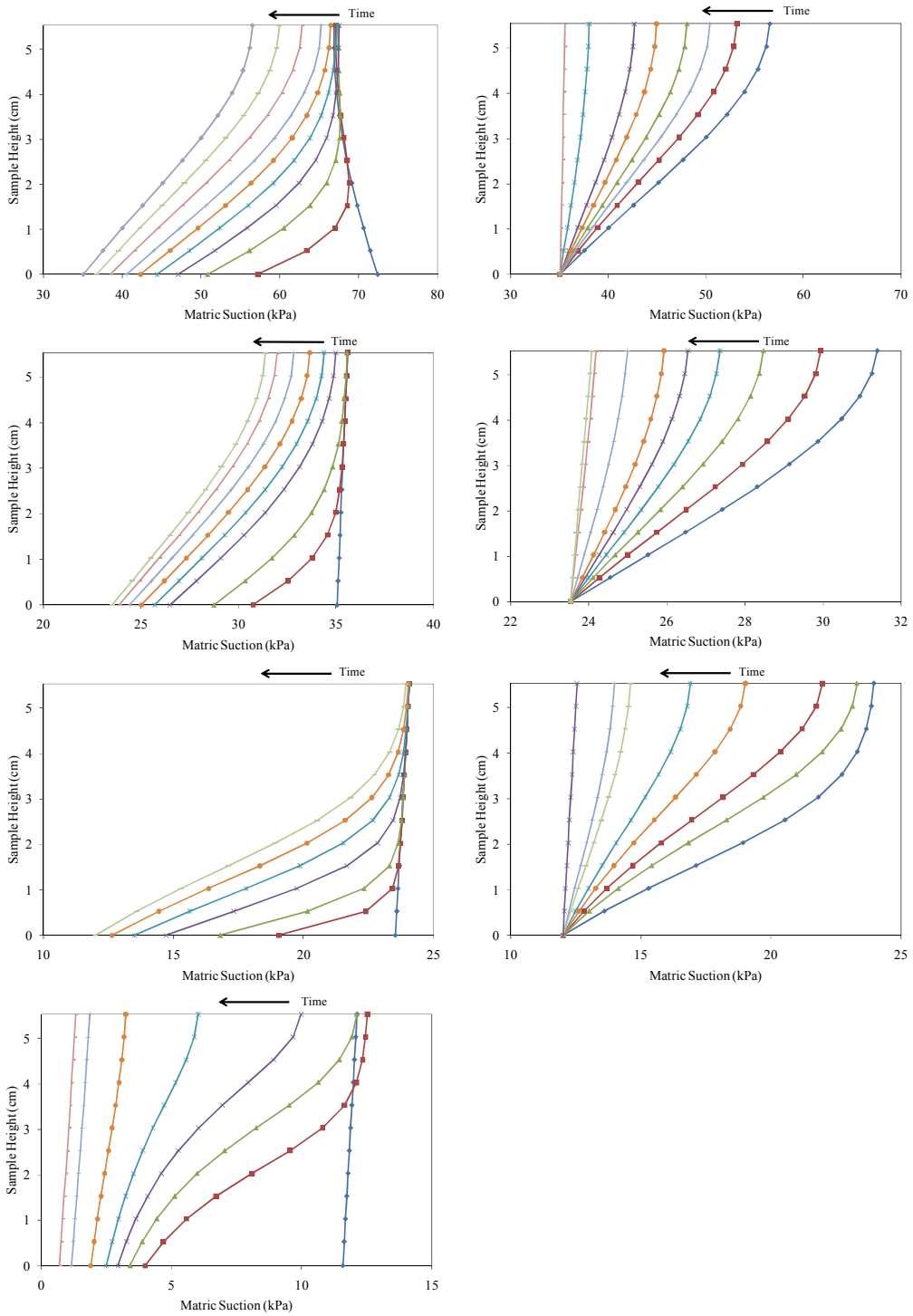

Figure C.1. Suction profiles at different time increments with the optimized of HCF (Pocheon Sand, MSM-P1)

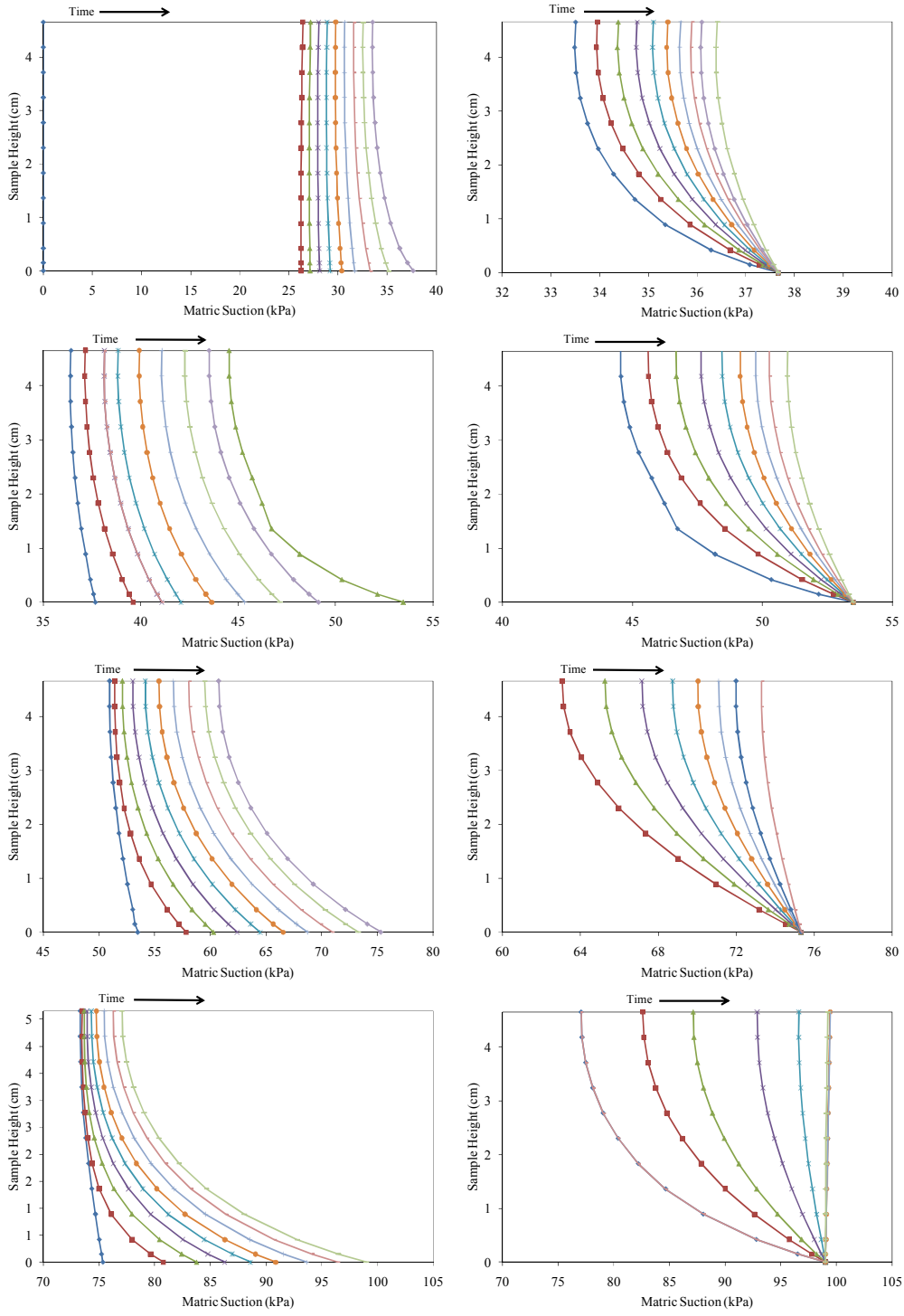

-continued-

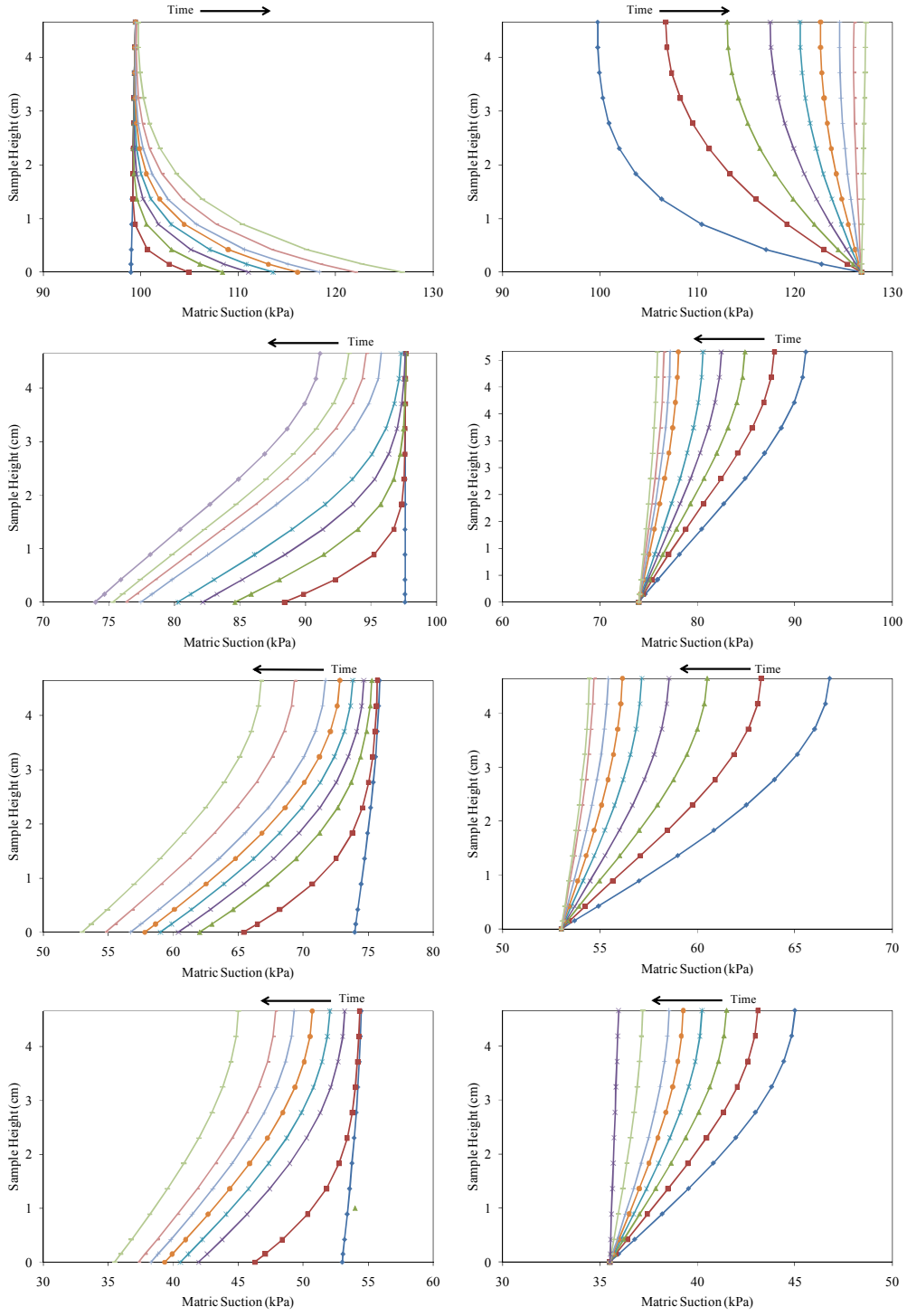

-continued-

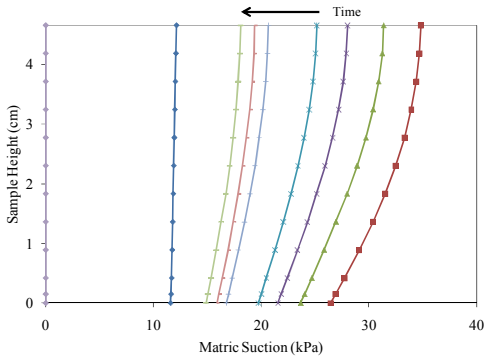

Figure C.2. Suction profiles at different time increments with the optimized HCF (Bonny Silt, MSM-B2)

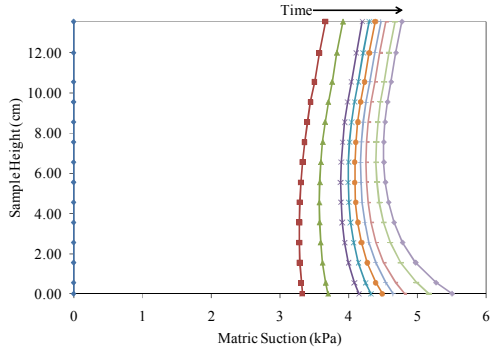

(a)first suction increasing stage

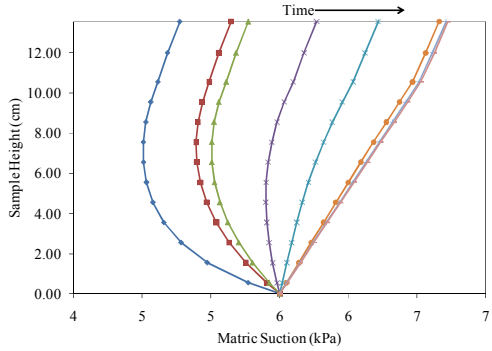

(b)first suction maintaining stage

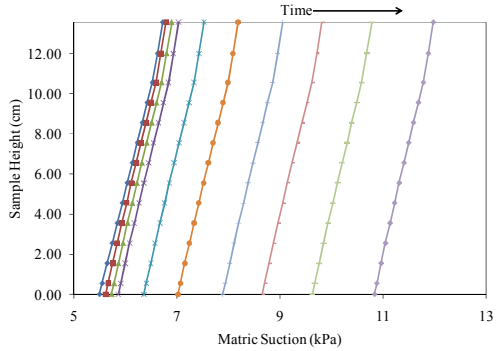

(c)second suction increasing stage

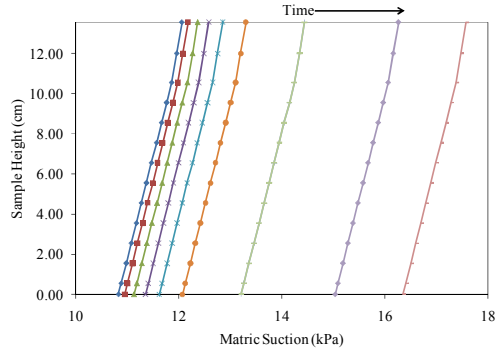

(d)third suction increasing stage

Figure C.3. Suction profiles at different time increments with the optimized HCF wetting cycle (F-75 Ottawa sand, MSM-F1)

Appendix D

Optimized Parameter Values and Coefficient of Determination in Tests #MSM-P1, #MSM-B1, #MSM-B-2, #MSM-F1, and # IT-B1

Table D.1. Optimized curve fitting parameters of drying cycle (Pocheon Sand, #MSM-P1)

Suction Range (kPa)	0→13.5	13.5→25.5	25.5→35.5	35.5→75.5
k_s(m/s)	1.0E-06	1.1E-08	5.6E-08	5.6E-08
ψ_e(kPa)	3.92	3.52	3.92	4.01
λ	0.92	1.24	10.00	0.20
R^2	0.95	0.88	0.90	0.89

Table D.2 Optimized curve fitting parameters of wetting cycle (Pocheon Sand, #MSM-P1)

Suction Range (kPa)	0←13.5	13.5←25.5	25.5←35.5	35.5←75.5
k_s(m/s)	3.1E-07	5.0E-08	2.1E-07	2.7E-07
ψ_e(kPa)	0.88	6.65	1.96	2.95
λ	0.35	1.00	0.23	0.29
R^2	0.91	0.97	0.85	0.86

Table D.3. Optimized curve fitting parameters of drying cycle (Bonny silt, #MSM-B1)

Sution Range (kPa)	0→45	45→85	85→120	120→171
k_s(m/s)	1.2E-07	8.5E-07	1.4E-06	1.4E-06
ψ_e(kPa)	18.64	9.86	12.78	14.13
λ	0.018	0.11	0.05	0.11
R^2	0.89	0.91	0.89	0.95

Table D.4 Optimized curve fitting parameters of drying cycle (Bonny silt, #MSM-B2)

Suction Range (kPa)	0→44	44→54	54→76	76→97	97→122
k_s(m/s)	5.1E-08	5.0E-08	4.6E-08	4.9E-08	5.5E-08
ψ_e(kPa)	25.51	25.93	10.81	24.60	24.53
λ	3.11	1.64	0.10	0.69	0.61
R^2	0.90	0.99	0.99	0.98	0.95

Table D.5. Optimized curve fitting parameters of wetting cycle (Bonny silt, #MSM-B2)

Suction Range (kPa)	0←44	44←54	54←76	76←97
k_s(m/s)	5.0E-09	5.5E-09	5.7E-09	5.8E-09
ψ_e(kPa)	15.30	20.50	24.86	51.36
λ	0.002	0.07	0.06	1.00
R^2	0.92	0.98	0.99	0.97

Table D.6 Optimized curve fitting parameters (F-75 Ottawa Sand, #MSM-F1)

Sution Range (kPa)	0→5.5	5.5→10.5	10.5→16
k_s(m/s)	6.2E-06	2.9E-06	2.9E-06
α(kPa^{-1})	0.21	4.48E-02	4.4E-02
n	2.48	3.6	3.6
R^2	0.95	0.99	0.99

Table D.7 Optimized curve fitting parameters (Bonny silt, #IT-B1)

BC Model			VG Model		
	SWRC	HCF		SWRC	HCF
ψ_e (kPa)	10.71	6.61	α(kPa^{-1})	0.05	0.06
λ	0.52	0.005	n	2.98	5.32
θ_r	0.10		θ_r	0.16	
R^2	0.98		R^2	0.99	

Appendix E

Difference between Air Entry Pressure and Air Entrapment Pressure

In general, air entry pressure is used for both the drying cycle and the wetting cycle for convenience. However, air entry pressure in the drying cycle is different from air entrapment pressure in the wetting cycle. The reason was discussed in Chapter 6.3.1. Table E.1 shows the difference between air entry pressure and air entrapment pressure. In general, air entry pressure in the drying cycle is 2 to 3 times higher than air entrapment in the wetting cycle. In the case of Bonny silt, air entry pressure is about 1.6 higher than air entrapment pressure. However, air entry pressure is significantly different from air entrapment pressure (i.e., 5 to 10 times higher than air entrapment in cases of F-75 Ottawa sand and Pocheon sand except test #MSM-P5). Therefore, a careful decision should be needed as to which process is to be modeled (i.e., the drying or wetting process) and with which kinds of soil are used.

Table E.1 Difference between air entry pressure and air entrapment pressure

Test #	Test Material	Air Entry Presure (kPa)	Air Entrampment Presure (kPa)	Difference ($\psi_{Air\ Entry}/\psi_{Air\ Entrapment}$)
MSM-P1	Pocheon sand	3.92	0.88	4.45
MSM-P2	Pocheon sand	5.93	0.68	8.72
MSM-P3	Pocheon sand	8.63	0.92	9.38
MSM-P4	Pocheon sand	9.45	0.94	10.05
MSM-P5	Pocheon sand	3.43	2.05	1.67
MSM-B1	Bonny silt	19.13	10.3	1.86
MSM-B2	Bonny silt	25.99	18.63	1.40
MSM-F2	F-75 Ottawa sand	2.58	0.28	9.21
MSM-F3	F-75 Ottawa sand	2.57	0.295	8.71